COUPLING FIELD DATA AND A FLOW MODEL TO CHARACTERIZE THE ROLE OF GROUNDWATER IN A MONTANE, SEMI-ARID, HEADWATER CATCHMENT, GORDON GULCH, COLORADO

by

LAUREN SALBERG

B.A., Geology, Carleton College, 2015

A thesis submitted to the
Faculty of the Graduate School of the
University of Colorado in partial fulfillment
of the requirement for the degree of
Master of Science
Department of Geological Sciences
2021

Committee Members:
Suzanne Anderson
Shemin Ge
Eric Small-Tilton

ABSTRACT

Salberg, Lauren (M.S., Geological Sciences)

Coupling Field Data and a Flow Model to Characterize the Role of Groundwater in a Montane, Semi-Arid, Headwater Catchment, Gordon Gulch, Colorado

Thesis directed by Professors Suzanne P. Anderson and Shemin Ge

Groundwater is critical in sustaining streamflow, especially in mountain catchments, because of its ability to supply baseflow in the absence of precipitation. In water-limited arid and semi-arid mountain environments, the need to characterize groundwater recharge and discharge has grown in tandem with demands to effectively manage current and future water resources. However, studying groundwater is challenging in complex terrain due to limited field measurements. Nearly a decade of monitoring data collection at Gordon Gulch in the Colorado Front Range provides a unique opportunity to study such an environment. The field data is used to parameterize and calibrate a groundwater flow model (MODFLOW-NWT). Model results reveal spatial and temporal patterns in groundwater recharge and discharge to the stream. Groundwater is recharged primarily by one to two recharge events each year, driven by spring snowmelt and rain. The majority of groundwater recharge occurs in upper Gordon Gulch and is stored in saprolite and weathered bedrock. Groundwater is discharged to the stream via long, deep flowpaths sourced from upper Gordon Gulch and short, shallow flowpaths from soil and saprolite in lower Gordon Gulch. Using Gordon Gulch as a case study, this model and data analysis contribute to a larger effort to understand and constrain the mechanisms driving groundwater recharge and groundwater-stream exchanges in semi-arid, montane environments.

ACKNOWLEDGEMENTS

I would like to thank my two incredible advisors, Suzanne Anderson and Shemin Ge, for their support throughout this project. This wonderful coupling of two advisors with very different subject matter expertise (Suzanne, a geomorphologist, and Shemin, a hydrogeologist) helped create a rich understanding of this catchment. I am incredibly grateful to Suzanne Anderson for her vast knowledge of Gordon Gulch and ability to contextualize the results of this project within the broader scope of the catchment. I am also incredibly grateful to Shemin Ge for her help troubleshooting MODFLOW and translating model terms. Thank you both for your endless guidance and patience throughout this process.

I would also like to thank Eric Small-Tilton for his efforts as the committee chair and helping shape the final version of this thesis.

Thank you to the Boulder Creek Critical Zone Observatory (BcCZO) and the field staff for all their work collecting the data and maintaining the databases; without their efforts. Without their efforts, I would not have had access to the vast Gordon Gulch dataset, which was a critical resource for this project.

I would also like to acknowledge the funding I received as I worked on this project. The BcCZO is funded under the National Science Foundation (NSF) grant (NSF-EAR-1331828). Thank you to Suzanne Anderson for funding my work in the form of a research assistantship.

Last but not least, thank you to my friends and family for your unwavering support.

Table of Contents

TABLES

FIGURES

1. INTRODUCTION

Groundwater discharge to headwater mountain streamflow is now recognized as a critical component of the hydrologic system. Studies recognizing and estimating mountain block recharge (MBR) have highlighted the importance of groundwater storage and discharge in mountain watersheds through the water balance method (Feth et al., 1966; Huntley, 1979), chloride mass balance (Anderholm, 2000; Maurer et al., 1997), and numerical modelling (Flint et al., 2001; Hibbs and Darling, 1995; Sanford et al., 2004). While snowmelt provides the majority of annual streamflow in mountain catchments (up to 80% of the total water budget, Caine, 1995), groundwater buffers streamflow supply in the absence of precipitation by discharging stored winter precipitation in the form of baseflow (Baraer et al., 2009; Carroll et al., 2018; Fujimoto et al., 2016; Gordon et al., 2015; Harrington et al., 2018; Saberi et al., 2019). In the Rocky Mountains, groundwater-derived baseflow can account for more than 75% of streamflow during dry conditions (Clow et al., 2003) and more than 60% during the early snowmelt season (Liu et al., 2004). This store and release process offers a mechanism for providing a reliable source to maintain streamflow, even during warmer and drier months, which often coincide with the highest environmental and anthropogenic demands (Markovich et al. 2019; Wilson and Guan, 2004). Somers and McKenzie (2020) summarized 26 studies on groundwater contributions to streamflow in a variety of high mountain catchments (from the Rocky Mountains to the Himalayas) and reported that groundwater contributes anywhere from 10% (Huth et al., 2004; Maurya et al., 2011) up to 100% (Harrington et al., 2018) of streamflow depending on the time of year and definition of baseflow.

Baseflow in mountain environments can be derived from both shallow and deep groundwater flow (Kosugi et al., 2008). Although early assumptions considered water that

infiltrated deep bedrock groundwater a lost component of the water budget, this deep groundwater has a prominent role in mountain water budgets. Deep groundwater recharge can be routed downstream, discharged to adjacent streams, driven deeper into bedrock groundwater, or recharge lower-lying aquifers (Caine et al., 2006; Duffy, 2004; Markovich et al., 2019; Wilson and Guann, 2004). Over the past twenty-five years, studies have identified substantial groundwater flow through bedrock through the use of numerical modelling (Frisbee et al., 2011; Gleeson et al., 2008), field experiments (Montgomery et al., 1997), tracers (Frazier et al., 2002; Liu et al., 2008; Noguchi et al., 1999; Liu et al., 2008; Anderson et al., 1997), soil temperature variations (Uchida et al., 2003), pore water pressure measurements (Kosugi et al., 2006), groundwater level measurements (Katsura et al., 2008), and noble gas, age, and temperature measurements (Manning and Caine, 2007). Studies have also identified bedrock groundwater contributions to streamflow through deep and slow discharge into soil layers adjacent to the stream channel (Anderson et al., 1997; Hattanji and Onda, 2004; McGlynn et al., 1999; Mulholland, 1993; Uchida et al., 2003), and in some cases, identified that deep groundwater contributes up to 50-95% of streamflow during low-flow conditions (Uchida et al., 2003).

The growing recognition of the importance of groundwater in the mountain water budget has highlighted the need to quantify groundwater in specific settings such as semi-arid, subalpine, and/or forested catchments. Semi-arid catchments increase groundwater storage during wet periods and release groundwater to sustain streamflow when precipitation is low; in this setting, studies have shown that groundwater contributions to streamflow can range from 19 to 31% annually (Cowie et al., 2017) and can range from 28% during snowmelt (Liu et al., 2004) to 50% from mid-July to September (Carroll et al., 2018). However, very few studies explicitly examine how groundwater interacts with the stream in mountain environments and even fewer

model these interactions. For the studies that have coupled groundwater-surface water models, the focus has been on a mountain-to-coast watershed scale (Foster and Allen, 2015), bedrock outflow (Voeckler et al., 2014), and responses to climate-driven recharge rates (Engdahl and Maxwell, 2015).

The limited number of studies on groundwater processes in mountain aquifers reflects some of the challenges in studying these systems.; e.g., mountain environments involve complex topography and geology, often lack data or instrumentation, require expensive and prohibitive monitoring of deep aquifer layers, and flow and transport systems are heterogeneous. All of these factors complicate the ability to create a regional flow model (Manning and Solomon, 2005). To reconcile these challenges, the community must develop approaches to study subsurface responses that rely on shallower measurements that can constrain deeper flow and transport (Tokunaga et al., 2019).

The nearly continuous, nine-year record of monitoring in Gordon Gulch provided a unique opportunity to study the interaction of groundwater and streamflow. Field measurements of groundwater elevation and stream discharge were used to constrain shallow and deep groundwater flow with the numerical groundwater flow model MODFLOW-NWT. This study seeks to identify spatio-temporal distributions of groundwater recharge and discharge to streamflow in a semi-arid, montane environment and uses Gordon Gulch as a case study. We rely on model results and the analysis of field data to gain insights on the following:

1. When and where is groundwater recharged in a semi-arid, montane, headwater catchment?
2. When and where does groundwater contribute to streamflow in a semi-arid, montane, headwater catchment?

2. STUDY AREA

Gordon Gulch is a small (2.6 km^2), semi-arid, montane, headwater catchment within the Colorado Front Range (**Figure 1**). The catchment (40.02°N, 105.48°W) is located approximately 30 km west of Boulder, Colorado, within the Boulder Creek watershed at an elevation of 2,500 to 2,700 meters above sea level. The catchment averages 580 mm of precipitation annually with a mean annual air temperature of 6.5°C, as summarized in **Table 1**. The catchment is divided into two sub-catchments, informally called upper and lower Gordon Gulch. The stream in Gordon Gulch is both ephemeral (upper Gordon Gulch) and perennial (lower Gordon Gulch).

Gordon Gulch is part of Boulder Creek Critical Zone Observatory (BcCZO), one of ten U.S National Science Foundation (NSF) research sites across the United States and Puerto Rico that examine climate, geology, vegetation, and watershed dynamics (White et al., 2015). As such, the catchment is instrumented with six groundwater monitoring wells (three with automated pressure transducers), two meteorological (MET) stations, two stream gauges, soil moisture sensors, time-lapse cameras, and snow depth poles (**Figure 1**). Additional data collection in the catchment includes weekly and monthly water sampling (e.g., Burns et al., 2016), airborne LiDAR (e.g., Harpold et al., 2014), and geophysical surveys (Befus et al., 2011; Leopold et al., 2013). These combined resources provide a wealth of data on the hydrology and climate of the Gordon Gulch and are utilized in the development of a groundwater flow model as part of this study.

Table 1. Climate summary of Gordon Gulch based on field measurements made at climate stations within the catchment (North-facing (NF)and South-facing (SF) MET stations) and nearby climate stations. The location of nearby climate stations and distance from Gordon Gulch are identified in the figure footnotes.

Parameter	Value	Climate Station	Period of Record
Mean annual temperature	6.5°C	NF and SF MET stations	2012 - 2020
Mean temperature, warmest month (July)	17.5°C		
Mean temperature, coldest month (February)	-3°C		
Temperature range over period of record	-23.7°C to 24.7°C		
Mean annual precipitation	580 mm	NADP CO94[a] station, NF MET and SF MET	
Mean annual precipitation as snow	59%[b] - 70%[c]	NADP CO94 station	2009 - 2011
Mean annual evapotranspiration	941 mm	B1 station	1987 - 2006
Mean annual wind speed	1.8 m/s	NF and SF MET stations	2012 - 2020

a. National Atmospheric Deposition Program (NADP) National Trends Network site CO94 is located 2 km southwest of Gordon Gulch at an elevation of 2,524 m.
b. Source: Cowie, 2010
c. Source: Anderson and Rock, 2020
d. B1 climate station, east of Niwot Ridge, Colorado at an elevation of 2591 m (Morse and Losleben, 2019)

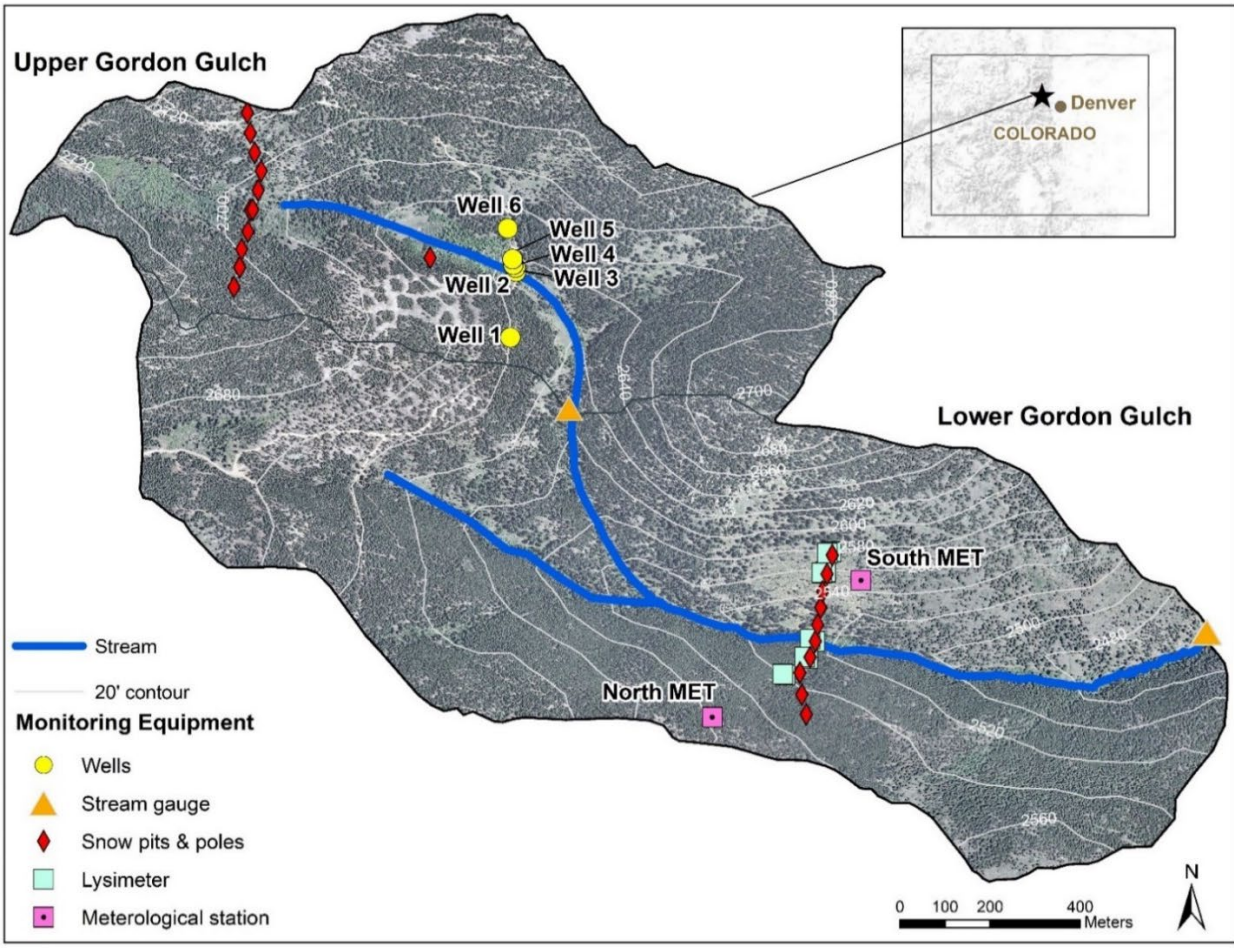

Figure 1. Gordon Gulch study area, located in the Colorado Front Range of the Rocky Mountains, USA. Selected instruments within the watershed are identified, including groundwater wells (wells 1, 2, and 6 are equipped with pressure transducers), stream gauges, meteorological (MET) stations, and snow poles. Site of snow pit digging is the solo red diamond near the transect of the wells. Inset: shaded relief map of Colorado; star locates Gordon Gulch.

2.1 Topography

Gordon Gulch is located between the steep topography of the crest of the Front Range and the western edge of the High Plains (Anderson et al., 2021). The catchment is in an area of rolling, low relief at an elevation below the extent of the Pleistocene glaciers but above the incised canyons (Aguirre et al., 2017; Anderson et al., 2006). Gordon Gulch is oriented approximately east to west, creating distinct north- and south-facing slopes. Slope aspect exerts control on weathering depths (Anderson et al., 2013; Anderson et al., 2014), snowpack depth and persistence (Langston et al., 2015), subsurface hydrology (Hinckley et al., 2014a), vegetation (Peet, 1981), and evapotranspiration rates (Barnard et al., 2017). On the north-facing slopes, vegetation is dense and populated by lodgepole pine (*Pinus contorta*); south-facing slopes are less vegetated and populated by shrubs, grasses and a scattering of ponderosa pine trees (*Pinus ponderosa*) (Adams et al., 2014) (**Figure 2**). South-facing slopes intercept a greater amount of solar, shortwave radiation than the north-facing slopes; at mid-winter, the south-facing slope receive 50% more radiation than a flat surface whereas the north-facing slope receives 50% less radiation (Anderson et al., 2021). Because the south-facing slope receive more solar radiation (Anderson et al., 2021), the snowpack is thin and experiences multiple cycles of snow accumulation and melt. Conversely, the north-facing slope retain a snowpack from the late fall through spring. On the north-facing slope, colder temperatures resulting from less solar radiation result in more pervasive frost (Rush et al., in press). In addition to greater thickness of weathered rock and saprolite on north-facing slopes (Befus et al., 2011), the saprolite is more porous and granulated than on south-facing slopes, where it is more intact and fractured (Bandler, 2016).

Figure 2. Photograph of north-and south-facing slopes in Gordon Gulch. The forest on the north-facing slope is a closed canopy of Lodgepole pine, while the forest on the south-facing slope is an open woodland composed of Ponderosa pine. Photo taken by Noah Hoffman, 2019.

Although slope aspect is not expressly addressed in this study, it is acknowledged that this may be a critical mechanism driving differences in groundwater recharge in the catchment (e.g., Hinckley et al., 2014; 2017). Differences in the annual precipitation, snow depth and duration, and evapotranspiration rates across the north- and south-facing slopes are apparent in field data and discussed in detail in Appendices B-E.

2.2 Geology

The bedrock underlying Gordon Gulch is Precambrian biotite gneiss, with minor granodiorite intrusions (Gable, 1996). We recognize four hydrogeologic units: soil, saprolite, weathered bedrock, and fresh bedrock (Anderson et al., 2007; Anderson et al., 2021). Weathered bedrock is fractured and moderately chemically altered bedrock (Anderson et al., 2007). Saprolite is defined as in-situ chemically weathered material that retains its original rock fabric and represents a transitional phase between bedrock and soil. Soils are sands and silty sands (Dethier et al., 2012; Hinckley et al., 2014a).

Depth of the weathering front (representing the base of weathered bedrock) averages 12 m in Gordon Gulch based on seismic refraction surveys (Befus et al., 2011), but varies

considerably (see Appendix A for a summary). Bedrock may be at the surface (~10% of the catchment is comprised of bedrock outcrops (or tors), Anderson et al., 2021), or up to 30 m deep (Dethier and Lazarus, 2006). The weathering front tends to be deeper on the north-facing slopes (10-15 m) than the south-facing slopes (5-10 m), resulting in different thicknesses of saprolite and weathered bedrock across the two aspects (Befus et al., 2011) (**Figure 3**). Soil is uniformly 0.4±0.2 m on both aspects, not including tors (Anderson et al., 2021).

Groundwater is unconfined in the soil, saprolite, and weathered bedrock and within fractured bedrock (Henning, 2016). Hydraulic conductivity varies greatly across these hydrogeologic units, which exerts control over groundwater flow. Based on field measurements and literature reviews, soil has the highest hydraulic conductivity and bedrock has the lowest (see Appendix A). Fractures in the weathered bedrock and bedrock act as channels for groundwater (Pandey and Rajaram, 2016). The differences in the hydraulic conductivity and layer thickness are believed to result in different rates of recharge, hydraulic gradients, fracture vs. matrix flow, and water table elevations across the north-and south-facing slopes (Bandler, 2016; Henning, 2016; Bandler, 2016).

3. DATA AND METHODS

3.1 Data

A groundwater-specific version of the water budget guided the data analysis process. This groundwater-specific budget is referred to as the groundwater budget of Gordon Gulch. The groundwater budget was modified from a catchment-scale water budget, which includes processes both above and below the water table. The catchment-scale water budget for a headwater catchment is:

$$P - ET_c - \Delta Q_C = \Delta S_c = 0 \quad (1)$$

where the subscript c denotes that the term is catchment-scale and includes surface and subsurface processes, P is total precipitation, ET_c is the total evapotranspiration (sum of evaporative losses from surface and soil waters and plant transpiration), ΔQ_c is streamflow out of the catchment, and ΔS_c is the change in water storage (**Figure 3**). If the system is in equilibrium, there are no changes in storage ($\Delta S_c = 0$).

To assess the processes occurring at and below the water table, the groundwater budget was extracted from the catchment-scale water budget, as follows (modified from King, 2011; Scanlon et al., 2002):

$$R - ET \pm \Delta Q = \Delta S \quad (2)$$

where R is recharge (the fraction of precipitation that reaches the groundwater table), ET is evapotranspiration water from the saturated zone, ΔQ is net groundwater-stream exchanges (defined as the difference between groundwater losses to streamflow (Q_{out}) and groundwater gains from stream leakage to the aquifer (Q_{in})), and ΔS is the change in groundwater storage in the saturated zone (**Figure 3**) (King, 2011; Scanlon et al., 2002).

Data collected in Gordon Gulch from 2011 through 2020 were used for the development and calibration of a groundwater flow model and to calculate the catchment-scale water budget (**Figure 4**). When data gaps occurred, data from nearby sites were used. Data were processed and analyzed by water year (defined as October 1 through September 30) to identify seasonal, annual, and interannual trends (**Figure 5**).

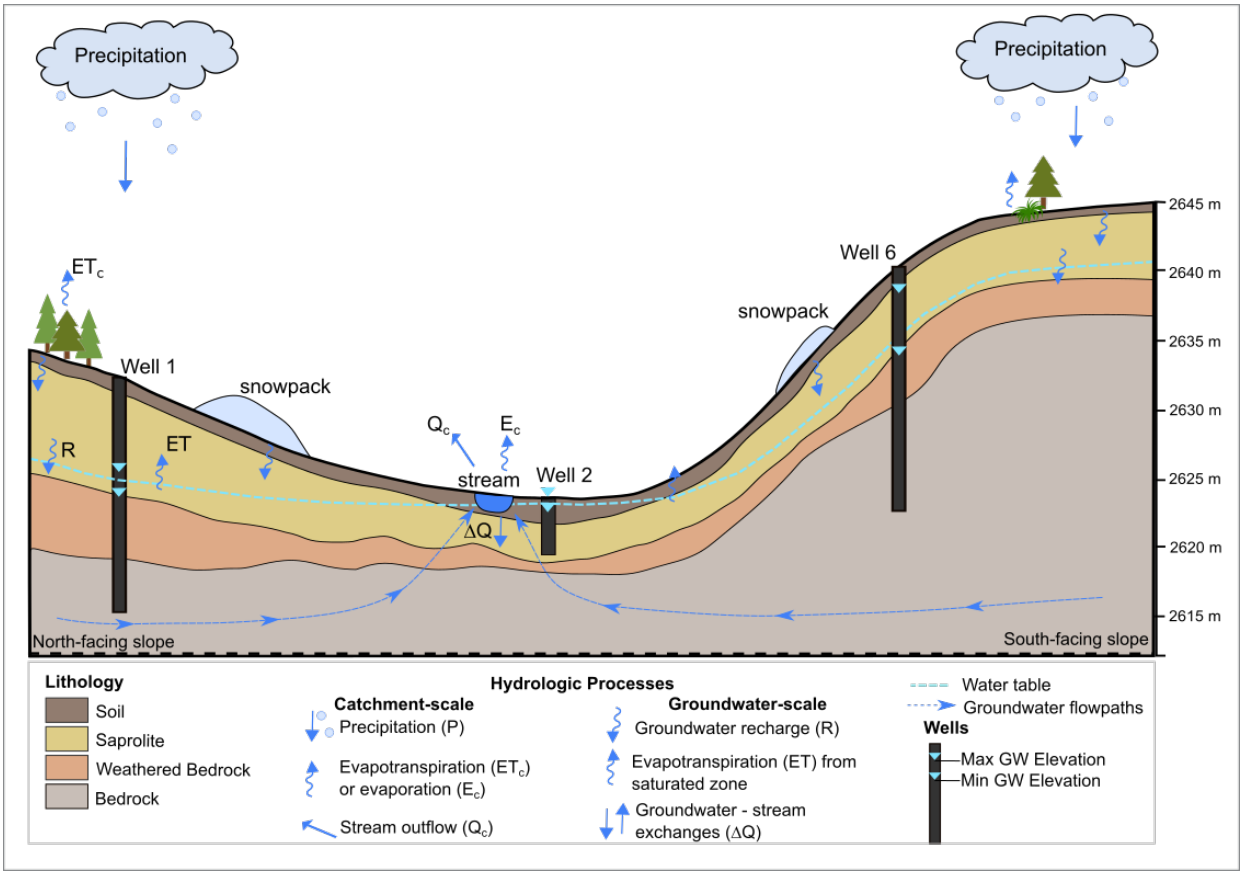

Figure 3. Conceptual model of Gordon Gulch. This figure presents a cross-sectional view of the catchment, identifying the four primary geologic layers and the sources and sinks of in the mountain water budget. Minimum and maximum recorded water table measurements for the three monitoring wells are identified, along with the average depth of the water table. Geologic layers are interpreted from well drilling logs and seismic refraction studies (Anderson and Ragar, 2021d; Befus et al., 2011; Bandler, 2016).

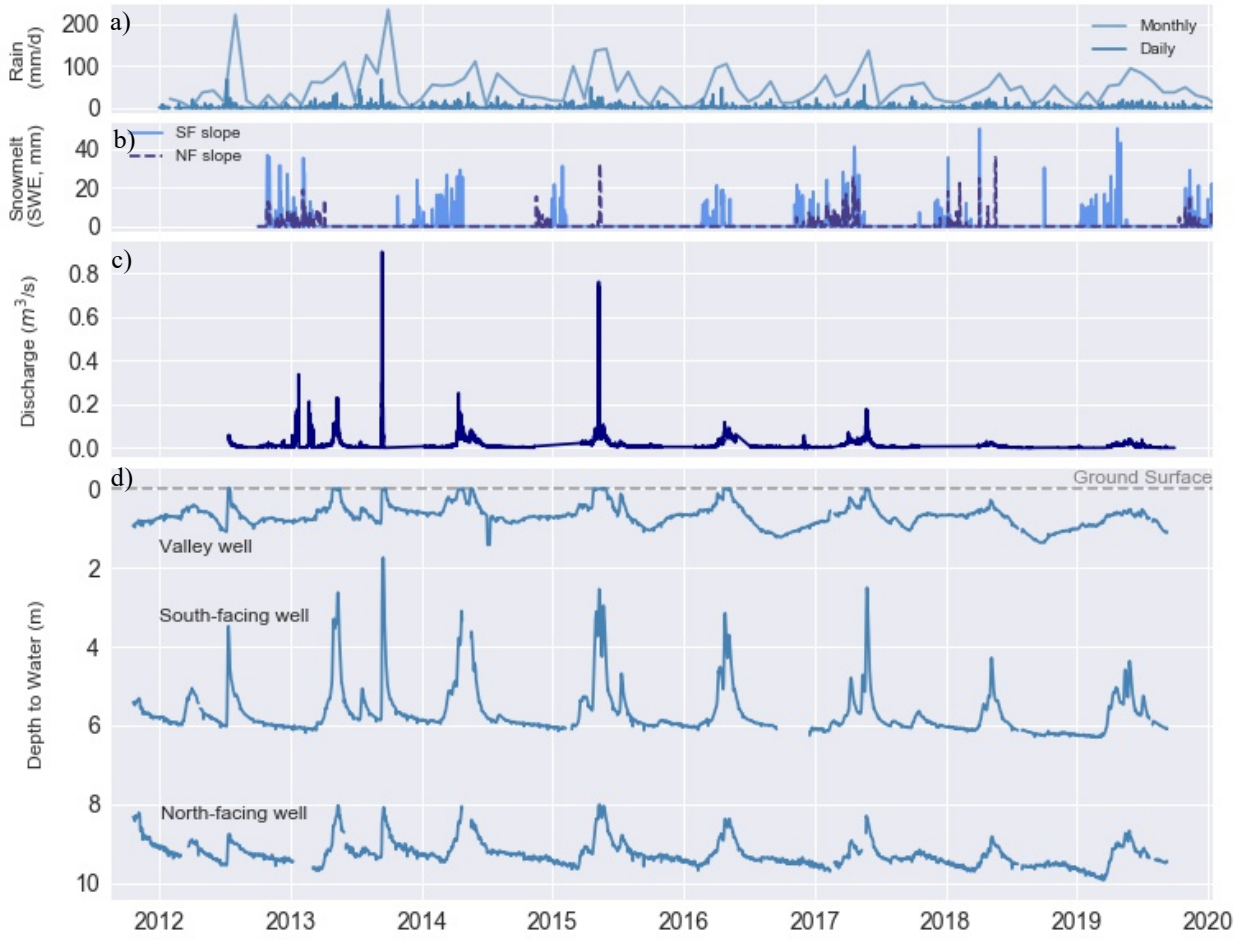

Figure 4. Time series of data from Gordon Gulch for water years 2012 to 2019. a) daily and total monthly rainfall, b) daily snowmelt (as SWE) on the north-facing (NF) and south-facing (SF) slopes, c) stream discharge in lower Gordon Gulch, and d) depth to water table at the valley well (2), south-facing well (6), and north-facing well (1).

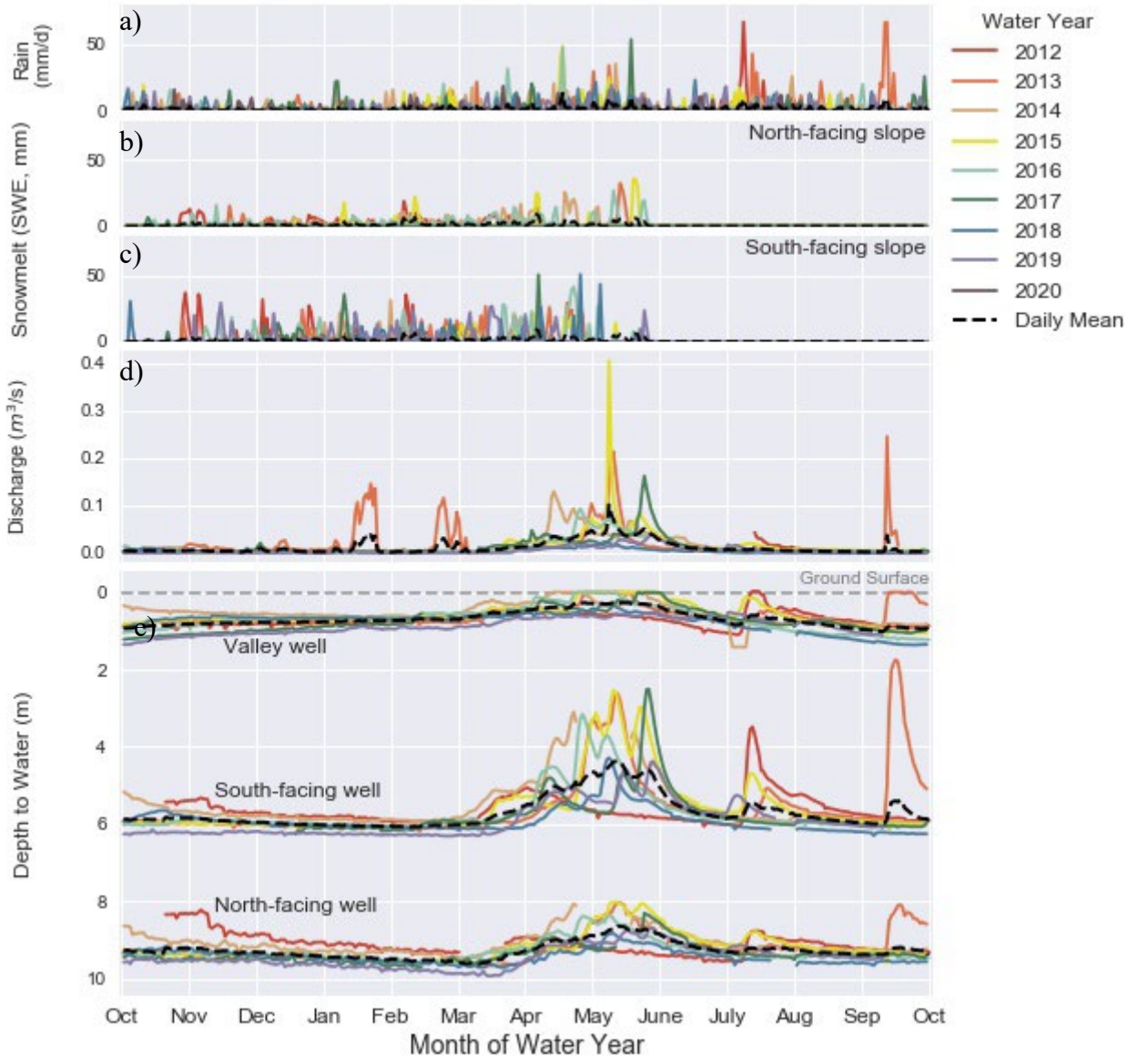

Figure 5. Daily values for individual water years (colored lines) and the average water year based on daily mean values (black dashed line) for data in Gordon Gulch from 2012 to 2019. a) rain, b) snow depth on the south-facing slope, c) snow depth on the north-facing slope, d) stream discharge, and e) depth to the water table for the valley well (well 2), south-facing well (well 6), and north-facing well (well 1).

3.1.1 Precipitation

Precipitation measurements were recorded at three meteorological stations. Two stations, the north-facing (NF) and south-facing (SF) meteorological (MET) stations, are located within Gordon Gulch and recorded daily precipitation in an unheated tipping bucket at 10-minute intervals from 2012 to 2020 (Anderson and Ragar, 2021a; Anderson and Ragar, 2021b). NF MET station is located under canopy on a north-facing slope while SF MET station is located in the open on a south-facing slope. The third station, National Atmospheric Deposition Program (NADP) National Trends Network site CO94, is a heated tipping bucket located approximately 2 km southwest of Gordon Gulch at an elevation of 2,524 m. CO94 has collected daily precipitation measurements since 1986, but data available and used in this study was from 2011 to 2017. None of the stations had a complete precipitation record. Therefore, a ranked, gap-fill procedure was performed to create a complete daily precipitation record for water years 2012 – 2020, with precipitation records from CO94 ranked highest and records from the NF MET station ranked lowest (see Appendix B). None of the stations accounted for undercatch or vegetation interception; we assumed these processes to have a minimal impact on the overall record and did not adjust the data to account for them.

Average annual precipitation in Gordon Gulch ranged from 415 mm to 836 mm, with a mean value of 580 mm. April, May, and July were the wettest months of the year, accounting for approximately 42% of the annual precipitation (**Figure 3a** and **Figure 4a**). July was the most variable month (outside of the exceptional September event in 2013; Gochis et al., 2015), with mean monthly precipitation ranging from 29 mm to 214 mm. The winter months (November through January) were the driest, contributing only 12% to the total precipitation.

3.1.2 Snowmelt

As snow melts, the water becomes available for evaporation, runoff, and/or infiltration. We used changes in snow depth (ignoring compaction) and average snow density to compute snowmelt. Snow depth was visually estimated by reviewing 10-minute time-lapse imagery, when available, from two cameras in Gordon Gulch for water years 2012 – 2019 (Anderson and Ragar, 2021c). These cameras are aimed at snow poles on the north- and south-facing slopes, so the depth of the snow can be visually estimated using the markers on the snow poles as a guide. There were significant gaps in the snow depth images; the camera on the north-facing slope lacked consistent wintertime imagery in 2013, 2015, and 2018. Peak snow depths recorded up to 0.80 m on the north-facing slopes (water year 2012) and 0.76 m on the south-facing slopes (water year 2016) (**Figure 3b** and **Figure 4b, c**).

Average snow density in Gordon Gulch was calculated from measurements made in snow pits dug on 16 dates between 2008 and 2017 (Anderson and Rock, 2020). Pits were sited in the same general area in upper Gordon Gulch; a snow cutter was used to measure density at 10 cm increments through the full snow depth. On average, snow density was 264 kg/m^3 but ranged from 214 to 323 kg/m^3.

Snow melt, as snow water equivalent (SWE), was calculated by multiplying negative changes in daily snow depth by the ratio of average snow density to the density of liquid water. Average annual SWE was approximately 254 mm per water year and ranged from 170 to 320 mm (**Table 2**). The majority of snowmelt occurred in April, and 54% of total annual snowmelt occurred between February through April. The SWE estimate procedure and a more detailed analysis of findings are described in Appendix C.

Table 2. Total annual snowmelt, as SWE for Gordon Gulch for water years 2012 – 2019. The percentage of total annual precipitation as snow represents snowmelt as a fraction of total annual precipitation.

Water year	Total annual snowmelt (SWE, mm)	% of precipitation as snow
2012	208	39
2013	310	37
2014	320	56
2015	270	42
2016	202	43
2017	290	50
2018	170	41
2019[a]	259	47
Mean	254	44
SD	51	6

a. Incomplete year, so total annual snowmelt was estimated using by multiplying total annual precipitation by the average annual percent of precipitation as snow.

3.1.3 Groundwater Levels

Six groundwater monitoring wells, located in upper Gordon Gulch (**Figure 1**), were drilled and completed during the winter of 2010-2011 (Anderson and Ragar, 2021e; Anderson and Ragar, 2021f; Anderson and Ragar, 2021g). Three of the wells (wells 1, 2, and 6) are equipped with pressure transducers to measure water table position at ten-minute intervals (Anderson and Ragar, 2021d). The steps to convert raw pressure measurements to water table depth are described in Appendix E. Well construction details for all six wells are presented in **Table 3**, a cross-section is presented in **Figure 3**, and well characteristics for the three active monitoring wells are summarized below:

North-facing well (well 1) is located on the north-facing slope side of a broad divide between upper and lower Gordon Gulch. It is the deepest well, drilled to a total depth of 18.55 m. The well is screened from 9.41 m to 18.55 m, an interval that includes saprolite, weathered bedrock, and bedrock (Anderson and Ragar, 2021e).

Valley well (well 2) is located in the valley bottom, approximately five meters north of the perennial stream. Well 2 is approximately 4 m deep and screened exclusively in soil and saprolite (Anderson and Ragar, 2021f).

South-facing well (well 6) is located on the south-facing slope of upper Gordon Gulch and is drilled to a total depth of 17.34 m. Well 6 is screened from 8.20 m to 17.34 m, an interval that includes weathered bedrock and bedrock (Anderson and Ragar, 2021g). Bedrock is encountered at a much shallower depth in well 6 than well 1 (7.6 m and 14.6 m, respectively).

Depth to water measurements were made at the three monitoring wells during water years 2012 – 2019 (see **Figure 3d** and **Figure 4e**). The groundwater table mimics topography with deeper groundwater on the hillslopes (wells 1 and 6) and shallower groundwater in the valley floor (well 2). On average, depth to water ranged from 0.68 m (well 2) to 5.70 m (well 6) to 9.27 m (well 1), as shown in **Table 3**. Peak groundwater elevations occurred in the spring (peak dates ranging from April 14 through May 29), following spring rain and snowmelt, and generally decreased throughout the summer, with the exception of summer rainstorms. During a typical water year, the valley well was first to peak, occurring on average on May 8 (**Table 4**). The south-facing well peaks a few days later, followed by the north-facing well approximately five days after the peak in the valley well. The lowest groundwater elevations typically occurred in early spring for the deeper wells, ranging from March 18 (north-facing well) to April 18 (south-facing well), while the shallow valley well experienced its annual low in mid-September. Throughout the water year, groundwater elevations fluctuated by approximately 1.8 m but ranged from 0.8 m (at the valley well in 2019) up to 4.5 m (at the south-facing well in 2013).

Table 3. Well construction parameters for the monitoring wells in Gordon Gulch. The total depth, depth to first water, screened interval, and depth to bedrock were recorded during drilling in the winter of 2010-2011.

Well ID	Elevation of well top (m)	Well depth (m)	Screened interval (m)	Average depth to water table (m)	Weathering description	Position in catchment
Well 1	2633	18.55	9.41 – 18.55	9.27	Tan/brown weathering to 12.2 m; gray weathered rock to 14.60 m; unweathered below	North-facing slope
Well 2	2623	4.45	1.41 – 4.45	0.68	Brown "loamy" material to 4.45 m[c]	Riparian / catchment valley
Well 3	2624	4.48	1.44 – 4.48	-		
Well 4	2625	4.53	1.49 – 4.53	1.90[c]		South-facing slope
Well 5	2627	6.30	0 – 6.30	-		
Well 6	2643	17.34	8.20 – 17.34	5.70	Slow drilling; unweathered bedrock at 7.60 m[d]	

a. Based on depth to water measurements from 2011 to 2019.
b. Anderson and Ragar, 2021e
c. Anderson and Ragar, 2021f
d. Anderson and Ragar, 2021g

Table 4. Summary of water table behavior for water years 2012 - 2019. The fluctuation of the water table is defined as the difference between the maximum and minimum groundwater elevation. The average dates of minimum and maximum depth to water (DTW) measurements identify when DTW is highest and lowest throughout the water year. Minimum DTW measurements identify when the peak in the water table occurs, typically following recharge, whereas maximum DTW measurements identify when the water table is deepest.

Parameters	North-facing well (well 1)	Valley well (well 2)	South-facing well (well 6)
Depth to water (m) mean (min - max)	9.3 (8.0 – 9.9)	0.7 (0 – 1.4)	5.7 (1.7 – 6.3)
Average annual water table fluctuation (m)	1.4	1.1	3.0
Average date of minimum DTW	May 13	May 8	May 11
Average date of maximum DTW	March 18	September 14	April 18
Average number of days per water year of water level rise	180	197	195
Average number of days per water year of water level decline	159	158	145

3.1.4 Streamflow

The unnamed stream in Gordon Gulch is ephemeral in upper Gordon Gulch and perennial in lower Gordon Gulch. Flow is intermittent in some segments of the channel during summer (Martin et al., 2021). The overall stream gradient is approximately 0.026, but the channel is steeper in the north-south oriented reach between the upper and lower basins. There are two stream gages in Gordon Gulch; one at the top of the steep reach between upper and lower

Gordon Gulch and one at the downstream end of lower Gordon Gulch (**Figure 1**). Stage measurements were recorded at 10-minute intervals using pressure transducers (Anderson and Ragar, 2021h). Streamflow for the lower gauge is computed using a stage-discharge rating curve derived from the automatic stage and manual discharge measurements made by salt dilution. Because of challenges imposed by snow and ice, and very low discharge in winter, streamflow data is unavailable from approximately November to April each year (dates vary). Streamflow from the lower gauge is exclusively used as part of this study because of its location at the catchment outlet which represents streamflow moving downstream, out of Gordon Gulch.

Streamflow statistics for water years 2012 – 2019 are shown in **Table 5**. Stream discharge averages 0.013 m^3/s. There are three distinct seasonal streamflow regimes in Gordon Gulch; low-flow period from August through March, a period of peak streamflow associated with spring snowmelt and rain (April through May), and a period of streamflow recession in the summer (June and July) (see **Figure 3c** and **Figure 4d**). During the low-flow period streamflow averages 0.0064 m^3/s. Peak streamflow averages 0.037 m^3/s, while streamflow during the recession period ranges from 0.0004 to 0.05 m^3/s. The highest discharge peak monitored occurred on May 9, 2015, where streamflow measured 0.41 m^3/s and remained above 0.10 m^3/s through May 11, 2015. A much larger flow on Sept. 13, 2013 destroyed the gage during an exceptional storm that hit the Front Range (Gochis et al., 2015); peak flow was estimated at 3-5 m^3/s from a post-flow analysis using Manning's equation and measured channel cross section (Brenner et al., 2014).

From 2012 – 2019, peak spring streamflow in most years occurred between mid-April and late May. In 2012, absence of spring rain prevented a spring peak. That year, a series of heavy summer monsoon storms produced peak flow in July that was comparable to typical

spring peaks. In 2013, the flood in the September storm surpassed the spring discharge peak. Spring peaks in streamflow are attributed to sustained melt of the snowpack on the north-facing slopes in April and May augmented by rain and rapidly melted spring snowfall. The late-spring snowmelt results in a hydrograph with a steep rising limb and a falling limb that lasts from summer through early fall. However, as 2012 illustrates, rapid increases in stream discharge can occur during the summer due to heavy rainfall events. Over the study period, three summer rainstorms were large enough to show up in the streamflow record; July 2012, September 2013, and July 2015. Cowie (2010) identified that no significant increases in discharge occur after the summer monsoon season (mid-July to September)*, suggesting* that the water table may remain elevated enough and keep the unsaturated zone moisture levels high enough to push soil water out of the aquifer and into the stream channel during summer rain events during June and July (Cowie, 2010).

Table 5. Stream and streamflow statistics for Gordon Gulch calculated from data measured during water years 2012 through 2019.

Parameter	Value
Elevation of stream gauge (m amsl)	2435.75
Average stream gradient (m/m)	0.026
Mean annual discharge (m^3/s)	0.013
Mean annual low-flow (m^3/s) (August – March)	0.00064
Mean annual recession flows (m^3/s) (June – July)	0.0097
Mean annual maximum discharge (m^3/s) (April – May)	0.1425
Range of mean annual maximum discharge (m^3/s)	0.023 - 5
Mean date of annual maximum discharge	May 8
Range of date of annual maximum discharge	April 13 - September 12

3.2 Groundwater Flow Model

A catchment-scale model was developed for Gordon Gulch using MODFLOW NWT with ModelMuse as a graphical user interface. MODFLOW is a three-dimensional, finite-difference numerical model used to solve equations of groundwater flow (Harbaugh, 2005). MODFLOW-NWT is the Newton-Raphson formulation of MODFLOW-2005, which applies a smoothed continuous function of groundwater heads to rewet unconfined cells that have run dry, ensuring that these cells remain active (Niswonger et al., 2011). MODFLOW-NWT is better suited to model unconfined aquifer conditions, like headwater catchments such as Gordon Gulch. MODFLOW-NWT calculates head at the center of each model cell and groundwater flow at the interface of adjoined cells (Harbaugh, 2005; Niswonger et al., 2011).

Inflows and outflows to the modeled aquifer system are based on the groundwater budget (Eq. 2). Inflows include groundwater recharge from precipitation and SWE and stream leakage to the aquifer. Outflows include groundwater seepage to the stream and evapotranspiration of groundwater.

3.2.1 Development of a Groundwater Flow Model

The three-dimensional groundwater flow model domain was delineated by the catchment boundaries of Gordon Gulch (**Figure 6**). The model topography was defined by a 20 m digital elevation model (DEM) derived from a 1 m digital surface model (DSM) from airborne LiDAR collected in August 2010 (Anderson et al., 2012). The four primary hydrogeologic units (soil, saprolite, weathered bedrock, and bedrock) were discretized into 13 model layers. In total, the model domain extends 75 m below the surface and model layers range from 1 m to 30 m in thickness, as summarized in **Table 6**. Hydrogeologic unit thicknesses were estimated using a literature review, soil pits, and well logs (see Appendix A), and are treated as homogenous in the

model. Initial values of hydraulic conductivity were based on field measurements, including double-ring infiltrometer tests in soil (Buraas, 2009), slug tests in saprolite and weathered bedrock (Henning, 2016), lab measurements on field samples (Hinckley et al., 2014a), and on literature values for similar rock types (see Appendix A). The model is unconfined to a depth of 11 m, representing the base of the saprolite.

Table 6. Hydraulic parameters and calibrated values for the hydrogeologic units and associated model layers used in the MODFLOW-NWT model.

Hydrogeologic unit	Unit discretization (# of model layers)	Aquifer type	Cited range of K (m/d)	Selected value of K (m/d)	Model layer thickness (m)
Soil	1	Unconfined	0.2 – 20.7	16	1
Saprolite	5		0.006 – 3.5	0.17 - 0.57	10
Weathered Bedrock	3	Confined	0.032 – 17.3	0.01	5
Bedrock	4		0.00009 – 2	0.000032	59
Streambed	-	-	-	7.6	0.75

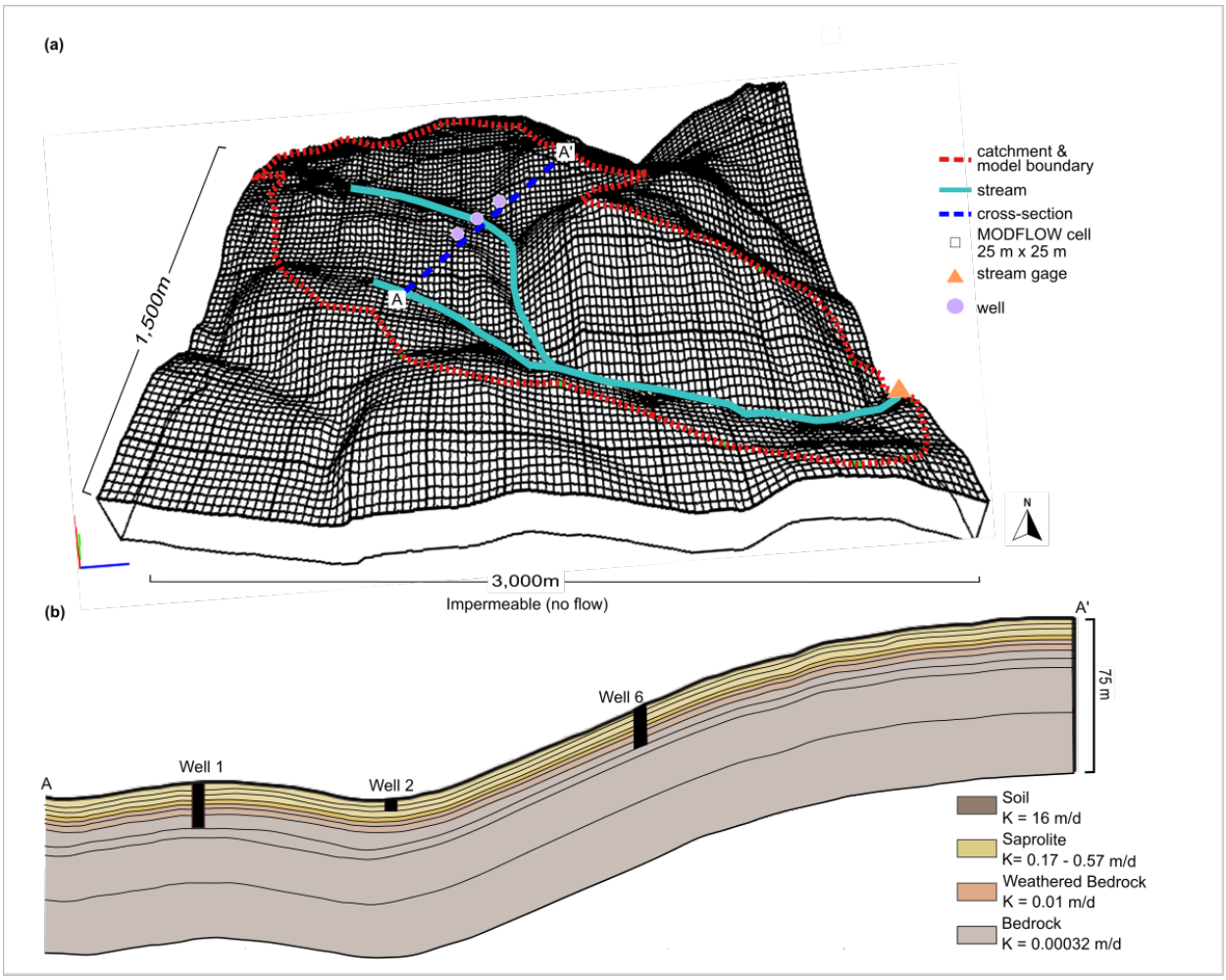

Figure 6. Model geometry and cross-section of Gordon Gulch used in MODFLOW-NWT. (a) 3-dimensional perspective view of the model domain, showing channel, locations of groundwater wells and stream gauge, and 25 x 25 m MODFLOW grid cells. (b) Cross-section of the model domain from A to A' identifying the13 model layers used to discretize the four primary hydrogeologic units in the catchment.

The model is approximately 2700 m by 1930 m, capturing the entire 2.6 km^2 area of Gordon Gulch (**Figure 6**). The model is discretized to 25 m by 25 m cells. There are 77 rows and 108 columns and 13 layers of these cells for a total of 15,246 active cells. The base of the groundwater flow model represents low-permeability bedrock and is defined by a no-flow Neumann boundary. The catchment boundaries are topographic highs (inferred to act as groundwater divides) are also defined by no-flow boundaries. Five constant head cells (four on the model boundary and one at an internal topographic high) were assigned to maintain topographic control on the head values at these locations.

MODFLOW's streamflow-routing (SFR) package was assigned to the stream in Gordon Gulch to simulate exchanges between groundwater and surface water and to route streamflow through the model domain. The SFR package calculates fluxes between groundwater and the stream (Prudic et al., 2004) based on head values and the hydraulic gradient between them during each time step, using Darcy's law. The stream was assigned a stage of 0.10 m across the span of the channel (representing a spring discharge levels), a stream width of 0.25 m, a stream gradient of 0.026, and streambed thickness of 0.75 m. The streambed conductance was initially set to 2 m/d and adjusted during the calibration process. A model gauge was assigned at the outlet of the lower reach (aligned with the true location) to report modeled baseflow moving out of the catchment (see **Figure 1** and **Figure 6**).

MODFLOW recharge (RCH) and evapotranspiration (ET) packages were applied to simulate inputs and outputs to the aquifer system. Recharge is defined as the total water available to enter the subsurface, which includes rainfall and snowmelt as SWE. Recharge and ET rates were assigned to the model top across the entire model domain. ET was assigned an extinction depth of 5 m. Recharge rates in the model vary monthly and were based on mean daily rates

calculated using data from water years 2012 to 2019. ET rates were initially based off a literature review for values of ET at sites with similar elevations and/or vegetation communities to Gordon Gulch (Appendix D), but rates were ultimately used as a fitting parameter during model calibration.

3.2.2 Model Calibration

Estimating Baseflow for Model Calibration

Baseflow is the portion of streamflow that comes from groundwater storage and is often used interchangeably with the term groundwater discharge (Hall, 1968). Baseflow was estimated by applying the Eckhardt digital filter to measured stream discharge from lower Gordon Gulch for water years 2012 - 2019. The Eckhardt method uses a two-parameter recursive digital filter (RDF) to parse hydrographs into two components: direct runoff and baseflow (Eckhardt, 2005). High-frequency discharge variations are assumed to be direct runoff derived from surface runoff and interflow, while low-frequency discharge variations are considered baseflow derived from stored groundwater (Eckhardt, 2005). The USGS Groundwater Toolbox was employed to estimate baseflow using the Eckhardt two-parameter method (Barlow et al., 2017; Eckhardt, 2005). Appendix F describes the baseflow separation process in more detail.

Steady State initial condition and transient model calibration

MODFLOW was run in steady state to set initial background conditions for transient model runs. Initially, the steady state run was done using long-term mean annual recharge (precipitation and snowmelt), but the monthly fluctuations of these values created mean values higher than values typical of the fall (October, the start of the water year). Instead, recharge values for the steady state run were derived from average values for the months of July, August, and September, i.e., recession conditions at the end of the water year. Steady-state head values

derived from the steady-state run were then used as initial conditions to simulate transient conditions.

After establishing initial conditions, a ten-year transient simulation was run, driven by measured climate parameters (precipitation and snowmelt) for water years 2012-2019. Stress periods identify changes in aquifer 'stresses' like monthly fluctuations in evapotranspiration or recharge rate, and stresses are held constant until the subsequent period where they can change. A total of 140 stress periods were run in the transient simulation. Each stress period represented monthly rates of ET and recharge, except for May, which was broken into three separate stress periods to account for high rates of recharge during the middle of the month. Stress periods were discretized into three-day time steps.

The transient model was calibrated using mean daily groundwater levels recorded at the north-facing well and south-facing well (the wells on hillslopes that accessed groundwater in weathered rock) and mean estimated baseflow. A typical water year profile of the groundwater table was created from the 2012-2019 monitoring data by computing the average daily depth to water (DTW) at wells 1 and 6 for each day of the year (**Figure 7a, b**); the resulting annual behavior was used as calibration targets for modeled head. The same process was applied to baseflow estimates; the average value for each day across water years 2012 to 2019 was computed to create a typical water year history of baseflow (**Figure 8a**), and used as a calibration target for modeled baseflow. During calibration, values of recharge, ET, and hydraulic conductivity of the model layers were adjusted through trial-and-error until simulated seasonal patterns of baseflow and groundwater elevation produced a good visual match to observed patterns and values. Calibrated hydraulic conductivity values (**Table 6**) were comparable to previously cited values for similar rock types (Appendix A).

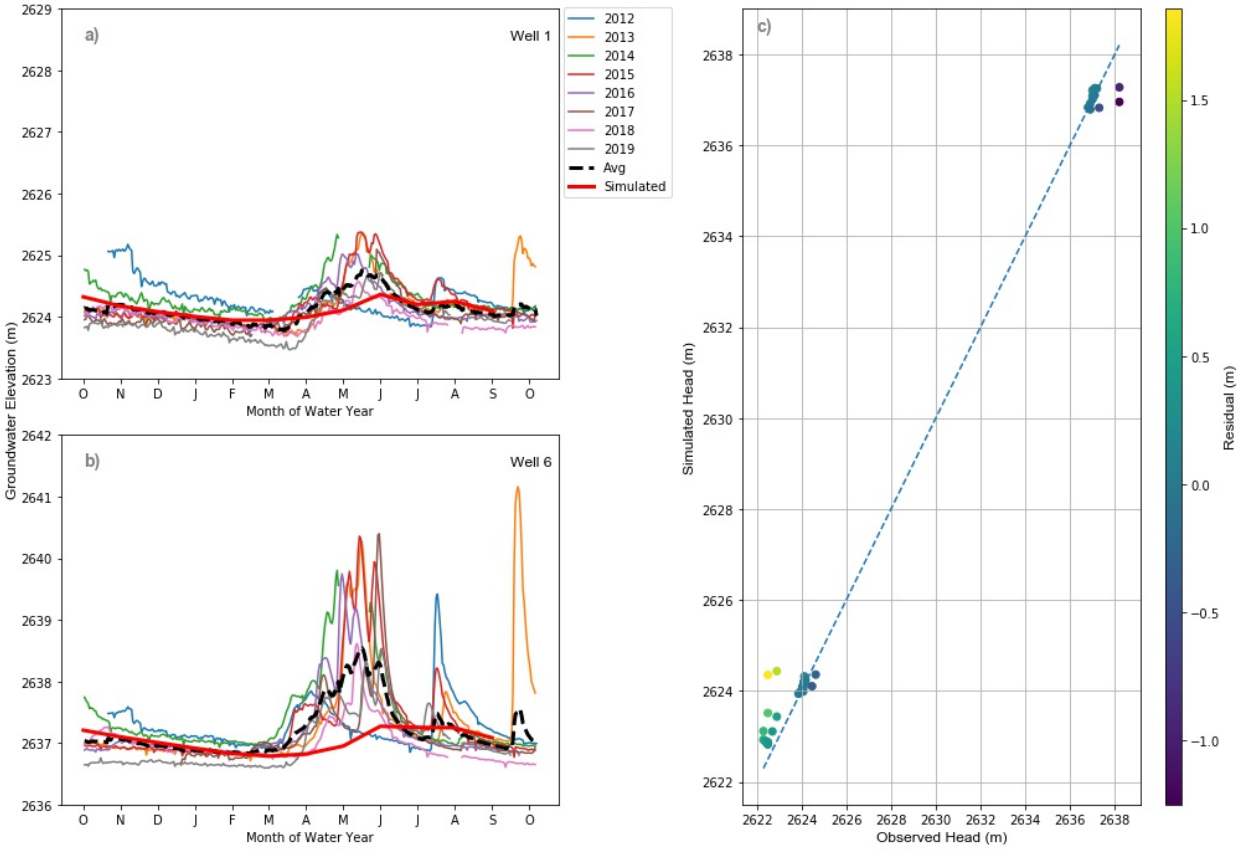

Figure 7. Observed vs. simulated groundwater head values for wells 1 and 6. (a) Well 1 simulated head for an average water year (red line), average daily observed head (black dashed line), and observed head values measured for each water year 2012 – 2019 (colored lines); (b) Well 6 simulated head for an average water year (red line), average daily observed head (black dashed line), and observed head values measured for each water year 2012 – 2019 (colored lines); (c) scatter plot of residuals calculated from simulated and observed groundwater head values at wells 1 and 6. Observed head values plotted are the mean daily measurements calculated from water years 2012-2019 for wells 1 and 6.

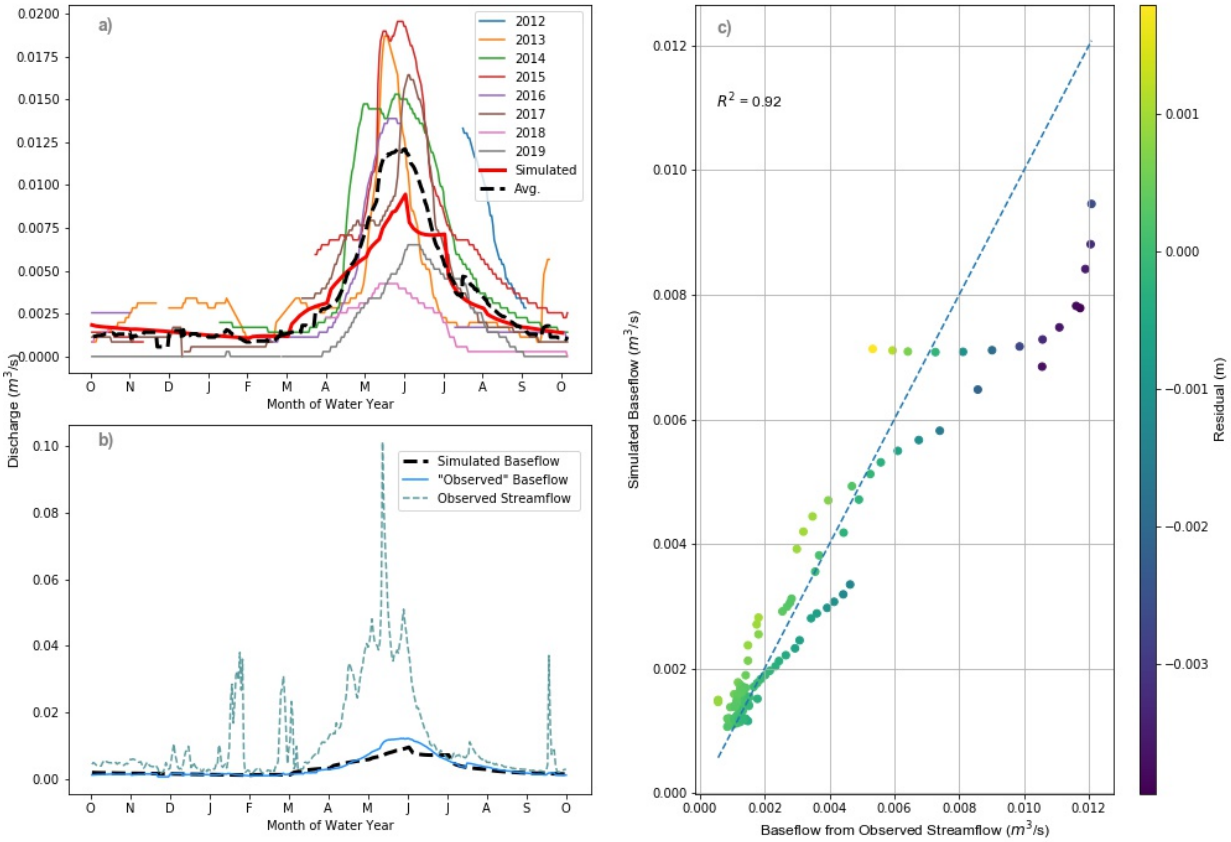

Figure 8. "Observed" vs. simulated baseflow values. "Observed" values of baseflow are estimated from measured values of streamflow, as described in Section 3.2.2 (a) Simulated baseflow values for an average water year (black dashed line) and observed baseflow values from measured streamflow recorded for water years 2012 – 2019 (colored lines); (b) Simulated baseflow (black dashed line), average daily baseflow estimated from streamflow (solid blue line), and average daily streamflow values (blue dashed line) repeated over a three-year simulation period. The average daily streamflow values were calculated from mean daily measurements across the eight water years of data from water years 2012 – 2019; (c) scatter plot of residuals calculated from simulated and observed baseflow, along with the reported R^2 value. Observed baseflow values plotted are the mean daily measurements calculated from water years 2012-2019.

Calibrated model results show good agreement between simulated and observed groundwater head (**Figure 7**) and baseflow (Figure 8). Notably, the model underestimates values of both baseflow and head in the spring. This pattern is most pronounced in the south-facing well. Although modeled values of head and baseflow don't quite capture the magnitude of the spring peak, modeled values closely match observed values for the rest of the simulated water year. Additionally, by plotting modeled values of baseflow and head over the water years of observed data (as done in **Figure 7a, b** and **Figure 8a**), it was apparent that model results fall within reasonable bounds of observed values.

R^2 values were calculated for simulated and observed values of head and baseflow as a first order assessment of the correlation between the modeled values and the field data. The R^2 value for baseflow was 0.92, indicating a strong correlation between the modeled and observed values (**Figure 8**c). The mean absolute error was 0.0007 m^3/s. R^2 values for simulated and observed heads were lower than baseflow; R^2 of 0.50 at the north-facing (well 1) and R^2 of 0.10 at the south-facing well (well 6). For the north-facing well, the R^2 value indicates there is a moderate correlation between observed and modeled head values; the R^2 value for the south-facing slope indicates the correlation between the two data sets is weak. Values of the mean absolute error further corroborate this difference. The mean absolute error for the north-facing well was 0.10 m and 0.28 m for the south-facing well. The springtime elevation in head is lagged at the south-facing well, offering explanation (in addition to underestimated spring values) as to why the correlation between the observed and modeled data is weaker at the south-facing well than the north-facing well.

During model calibration it was found that baseflow was more sensitive to recharge and ET rates than groundwater elevations, since baseflow is closer to the surface than the

groundwater levels and most influenced by these rates applied directly to the surface. Groundwater elevations were most sensitive to values of hydraulic conductivity.

The distribution of groundwater head from the final time step of the calibrated transient model was plotted to ensure the model produced reasonable results (**Figure 9**). Groundwater contours indicate that groundwater is driven by topography, flowing from high to low elevations in the catchment.

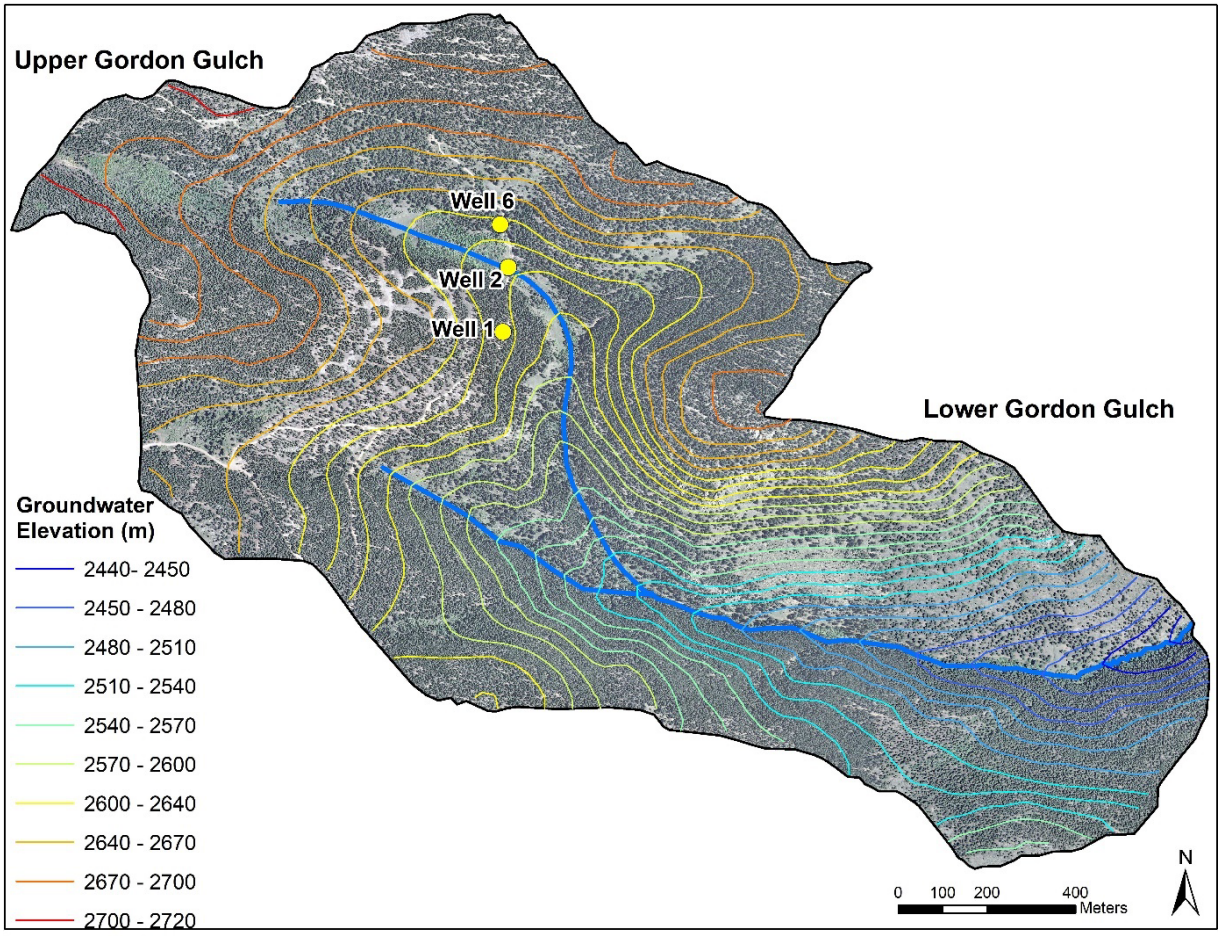

Figure 9. Modeled distribution of groundwater elevation in Gordon Gulch.

Groundwater Flowpath Tracking

To examine groundwater flowpaths, advective transport was simulated during the ten-year transient period using the forward particle tracking method in MODPATH. MODPATH is a MODFLOW post-processor that uses the distribution of head to calculate velocity and trace particle flowpaths (Pollock, 2012). Particles were placed in upstream locations and tracked to reveal groundwater flowpaths in soil, saprolite, weathered bedrock, and bedrock.

4. RESULTS

4.1 Catchment-Scale Water and Groundwater Budgets of Gordon Gulch

4.1.1 Catchment-Scale Water Budget

The catchment-scale water budget (Eq. 1) for Gordon Gulch was estimated using data from water years 2012 – 2019 (**Table 7**). Precipitation (P) and streamflow (ΔQ_c) were measured in Gordon Gulch (Anderson and Ragar, 2021b; Anderson and Ragar, 2021h) and ET_c was estimated as the difference between total annual precipitation and streamflow. Based on this data, the runoff ratio (defined as the ratio between precipitation and streamflow) for Gordon Gulch is approximately 14%. The runoff ratio provides a first order estimate of how much water is available for groundwater recharge each year (up to 80 mm). ET_c removes the remaining 86% of precipitation from the catchment each year (580 mm).

Results from the catchment-scale water budget were compared to the results of the groundwater budget, in order to confirm the model was producing reasonable results (i.e., model results did not exceed values of precipitation, streamflow, or ET estimated for the catchment). This comparison is described in detail in Section 5.1.

Table 7. Catchment-scale water budget of Gordon Gulch based on measured mean data from water years 2012-2019.

Water budget component	Inflows		Outflows	
	Mean annual total (mm/yr)	% of catchment-scale water budget	Mean annual total (mm/yr)	% of catchment-scale water budget
Precipitation (P)	580	100%	-	-
Evapotranspiration (ET_c)	-	-	500	86%
Streamflow (ΔQ_c)	-	-	80	14%
Change in catchment storage (ΔS_c)	580	100%	580	100%

4.1.2 Groundwater Budget

The groundwater budget for Gordon Gulch was extracted from the results of the groundwater flow model. Following the groundwater budget (Eq. 2), recharge (a fraction of total precipitation that reaches the water table) is the inflow to the groundwater system and is balanced against losses to the system from evapotranspiration (ET). The net exchanges between groundwater and the stream (ΔQ) may be either a net gain or loss to the groundwater system, depending on the dominant exchange (balanced between groundwater discharge to the stream (Q_{out}) and stream leakage to the aquifer (Q_{in})).

The annual groundwater budget based off model results is presented in **Table 8**. The volume of these exchanges produced during model simulations (m^3/d) were area-corrected to Gordon Gulch to produce a net change represented in millimeters. During the simulated water year, recharge from precipitation and snowmelt totaled 62 mm (160,781 m^3) and 56 mm of groundwater were lost to ET. Groundwater exchanges with the stream represented a net loss of 13 mm from the aquifer; 6 mm were added to the aquifer from stream leakage (Q_{in}), but 19 mm of water were discharged from groundwater into the stream (Q_{out}). Although constant head cells were included in the model to exert a topographic control on head, water from these cells were a minimal component of the model groundwater budget, representing only 0.1% and 0.04% of inflows and outflows, respectively.

Table 8. Annual groundwater budget of Gordon Gulch based on the calibrated transient model. Values reported in mm/yr were normalized to the catchment area. R is recharge, ET is evapotranspiration, ΔS is the change in aquifer storage, ΔQ represents the net flux between groundwater and the stream and is calculated as the difference between groundwater discharge to the stream (ΔQ_{out}) and stream leakage to the aquifer (ΔQ_{in}). Constant head is a model term that represents flow from the modeled constant head cells to maintain head.

Groundwater Budget Component	Input			Output			Input - Output	
	m^3/yr	mm/yr	% of total	m^3/yr	mm/yr	% of total	m^3/yr	mm/yr
Recharge (R)	160,781	62	57%	-	-	0%	160,781	62
Evapotranspiration (ET)	-	-	0%	144,666	56	51%	-144,666	-56
Change in aquifer storage (ΔS)	105,487	41	37%	88,588	34	31%	16,899	6
Net groundwater-stream fluxes (ΔQ)								-13
Stream leakage to the aquifer (ΔQ_{in})	16,696	6	6%	-		-	16,696	6
Groundwater discharge to the stream (ΔQ_{out})	-	-	-	49,768	19	18%	-49,768	-19
Constant head	166	0.1	0.10%	101	0.0	0.04%	65	0
Total	*283,130*	109	*100%*	*283,124*	109	*100%*	*6*	*0.0*

4.2 Groundwater – Stream Exchanges

4.2.1 Spatial and Temporal Distribution of Exchanges

The spatial and temporal distributions of groundwater-stream exchanges over an average water year are presented in **Figure 10**. Stream leakage to the groundwater system ('losing' stream conditions) is represented as a positive rate and groundwater discharge to the stream ('gaining' stream conditions) is represented as a negative rate. Locations along the stream that are not plotted with a colored cell indicate there was no net gain or loss within that cell.

Overall, Gordon Gulch is a gaining system. Gaining stream conditions were observed consistently in lower Gordon Gulch throughout the water year and across the entire stream reach in the spring. Despite the presence of segments with losing conditions, the rates of stream leakage were consistently lower than those of groundwater discharge to stream. As identified in **Table 8,** stream leakage to the aquifer supplied approximately 6 mm of water to the aquifer

whereas groundwater discharge to the stream contributed approximately 19 mm to the stream as baseflow over the course of a water year.

The spatial extent of groundwater-surface water exchanges contracts and expands seasonally, as shown in **Figure 10**. The majority of groundwater discharge to the stream occured in the spring through late summer, with the highest rates occurring in May. In lower Gordon Gulch, the stream was consistently gaining throughout the water year but flux rates peaked in May at a rate of 15 m^3/d. In upper Gordon Gulch, exchanges in the main stream channel and branch were seasonally dependent. In the spring, these locations were extensively under gaining conditions, but the extent of exchanges contracted so that by the winter there were no net gains or losses to the system. Gaining stream conditions were still observed in lower Gordon Gulch in the winter, but the rates of groundwater discharge to the stream were at a minimum, ranging up to 6 m^3/d.

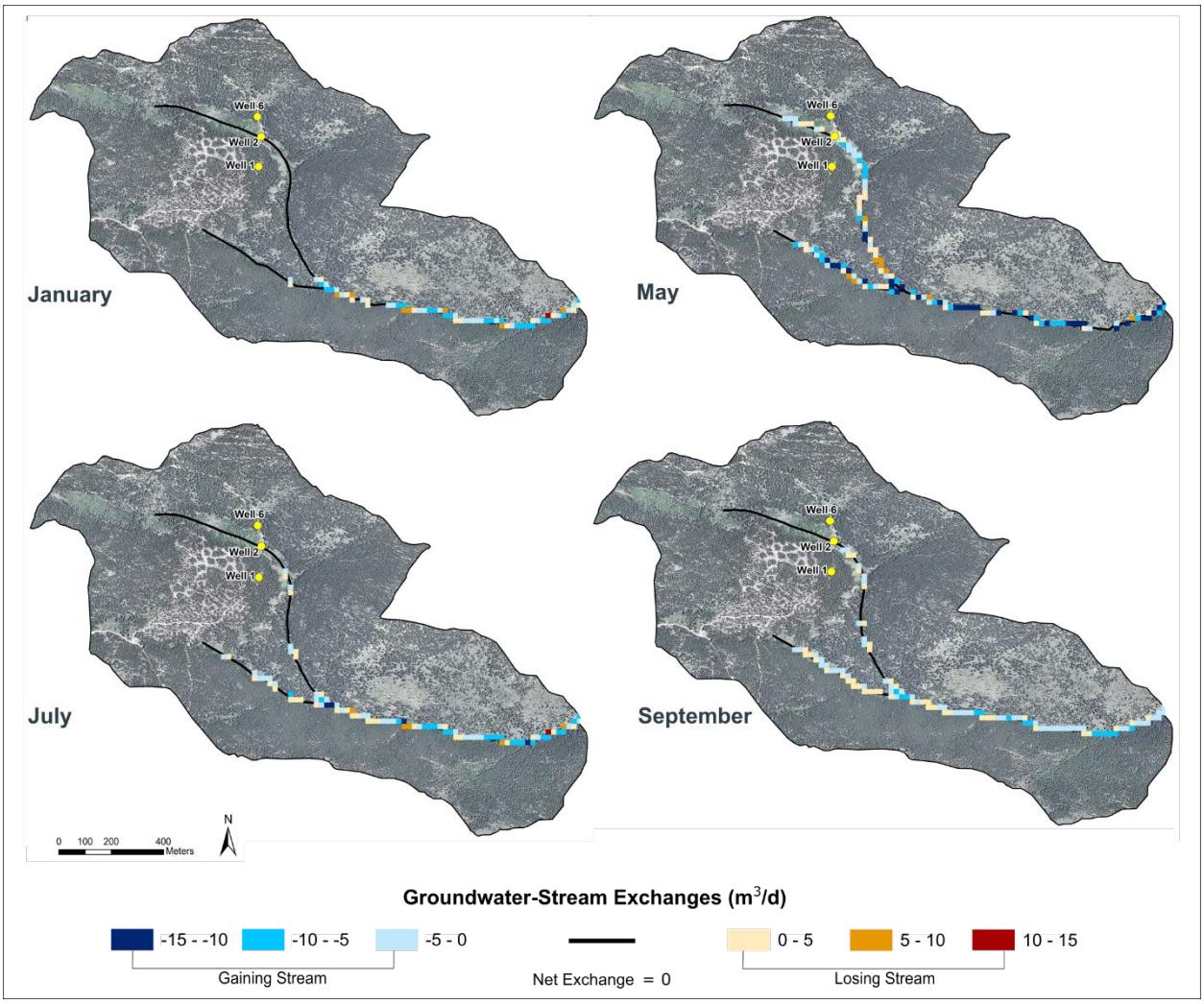

Figure 10. Groundwater – stream exchanges in Gordon Gulch over four distinct seasons over the average water year: January, May, July, and September. Positive values represent upwards groundwater seepage (gaining stream) and negative fluxes represent downwards streamflow leakage (losing stream).

4.2.2 Groundwater Flowpaths

Particle tracking showed that groundwater flow predominantly occurs in saprolite and weathered bedrock (**Figure 11**). Particles released in bedrock remained fairly stationary throughout the ten-year model period, indicating slow to minimal groundwater flow in the bedrock. Flowpaths indicate groundwater flow follows topography. Along the steepest topographic gradients (such as those along the catchment boundary), flow moved in the direction towards the catchment axis. Along the valley floor where topographic gradients are low, flow was in the downgradient direction which is generally to the southeast near the outlet stream in lower Gordon Gulch.

Flowpaths also identified the spatial distribution of groundwater recharge and discharge in the catchment. Downward flowpaths that transition to long, lateral flow were located mainly in upper Gordon Gulch (**Figure 11a**) whereas in lower Gordon Gulch flowpaths bent upwards at the channel, supporting baseflow and gaining conditions in the stream (**Figure 11b, c**)**.** Hillslope flowpaths showed long, slope-parallel flow within weathered bedrock toward the channel **(Figure 11c).** In lower Gordon Gulch, these emergent groundwater flowpaths coincided with consistent gaining stream conditions and the location of a perennial spring in the catchment. These shallow, upward flowpaths moved groundwater primarily from upper saprolite and soil into the stream.

Groundwater flow velocity estimates from MODPATH indicate that groundwater moved fastest in lower Gordon Gulch, especially in soil, where velocities averaged 2 m/d. Long, deeper flowpaths were observed moving from topographic highs in the catchment, such as those along the catchment boundary, towards the catchment valley and stream, as shown in **Figure 11b**. These longer groundwater flowpaths moved through saprolite and weathered bedrock upon

exiting into the stream. Groundwater flowed most slowly from the steepest portions towards the catchment axis at a rate of approximately 0.6 m/yr through saprolite, weathered bedrock, and bedrock.

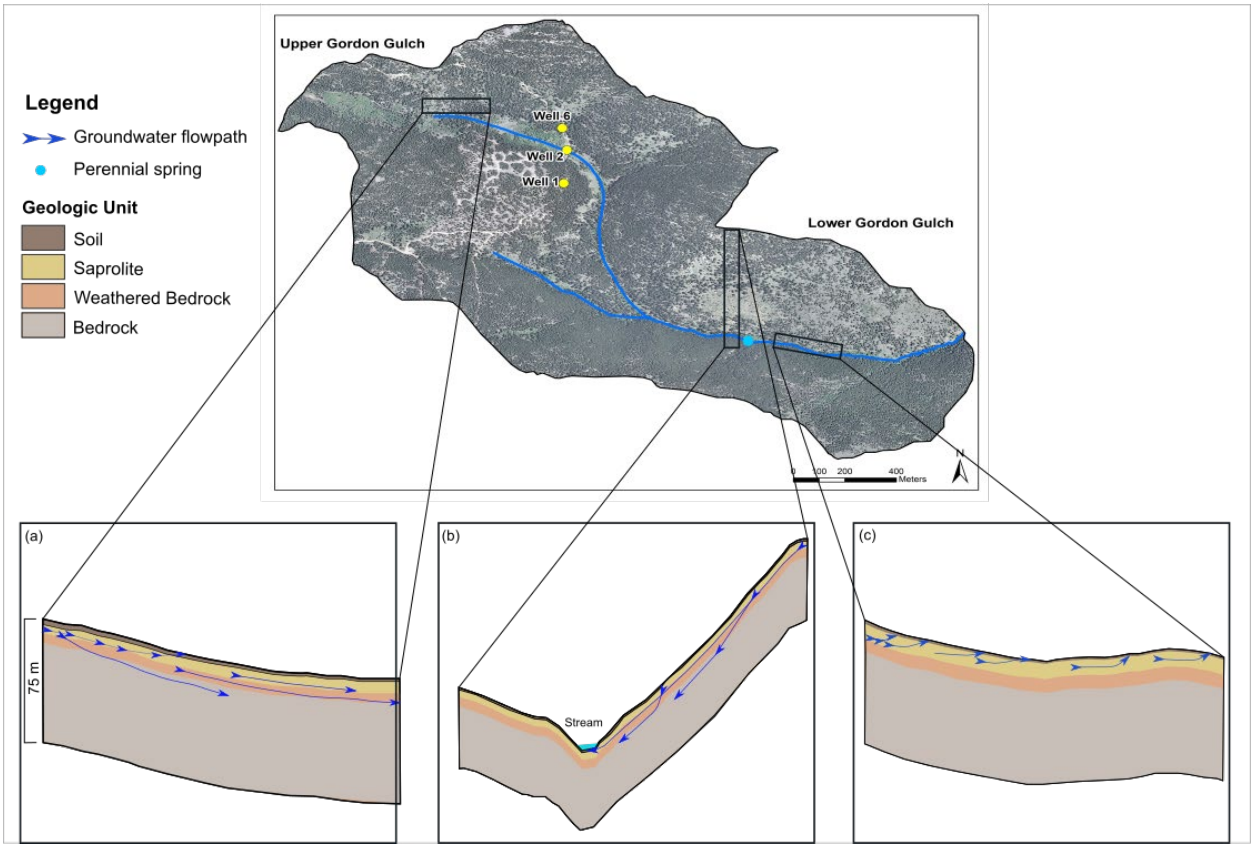

Figure 11. Simulated groundwater flowpaths in Gordon Gulch. Three distinct patterns of groundwater flowpaths are identified in a, b, and c. (a) Long horiztonal groundwater flowpaths along the stream channel in upper Gordon Gulch which move through the saprolite and weathered bedrock layers, along with concentrated groundwater recharge into the weathered bedrock and bedrock layers; (b) Groundwater flow from topographic highs of the catchment towards the valley, moving through the saprolite and weathered layers until ultimately discharged to the stream; (c) short, shallow groundwater flowpaths along the stream in lower Gordon Gulch where upwards, vertical gradients drive groundwater discharge to the stream. These flowpaths coincide with the location of a perennial spring in the catchment.

5. DISCUSSION

5.1 Catchment-Scale Water Budget vs. Groundwater Budget

The groundwater budget based on transient model results from MODFLOW was compared to the catchment-scale water budget for Gordon Gulch to gain perspective on the groundwater processes relative to catchment-wide processes (**Table 9**). The comparison shows that groundwater plays a significant role in the catchment. Groundwater recharge is approximately 62 mm/yr, indicating that approximately 11% of total annual precipitation (snowmelt and rain) infiltrates the subsurface and reaches the water table (**Figure 12**). ET from groundwater is approximately 56 mm/yr, indicating that approximately 11% of total catchment ET_c is sourced from below the water table. Groundwater discharge to stream baseflow accounts for approximately 13 mm/yr, which represents approximately 16% of total streamflow out (ΔQ_c) of Gordon Gulch.

Table 9. MODFLOW groundwater budget and comparison to the catchment-scale water budget of Gordon Gulch.

Ground-water budget component	Inflows		Outflow		Parameter from catchment-scale water budget used in comparison
	Mean annual total (mm/yr)	% of catchment-scale budget	Mean annual total (mm/yr)	% of catchment-scale budget	
Recharge	62	11%	-	-	P
ET	-	-	56	11%	ET_c
ΔQ	-	-	13	16%	ΔQ_c
ΔS	7	n/a			ΔS_c

Overall, model results produced a groundwater budget that was reasonable within the context of the catchment-scale water budget. MODFLOW-estimated recharge in Gordon Gulch was approximately 11% of total annual precipitation (including snowmelt and rain). Compared to studies of settings similar to Gordon Gulch, estimated recharge ranges from 14% (Huntley, 1979) to 52.5% (King, 2011) with a range of rates in-between (Earman et al., 2004; Kormos et al., 2015). To obtain a rough estimate of the percent of recharge from precipitation in Gordon

Gulch, the water table fluctuation method was applied to groundwater levels (see Appendix G). Based on results from the water table fluctuation method, recharge ranged from 19-38% of total annual precipitation. However, compared to the catchment-scale, modeled recharge is less than the calculated runoff ratio of 14%, indicating the total modeled recharge is consistent with catchment-scale groundwater recharge (up to 80 mm). Overall, modeled recharge is compatible with the supply estimated from the catchment-scale water budget.

The modeled groundwater budget had an overall percent discrepancy of 0.002% reflected in net loss of 7 mm of groundwater storage over the mean water year. The likely culprit for the loss in groundwater storage is due to overestimating ET in the model.

Overestimating ET likely underestimated ΔQ by removing excess groundwater that otherwise could have been discharged to the stream. Hydrograph analysis using the Eckhardt two-parameter method showed that baseflow in Gordon Gulch was approximately 34% of total streamflow; using the catchment-scale estimate of 80 mm of total streamflow (ΔQ_c), this means baseflow should have accounted for approximately 27 mm. However, MODFLOW-estimated baseflow (ΔQ) was approximately 13 mm (or 16%) of total streamflow. Modeled baseflow is approximately half of what was expected based on hydrograph separation estimate. Contextualizing modeled baseflow within the catchment-scale water budget further highlights that the model underestimated baseflow (initially observed during model calibration), but produced results reasonable enough to be interpreted.

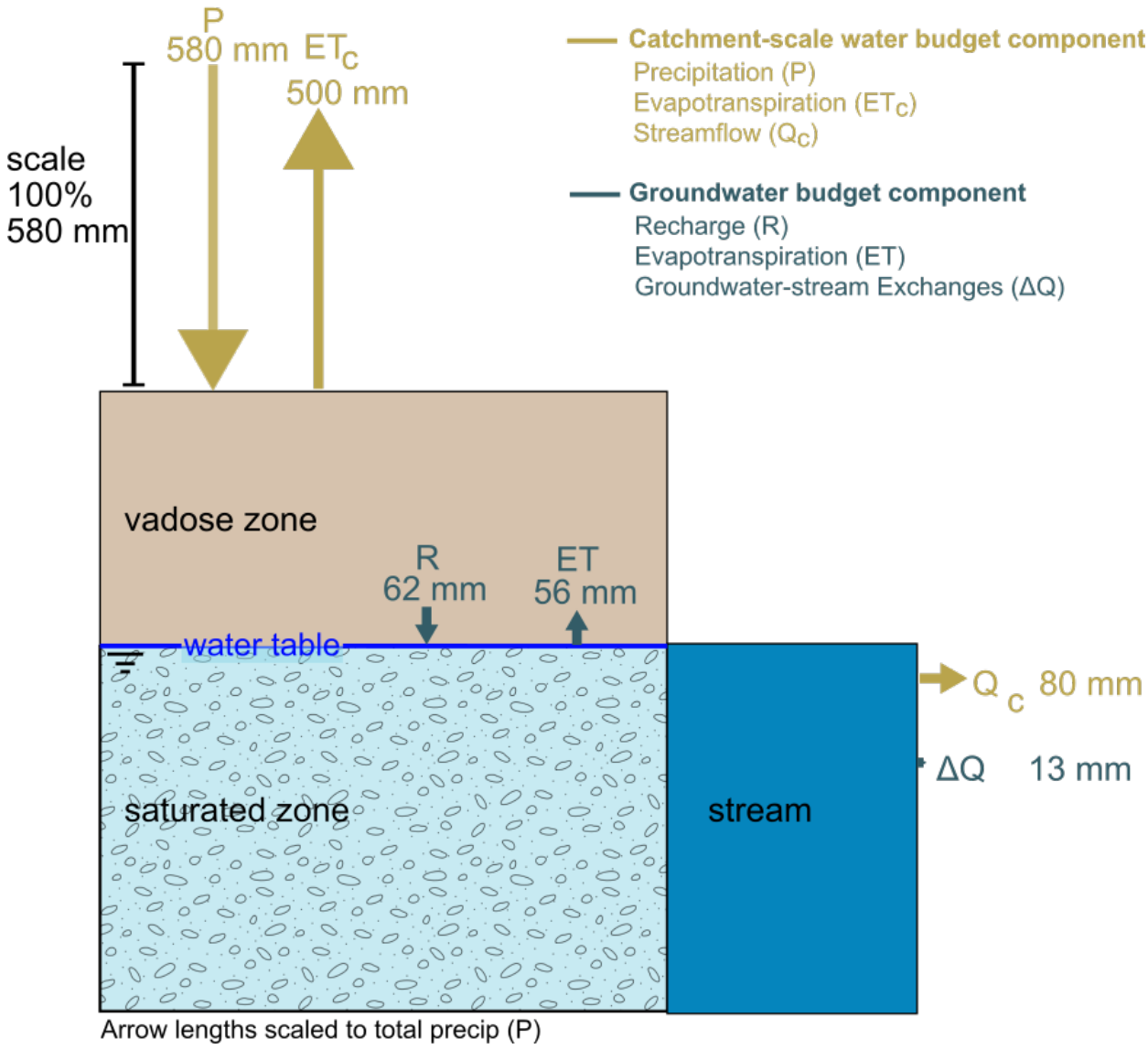

Figure 12. The annual catchment-scale water and groundwater budgets of Gordon Gulch. Catchment-scale water budget components are identified in gold and with a 'c' subscript. Catchment-scale and represents both surface and subsurface processes Groundwater budget components are listed in navy and pertain to all processes at or below the water table. Arrow lengths are scaled to total precipitation.

5.1.1 Seasonal Trends in the Groundwater Budget

The dominant components of the groundwater budget changed seasonally (**Figure 13**). Notably, precipitation, recharge, streamflow, and groundwater discharge to the stream were highest in the spring. Precipitation during April and May accounted for approximately 30% of total annual precipitation; total recharge during April and May represented 50% of total annual

recharge. This indicates that the spring snowmelt period is a significant driver of groundwater recharge.

Net groundwater-stream exchanges are positive throughout the year, indicating the stream is under gaining conditions year-round (meaning groundwater discharge to the stream (Q_{out}) exceeds stream leakage to the aquifer (Q_{in})). However, seasonally, the fraction of baseflow to total streamflow varies significantly. As shown in **Figure 13**, baseflow accounts for approximately 8% of total streamflow during April and May. In the winter and during periods with less total precipitation, baseflow accounts for nearly 30% of total streamflow. The variation in fraction of baseflow to total streamflow throughout the year highlights the importance of baseflow in this catchment especially during dry periods. In the spring, the relative contributions of baseflow to streamflow were low because rain and snowmelt were high and contributed to an overall higher total streamflow. In the winter and late summer when precipitation was low, baseflow was a more significant component of total streamflow.

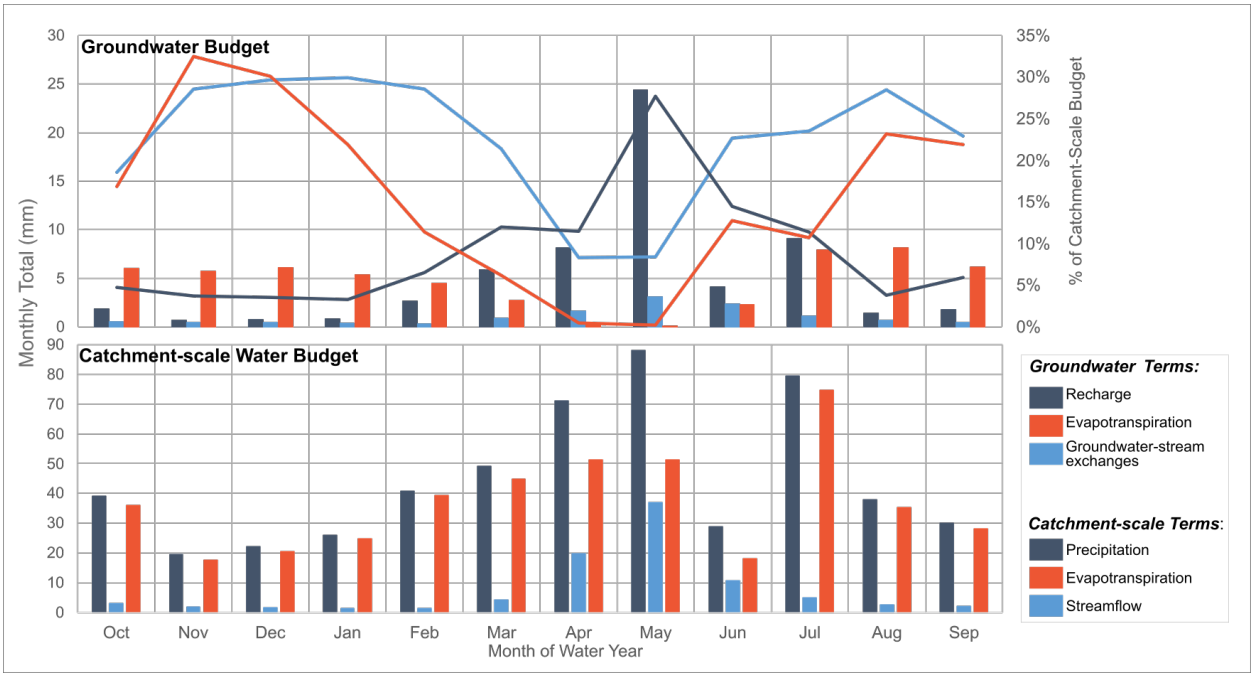

Figure 13. Monthly variations in the components of the groundwater budget (top) and catchment-scale water budget (bottom). The total monthly amount of each term is plotted as a bar graph. The top graph also overlays the fraction of the groundwater budget component compared to the total monthly catchment-scale water budget component (i.e., groundwater recharge as a fraction of total precipitation, groundwater evapotranspiration as a fraction of total evapotranspiration, and groundwater-stream exchanges as a fraction of total streamflow).

5.2 Groundwater Recharge

5.2.1 Temporal Trends

Model results indicate recharge is approximately 11% of total annual precipitation. Based on the nine-year data record and trends in groundwater table fluctuations, this recharge is concentrated within one to two major groundwater recharge events per water year. Annually, the primary recharge event occurs in the spring driven by rainfall and widespread snowmelt on north-facing slopes. The groundwater recharge period begins in March and ends in May, as supported by the model water budget, which shows that rising groundwater levels occur during this period. Maximum recharge varies from 0.002 m/d to 0.009 m/d during these three months. With the exception of a secondary recharge event (discussed below), groundwater elevations recede until the following recharge period in the spring of the following water year.

In some years, a secondary recharge event occurs in the summer driven by heavy, sustained rainfall in convective storms. Recently, such events have been identified as significant in snow-dominated alpine settings (Carroll et al., 2020). In Gordon Gulch, these recharge events are observed approximately every three years, with events occurring in the summers of 2012, 2013, and 2015. Though the response of the groundwater table to the second recharge event is usually not as pronounced as that to the primary recharge event, the secondary event results in an overall elevated water table, which promotes a greater groundwater response to recharge events in the following spring. For example, the July 2015 storm added 0.06 m of rain over a five-day period (64% of the total monthly precipitation), resulting in 1 m and 0.48 m rise in groundwater elevations at well 6 and well 2, respectively, five days after the start of the rain event and a 0.32 m rise in the groundwater elevation at well 1 nine days after. In the following spring (2016) depth to water peaked at 8.4 m, the surface, 3.1 m at wells 1, 2, and 6, respectively.

Comparatively, the summer of 2017 was relatively dry with only 0.03 m cumulative rainfall in the month of July and depth to water at all wells declined. During the spring recharge event of the following year (2018), depth to water levels peaked at 8.8 m, 0.3 m, and 4.3 m at wells 1, 2, and 6. In this sense, the secondary recharge event 'preps' the system for future recharge, allowing for a more substantial rise in the water table the following year.

5.2.2 Spatial Trends

Modeled groundwater flowpaths illuminate differences in the spatial distribution of groundwater recharge. The majority of groundwater recharge occurs in upper Gordon Gulch whereas the majority of groundwater discharge occurs in lower Gordon Gulch. This is consistent with patterns in the exchange between groundwater and the stream, which show that groundwater discharges to the stream in lower Gordon Gulch throughout the water year and that groundwater flow is driven by topography (**Figure 9**). The topographic highs and hillslopes create hydraulic gradients that drive groundwater towards lower elevations along the catchment valley and outlet. These gradients drive recharge into the saprolite and weathered bedrock in upper Gordon Gulch; these are the layers where the majority of groundwater recharge occurs. Some deep recharge occurs into the bedrock also, but widespread groundwater flow in this layer is minimal. In lower Gordon Gulch, gradients are mostly upwards, moving groundwater into the stream channel. Here, groundwater flow is shallow and generally confined to the upper portion of saprolite.

5.3 Groundwater-Stream Interactions

The model attributes 16% of streamflow as sourced from groundwater discharge (baseflow). Results from the Eckhardt two-parameter method estimated baseflow as approximately 34% of streamflow for water years 2012 - 2019. This estimate of baseflow is

similar to findings from an EMMA, which found that baseflow ranged from 23 – 33% of streamflow from 2010 to 2012, averaging 28% annually (Cowie et al., 2017). We conclude that annual baseflow ranges between 16% to 34% of total streamflow. The discrepancy between these two estimates is likely due to the differences in the components of baseflow estimated and because model results underestimated baseflow in the spring. The Eckhardt two-parameter method considers baseflow to be the low-frequency portion of streamflow that responds slowly to precipitation, while groundwater discharge simulated by MODFLOW is exclusively sourced from the saturated zone (Eckhardt, 2005; Harbaugh, 2005). Therefore, the lower estimate of 16% may be underestimated also because of unaccounted for unsaturated and vadose zone contributions to streamflow, which likely contribute to baseflow in Gordon Gulch (Smull, 2015). The Eckhardt two-parameter method results represent an upper estimate of 34% as it may be overestimated due to the oversimplification of baseflow generation processes by digital filter methods (Xie et al., 2020). Both estimates highlight the important role of groundwater in sustaining streamflow in Gordon Gulch.

5.3.1 Spatio-Temporal Distribution of Groundwater-Stream Interactions

Model results constrain the spatio-temporal distribution of groundwater-stream interactions. Groundwater discharge occurs throughout the water year, especially in lower Gordon Gulch, but peaks during periods of increased precipitation and streamflow (April through July). The highest rates of groundwater discharge occur in May, at rates up to 15 m^3/d. The months of April through July are the wettest (accounting for 42% of total annual precipitation), observe the highest rates of streamflow (77% of total annual streamflow moves through the downstream gage), and experience higher exchanges between the aquifer and the stream (accounting for 61% of total annual groundwater discharge to the stream). The connection

between increased streamflow and groundwater discharge corroborates Wilson's (2017) finding that the magnitude of groundwater-stream exchanges correlate with the magnitude of streamflow. During drier portions of the year, such as the late summer and winter, the connection between the stream and groundwater recedes. This result indicates drier, climate- driven conditions may likely result in overall less connectivity across the catchment, especially in upper Gordon Gulch.

Groundwater discharge also varies significantly depending on location in the catchment. The majority of groundwater discharge occurs in lower Gordon Gulch, driven by shallow, upward gradients towards the stream. Deeper flowpaths observed in upper Gordon Gulch also play a critical role in sustaining baseflow because the groundwater recharge that occurs in upper Gordon Gulch later supplies groundwater in the absence of precipitation and snowmelt through the long, deep flowpaths in saprolite and weathered bedrock. These deeper flowpaths emerge further downstream in lower Gordon Gulch.

The data record supports the importance of both deep and shallow flowpaths in sustaining streamflow when comparing the timing of peak stream discharge and peak groundwater elevation. Following peak snowmelt on the north-facing slope, peak stream discharge occurs approximately two days afterwards, followed by a peak in groundwater level at the valley well one day later, the south-facing well three days later, and the north-facing well four days later. Based on the various depths of the groundwater levels (the valley well being the shallowest and the north-facing well being the deepest) and hillslope positions, we observe the rise in the water table and thus groundwater storage in upper Gordon Gulch, the dominant locale of recharge in the catchment. The saprolite and weathered bedrock layers act as a storage and delivery system, delivering groundwater to lower Gordon Gulch and ultimately to the stream throughout the year.

Previous studies of groundwater-stream interactions in Gordon Gulch applied chemical separation methods to parse streamflow hydrographs. Smull (2015) and Mills et al. (2017) identified baseflow conditions in Gordon Gulch in the late summer and early fall. Smull (2015) identified the baseflow period in Gordon Gulch occurs from October to November using observations of in-stream nitrate removal (losing lateral hydraulic gradients were associated with increased baseflow). Mills et al. (2017) used the absence of silica colloids (characteristic of groundwater, but not surface water) in stream water and identified the baseflow period from late July through early October in 2011. However, Wilson (2017) found the opposite and identified primarily losing conditions in lower Gordon Gulch using tracer tests to show that a 100 m reach in lower Gordon Gulch lost water to the subsurface from late-July to late-October. Wilson (2017) found that leakage is heavily dependent on stream discharge, with higher rates of stream discharge driving in higher rates of leakage. Her observations, however, are confined to late summer months and a small reach.

Our model results support the former conclusions that baseflow supports streamflow in lower Gordon Gulch throughout the water year, including during the baseflow period from late summer through early fall. However, we acknowledge that rates of groundwater discharge are tied to rates of stream discharge, observing that peak groundwater discharge occurs in the spring (associated with peak streamflow) and declines throughout the water year. We conclude that the stream in Gordon Gulch is typically under gaining conditions, though temporal and spatial variations exist.

6. CONCLUSIONS

MODFLOW was employed to study the spatial and temporal distribution of groundwater recharge and groundwater-surface water interactions in Gordon Gulch as an example of the hydrogeologic system in a semi-arid, montane environment. Field measurements of groundwater elevation and baseflow estimated from stream discharge measurements were used to calibrate the model. Model results and supporting field data characterize Gordon Gulch as an interconnected system highly dependent on and responsive to precipitation and snowmelt, and with connectivity between groundwater and the stream and from upper to lower Gordon Gulch. Below are the key findings from this study:

- Groundwater recharge is highly dependent on snowmelt and rain.
    - Temporally, groundwater recharge is concentrated in one or two events each water year, driven by spring snowmelt and summer rainstorms. The spring snowmelt period in April and May accounts for approximately 50% of total annual recharge.
    - Spatially, groundwater recharge mainly occurs in upper Gordon Gulch where water is driven into saprolite and weathered bedrock.
- The stream in Gordon Gulch is overall a gaining system. Groundwater discharge to the stream as baseflow accounts for 16 to 34% of total annual streamflow.
    - Spatially, the majority of groundwater discharge to the stream occurs in lower Gordon Gulch. Groundwater flowpaths to the stream are derived from storage in saprolite and weathered bedrock and may be primarily sourced from the deeper, upstream flowpaths coming from upper Gordon Gulch topographic highs in the catchment. The short, shallow, and emergent flowpaths in lower Gordon Gulch ultimately deliver groundwater to the stream.

- Temporally, the highest rates of groundwater discharge to the stream occur in the spring.

This study highlights the importance of groundwater in a semi-arid, montane, headwater catchment. Our model offers a promising use as an assessment of the groundwater budget in similar environments. Future investigations on the spatial and temporal distribution of groundwater recharge and groundwater-surface water interactions are warranted considering the importance of water resources in montane, headwater environments.

REFERENCES

Adams, H.R., Barnard, H.R., and Loomis, A.K. (2014): Topography alters tree growth-climate relationships in a semi-arid forested catchment, Ecosphere 4: art148, doi:10.1890/ES14-00296.1.

Aguirre, A. A., Derry, L. A., Mills, T. J., and Anderson, S. P. (2017). Colloidal transport in the Gordon Gulch catchment of the Boulder Creek CZO and its effect on C-Q relationships for silicon, *Water Resources. Res.*, 53, 2368– 2383, doi:10.1002/2016WR019730.

Anderholm, S.K., Mountain-front recharge along the eastern side of the Middle Rio Grande Basin, central New Mexico, U.S. Geological Survey Water-Resources Investigation Report 00-4010, 2000.

Anderson, R.S., Riihimaki, C.A., Safran, E.B., and Macgregor, K.B. (2006). Facing reality: Late Cenozoic evolution of smooth peaks, glacially ornamented valleys, and deep river gorges of Colorado's Front Range. 10.1130/2006.2398(25).

Anderson, RS, Anderson, SP, and Tucker, GE (2013): Rock damage and regolith transport by frost: An example of climate modulation of critical zone geomorphology. Earth Surface Processes and Landforms 38: 299-316, doi:10.1002/esp.3330

Anderson, R.S., Rajaram, H., Anderson, S.P. (2019). Climate driven coevolution of weathering profiles and hillslope topography generates dramatic differences in critical zone architecture. *Hydrological Processes*. 2019; 33: 4– 19. https://doi.org/10.1002/hyp.13307

Anderson, S. (2020). BCCZO -- Snow Survey -- Gordon Gulch -- (2008-2009), HydroShare, http://www.hydroshare.org/resource/c8d95e8119304d5396a9cecdded22fcc

Anderson, S., and Ragar, D. (2021a). BCCZO -- Air Temperature, Meteorology -- North-Facing Meteorological Tower (GGL_NF_Met) -- Gordon Gulch: Lower -- (2012-Ongoing), HydroShare, http://www.hydroshare.org/resource/d30b44383d154225b3c99e557d124b7d

Anderson, S., and Ragar, D. (2021a). Gordon Gulch: Upper Well Water Levels -- (GGU_GW_1_Pducer) -- Gordon Gulch: Upper -- (2011-2017), BcCZO, https://bcczo.colorado.edu/query/ggu_gw_1_pducer.shtml

Anderson, S., and Ragar, D. (2021b). Gordon Gulch: Upper Well Water Levels -- (GGU_GW_6_Pducer) -- Gordon Gulch: Upper -- (2011-2017), BcCZO, https://bcczo.colorado.edu/query/ggu-gw-6-pducer.shtml

Anderson, S., and Ragar, D. (2021c). BCCZO -- Snow Depth -- Snow Pole Transects (manual) (GGU_SP_1-10_Tran) -- Gordon Gulch: Upper -- (2008-2017), HydroShare, http://www.hydroshare.org/resource/48e04554b0b044c095a85c8ee2314134

Anderson, S., and Ragar, D. (2021d). BCCZO -- Well Water Levels -- (GGU_GW_1,2,6_Pducer_Tran) -- Gordon Gulch: Upper -- (2011-2020), HydroShare, http://www.hydroshare.org/resource/4a4b2b04790147828072151b2a4820e1

Anderson, S., and Ragar, D. (2021e). Gordon Gulch: Upper Well Water Levels -- (GGU_GW_1_Pducer) -- Gordon Gulch: Upper -- (2011-2017), BcCZO, https://bcczo.colorado.edu/query/ggu_gw_1_pducer.shtml

Anderson, S., and Ragar, D. (2021f). Gordon Gulch: Upper Well Water Levels -- (GGU_GW_2_Pducer) -- Gordon Gulch: Upper -- (2011-2017), BcCZO, https://bcczo.colorado.edu/query/ggu_gw_2_pducer.shtml

Anderson, S., and Ragar, D. (2021g). Gordon Gulch: Upper Well Water Levels -- (GGU_GW_6_Pducer) -- Gordon Gulch: Upper -- (2011-2017), BcCZO, https://bcczo.colorado.edu/query/ggu-gw-6-pducer.shtml

Anderson, S., and Ragar, D. (2021h). BCCZO -- Streamflow / Discharge -- (GGL_SW_0_Dis) -- Gordon Gulch: Lower -- (2011-2019), HydroShare, http://www.hydroshare.org/resource/c2384bd1743a4276a88a5110b1964ce0

Anderson, S., and Rock, N. (2020). BCCZO -- Snow Pits -- Snow Pit Stratigraphy, Density - SWE (GG_SN_Array) -- Gordon Gulch -- (2008-2017), HydroShare, http://www.hydroshare.org/resource/e876ee4739b34f3c840c2588942f0381

Anderson, SP, Dietrich, WE, Montgomery, DR, Torres, R, Conrad, ME, and Loague, K (1997): Subsurface flow paths in a steep, unchanneled catchment. Water Resources Research 33 (12): 2637-2653.

Anderson, SP, von Blanckenburg, F, and White, AF (2007) Physical and chemical controls on the critical zone. Elements 3: 315-319.

Anderson, S.P., Qinghua, G., and Parrish, E.G. (2012). Snow-on and snow-off Lidar point cloud data and digital elevation models for study of topography, snow, ecosystems and environmental change at Boulder Creek Critical Zone Observatory, Colorado: Boulder Creek CZO, INSTAAR, University of Colorado at Boulder, digital media.

Anderson, S.P., Anderson, R.A., Tucker, G.E., & Dethier, D. (2013). Critical zone evolution: Climate and exhumation in the Colorado Front Range, Classic Concepts and New Directions: Exploring 125 Years of GSA Discoveries in the Rocky Mountain Region, Lon D. Abbott, Gregory S. Hancock. https://doi.org/10.1130/2013.0033(01)

Anderson, SP, Hinckley, E-L, *Kelly, P, *Langston, A (2014): Variation in critical zone processes and architecture across slope aspects, Procedia Earth and Planetary Science 10: 28-33, doi:10.1016/j.proeps.2014.08.006

Anderson, SP, Kelly, PJ, Hoffman, N, Barnhart, K, Befus, K, and Ouimet, W. (2021): Is this steady state? Weathering and critical zone architecture in Gordon Gulch, Colorado Front Range. In Hydrogeology, Chemical Weathering, and Soil Formation, AGU Geophysical Monograph 257, ed. by AG Hunt, M Egli, and B Faybishenko, John Wiley & Sons, Inc., p. 231-252, doi: 10.1002/9781119563952.ch13

Bandler, A. (2016). Geophysical Constraints on Critical Zone Architecture and Subsurface Hydrology of Opposing Montane Hillslopes [master's thesis]. Colorado School of Mines.

Baraer, M., Mckenzie, J. M., Mark, B. G., Bury, J., & Knox, S. (2009). Characterizing contributions of glacier melt and groundwater during the dry season in a poorly gauged catchment of the cordillera Blanca (Peru). Advances in Geosciences, 22, 41–49. https://doi.org/10.5194/adgeo-22-41-2009

Barlow, P.M., Cunningham, W.L., Zhai, T., and Gray, M. (2017). U.S. Geological Survey Groundwater Toolbox version 1.3.1, a graphical and mapping interface for analysis of

hydrologic data: U.S. Geological Survey Software Release, 26 May 2017, http://dx.doi.org/10.5066/F7R78C9G

Barnard, DM, Barnard, HR, and Molotch, NP (2017): Topoclimate effects on growing season length and montane conifer growth in complex terrain. Environmental Research Letters 12, doi:10.1088/1748-9326/aa6da8

Bearup, L.A., Maxwell, R.M., Clow, D.W., and McCray, J.E. (2014). Hydrological effects of forest transpiration loss in bark beetle-impacted watersheds, Nature Climate Change, 4, doi: 10.1038/NCLIMATE2198.

Befus, K. M., Sheehan, a. F., Leopold, M., Anderson, S. P., & Anderson, R. S. (2011). Seismic Constraints on Critical Zone Architecture, Boulder Creek Watershed, Front Range, Colorado. *Vadose Zone Journal*, *10*(4), 1342. https://doi.org/10.2136/vzj2010.0108er

Bloomfield, J.P., Allen, D.J., and Friffiths, K.J. (2009). Examining geological controls on baseflow index (BFI) using regression analysis: An illustration from the Thames Basin, UK. Journal of Hydrology 373: 164-176.

Brenner, AE, Anderson RS, Anderson, SP, Winchell, EW, Schellhase, D, and Marquez, JA (2014): Reconstructing peak discharge in a Colorado Front Range headwater stream during the September 2013 storm. Eos Trans. AGU 95 (52), Fall Meeting Suppl., Virtual Abstract.

Brutsaert, W., and Lopez, J. P. (1998), Basin-scale geohydrologic drought flow features of riparian aquifers in the Southern Great Plains, Water Resour. Res., 34(2), 233– 240, doi:10.1029/97WR03068.

Buraas, E. (2009). Getting water into the ground and to the channel, Gordon Gulch, Colorado [undergraduate thesis]. Williams College.

Burns, D. A., Murdoch, P. S., Lawrence, G. B., and Michel, R. L. (1998), Effect of groundwater springs on NO3 _ concentrations during summer in Catskill Mountain streams, Water Resour. Res., 34, 1987 – 1996, doi:10.1029/98WR01282.

Burns, M.A., Barnard, H.R., Gabor, R.S., McKnight, D.M., and Brooks, P.D. (2016): Dissolved organic matter transport reflects hillslope to stream connectivity during snowmelt in a montane catchment. *Water Resources Research* 52 (6), Doi: 10.1002/2015WR017878

Caine, J.S. Manning, A.H., Verplanck, P.L., Bove, D.J., Kahn, K.G., and Ge, S. (2006). Well Construction Information, Lithologic Logs, Water Level Data, and Overview of Research in Handcart Gulch, Colorado: An Alpine Watershed Affected by Metalliferous Hydrothermal Alteration: U.S. Geological Survey Open-File Report 2006-1189, 14 pp., < http://pubs.usgs.gov/of/2006/1189/

Caine, N. (1995). Temporal Trends in the Quality of Streamwater in an Alpine Environment: Green Lakes Valley, Colorado Front Range, U.S.A., Geografiska Annaler: Series A, Physical Geography, 77:4, 207-220, DOI: 10.1080/04353676.1995.11880441

Carroll, R. W. H., Bearup, L. A., Brown, W., Dong, W., Bill, M., & Willlams, K. H. (2018). Factors controlling seasonal groundwater and solute flux from snow-dominated basins. Hydrological Processes, 32(14), 2187–2202. https://doi.org/10.1002/hyp.13151

Carroll, R. W H., Deems, J. S., Niswonger, R., Schumer, R., & Williams, K. H. (2019). The importance of interflow to groundwater recharge in a snowmelt-dominated headwater basin. *Geophysical Research Letters*, 46, 5899– 5908. https://doi.org/10.1029/2019GL082447

Carroll, R. W. H., Gochis, D., & Williams, K. H. (2020). Efficiency of the summer monsoon in generating streamflow within a snow-dominated headwater basin of the Colorado River. Geophysical Research Letters, 47, e2020GL090856. https://doi.org/10.1029/2020GL090856

Chapman, TG. (1991). Comment on "Evaluation of automated techniques for base flow and recession analyses' by R.J. Nathan and T.A. McMahon. Water Resources Research 27: 1783-1784.

Clow, D. W., Schrott, L., Webb, R., Campbell, D. H., Torizzo, A., and Dornblaser, M. M. (2003). Ground water occurrence and contributions to streamflow in an alpine catchment, Colorado Front Range. Ground Water, 41(7), 937−950.

Collischonn, W. and Fan, F.M. (2013), Defining parameters for Eckhardt's digital baseflow filter. Hydrol. Process., 27: 2614-2622. https://doi.org/10.1002/hyp.9391

Compaore, G., Lachassagne, P., Pointet, T. and Travi, Y. (1997). Evaluation du stock d'eau des altérites. expérimentation sur le site granitique de Sanon (Burkina-Faso). *In*: IAHS (Edited), Rabat IAHS conference. IAHS Publication. IAHS, Rabat, pp. 37–46.

Cowie, R. (2010). The Hydrology of Headwater Catchments from the Plains to the Continental Divide, Boulder Creek Watershed, Colorado. *Geological Sciences Graduate Theses & Dissertations*, (13), 131.

Cowie, R. (2014). Surface water and groundwater interactions in natural and mining impacted mountain catchments (doctoral dissertation). Retrieved from Proquest Dissertations Publishing. (UMI number: 3672393). Boulder, CO: University of Colorado Boulder

Cowie, R., Knowles, J. F., Dailey, K. R., Williams, M. W., Mills, T. J., & Molotch, N. P. (2017). Sources of streamflow along a headwater catchment elevational gradient. *Journal of Hydrology*, *549*, 163–178. https://doi.org/10.1016/j.jhydrol.2017.03.044

Creutzfeldt, B., Güntner, A., Wziontek, H., Merz, B. (2010). Reducing local hydrology from high-precision gravity measurements: a lysimeter-based approach, *Geophysical Journal International*, Volume 183, Issue 1, October 2010, Pages 178–187, https://doi.org/10.1111/j.1365-246X.2010.04742.x

Dailey, K. (2016). Streamflow and groundwater response to precipitation variability in a snow-dominated, subalpine headwater catchment, Colorado Rocky Mountains, USA [master's thesis]. University of Colorado Boulder.

Delin GN, Healy RW, Lorenz DL, Nimmo JR. (2007). Comparison of local- to regional-scale estimates of groundwater recharge in Minnesota, USA. J Hydrol 334:231–249

Dethier, D. P., and Lazarus, E. D. (2006). Geomorphic inferences from regolith thickness, chemical denudation and CRN erosion rates near the glacial limit, Boulder Creek catchment and vicinity, Colorado. *Geomorphology*, *75*(3–4), 384–399. https://doi.org/10.1016/j.geomorph.2005.07.029

Dethier, David P., Birkeland, Peter W., and McCarthy, James A. (2012) Using the accumulation of CBD-extractable iron and clay content to estimate soil age on stable surfaces and nearby slopes, Front Range, Colorado. Geomorphology 173-174: 17-29, doi:10.1016/j.geomorph.2012.05.022.

Dewandel, Benoit & Lachassagne, Patrick & Wyns, Robert & Maréchal, Jean-Christophe & N.s, Krishnamurthy. (2006). A generalized 3-D geological and hydrogeological conceptual model of granite aquifers controlled by single or multiphase weathering. Journal of Hydrology. 260-284. 10.1016/j.jhydrol.2006.03.026.

Duffy, Christopher. (2004). Semi-Discrete Dynamical Model for Mountain-Front Recharge and Water Balance Estimation, Rio Grande of Southern Colorado and New Mexico. 10.1029/009WSA14.

Durand, V. Léonardi, V., de Marsily, G., Lachassagne, P. (2017). Quantification of the specific yield in a two-layer hard-rock aquifer model. Journal of Hydrology, Elsevier, 2017, 551, pp.328-339. ff10.1016/j.jhydrol.2017.05.013ff. ffhal-01537837f

Earman, S., Campbell, A. R., Phillips, F. M., & Newman, B. D. (2006). Isotopic exchange between snow and atmospheric water vapor: Estimation of the snowmelt component of groundwater recharge in the southwestern United States. *Journal of Geophysical Research*,*111*, D09302. https://doi.org/10.1029/2005JD006470

Eckhardt, K. (2005), How to construct recursive digital filters for baseflow separation. Hydrol. Process., 19: 507-515. https://doi.org/10.1002/hyp.5675

Eckhardt, K. (2008). A comparison of baseflow indices, which were calculated with seven different baseflow separation methods. Journal of Hydrology 352(1-2): 168 – 173.

Eckhardt, K. (2012). Technical Note: Analytical sensitivity analysis of a two parameter recursive digital baseflow separation filter. Hydrology and Earth System Sciences. 16. 10.5194/hess-16-451-2012.

Eilers K.G., Debenport S., Anderson S., Fierer N. (2012): Digging deeper to find unique microbial communities: The strong effect of depth on the structure of bacterial and archaeal communities in soil. *Soil Biology and Biochemistry(50):58-65*. DOI: 10.1016/j.soilbio.2012.03.011

Engdahl, N. B., & Maxwell, R. M. (2015). Quantifying changes in age distributions and the hydrologic balance of a high-mountain watershed from climate induced variations in recharge. Journal of Hydrology, 522, 152–162. https://doi.org/10.1016/j.jhydrol.2014.12.032

Feth, J.H., D.A. Barker, L.G. Moore, R.J. Brown, and C.E. Veirs. (1966). Lake Bonneville: geology and hydrology of the Weber Delta District, including Ogden, Utah, *U. S. Geological Survey Professional Paper 518*.

Flint, A.L., L.E. Flint, G.SW. Bodvarsson, E.M. Kwicklis, and J. Fabryka-Martin. (2001). Evolution of the conceptual model of unsaturated zone hydrology at Yucca Mountain, Nevada, *J. of Hydrology*, 247, 1-30.

Foks, S., Raffensperger, J.P., Penn, C.A., & Driscoll, J. (2019). Estimation of Base Flow by Optimal Hydrograph Separation for the Conterminous United States and Implications for National-Extent Hydrologic Models. *Water, 11*, 1629.

Foster, S. B., & Allen, D. M. (2015). Groundwater-surface water interactions in a mountain-to-coast watershed: Effects of climate change and human stressors. Advances in Meteorology, 2015, 1–22. https://doi.org/10.1155/2015/861805

Frazier, C. S., R. C. Graham, P. J. Shouse, M. V. Yates, and M. A. Anderson (2002), A field study of water flow and virus transport in weathered granitic bedrock, Vadose Zone J., 1, 113–124.

Freeze, A. R., & Cherry, J. A. (1979). Groundwater. Englewood Cliffs, NJ: Prentice-Hall.

Frisbee, M. D., Phillips, F. M., Campbell, A. R., Liu, F., & Sanchez, S. A. (2011). Streamflow generation in a large, alpine watershed in the southern Rocky Mountains of Colorado: Is streamflow generation simply the aggregation of hillslope runoff responses? Water Resources Research, 47(6), 1–18. https://doi.org/10.1029/2010WR009391

Fujimoto, M., Ohte, N., Kawasaki, M., Osaka, K., Itoh, M., Ohtsuka, I., & Itoh, M. (2016). Influence of bedrock groundwater on streamflow characteristics in a volcanic catchment. Hydrological Processes, 30(4), 558–572. https://doi.org/10.1002/hyp.10558

Gable, D.J. (1996): Mineralogy, geochemistry, metamorphism, and provenance of the 940 early Proterozoic metamorphic rocks of the central Front Range, Colorado. 941 United States Geological Survey Open-File Report 96-522.

Gabor, RS, Eilers, KG, McKnight, DM, Fierer, N, and Anderson, SP (2014): From the litter layer to the saprolite: Chemical changes in water-soluble soil organic matter and their correlation to microbial community composition, Soil Biology and Biochemistry 68: 166-176, doi:10.1016/j.soilbio.2013.09.029

Gleeson, T., & Manning, A. H. (2008). Regional groundwater flow in mountainous terrain: Three-dimensional simulations of topographic and hydrogeologic controls. Water Resources Research, 44(10), 1–16. https://doi.org/10.1029/2008WR006848

Gochis, D. and 18 others (2015): The Great Colorado Flood of September 2013, Bulletin of the American Meteorological Society, https://doi.org/10.1175/BAMS-D-13-00241.1

Gordon, R. P., Lautz, L. K., McKenzie, J. M., Mark, B. G., Chavez, D., & Baraer, M. (2015). Sources and pathways of stream generation in tropical proglacial valleys of the cordillera Blanca, Peru. Journal of Hydrology, 522, 628–644. https://doi.org/10.1016/j.jhydrol.2015.01.013

Grace, B. and Quick, B. (1988) A Comparison of Methods for the Calculation of Potential Evapotranspiration Under the Windy Semi-arid Conditions of Southern Alberta, Canadian Water Resources Journal / Revue canadienne des ressources hydriques, 13:1, 9-19, DOI: 10.4296/cwrj1301009

Greenland, D. (1989). The climate of Niwot Ridge, Front Range, Colorado, U.S.A. *Arctic and Alpine Research*, *21*(4), 380−391.

Greenland, D. (1993). Spatial energy budgets in alpine tundra. Theor Appl Climatol 46, 229–239. https://doi.org/10.1007/BF00865710

Hale, K. (2018). Streamflow Sensitivity to Climate Warming and a Shift from Snowfall to Rainfall [master's thesis]. University of Colorado Boulder.

Hall, F. R. (1968), Base-Flow Recessions—A Review, Water Resour. Res., 4 (5), 973– 983, doi:10.1029/WR004i005p00973.

Hamilton, E. L., and P. B. Rowe. (1949). Rainfall interception by chaparral in California, Calif. Dept. Nat. Resources, Div. Forestry, and U.S. Forest Serv., California Forest and Range Expt. Sta., 43 pp.

Harbaugh, A.W. (2005) MODFLOW-2005, the U.S. Geological Survey Modular Ground-Water Model—The Ground-Water Flow Process. U.S. Geological Survey Techniques and Methods 6-A16.

Harpold, A.A., Q. Guo, N. Molotch, P. D. Brooks, R. Bales, J.C. Fernandez-Diaz, K.N. Musselman, and T.L. Swetnam, P. Kirchner, M. Meadows, J. Flanagan, R. Lucas. (2014). LiDAR-derived snowpack data sets from mixed conifer forests across the Western United States. *Water Resources Research 50(3): 2749-2755*. DOI: 10.1002/2013WR013935

Harrington, J. S., Mozil, A., Hayashi, M., & Bentley, L. R. (2018). Groundwater flow and storage processes in an inactive rock glacier. Hydrological Processes, 32(20), 3070–3088. https://doi.org/10.1002/hyp.13248

Hattanji, T., and Y. Onda (2004), Coupling of runoff processes and sediment transport in mountainous watersheds underlain by different sedimentary rocks, Hydrol. Process., 18, 623–636, doi:10.1002/hyp.1262.

Hely, A. G., Mower, R. W., and Harr, C. A. (1971). *Water resources of Salt Lake County, Utah*. Salt Lake City, UT: Utah Department of Natural Resources.

Henning, S. R. (2016). Dynamic Response of a Watershed Subsurface Systems to Extreme Precipitation Events [master's thesis]. University of Colorado Boulder.

Hibbs, B.J., and B.K. Darling, Environmental isotopes and numerical models for understanding aquifer dynamics in southwestern basins, In Advances in the Development and Use of Models in Water Resources, edited by T. G. Cleveland, 195-201, Houston, Texas, 1995.

Hinckley, E. L. S., Ebel, B. A., Barnes, R. T., Anderson, R. S., Williams, M. W., & Anderson, S. P. (2012). Aspect control of water movement on hillslopes near the rain-snow transition of the Colorado Front Range. *Hydrological Processes*, *28*(1), 74–85. https://doi.org/10.1002/hyp.9549

Hinckley, E-L, Ebel, BA, Barnes, RT, Anderson, RS, Williams, MW, and Anderson, SP (2014a): Aspect control of water movement on hillslopes near the rain-snow transition of the Colorado Front Range, U.S.A. Hydrological Processes 28: 74-85, doi:10.1002/hyp.9549

Hinckley, E-L, Barnes, RT, Anderson, SP, Williams, MW, and Bernasconi, S (2014b): Nitrogen retention and transport differ by hillslope aspect at the rain-snow transition of the Colorado Front Range, Journal of Geophysical Research-Biogeosciences 119 (7): 1281-1296, doi:10.1002/2013JG002588

Hinckley, ES, Ebel, BA, Barnes, RT, Murphy, SF, and Anderson, SP (2017): Critical zone properties control the fate of nitrogen during experimental rainfall in montane forests of

the Colorado Front Range. Biogeochemistry 132 (1): 213-231, doi:10.1007/s10533-017-0299-8

Hisz, D. and Murdoch, L. (2006). The Effect of Saprolite on Long-Term Performance of Wells in the Piedmont [Conference presentation]. AGU Fall Meeting Abstracts, San Francisco, CA, U.S.

Houston, J. and Lewis, R.T. (1988), The Victoria Province Drought Relief Project, II. Borehole Yield Relationships. Groundwater, 26: 418-426. https://doi.org/10.1111/j.1745-6584.1988.tb00407.x

Hudson, R.O., and D.L. Golding. (1997). Controls on groundwater chemistry in subalpine catchments in the southern interior of British Columbia, Journal of Hydrology, 201, pp 1-20.

Huntley, D. (1979). Groundwater recharge to the aquifers of northern San Luis Valley, Colorado. *Geological Society of America Bulletin*, Part II, 90(8), 1196-1281.

Huth, A. K., Leydecker, A., Sickman, J. O., & Bales, R. C. (2004). A two-component hydrograph separation for three high-elevation catchments in the Sierra Nevada, California. Hydrological Processes, 18(9), 1721–1733. https://doi.org/10.1002/hyp.1414

Isard, S.A, and Belding, M.J. (1989). Evapotranspiration from the Alpine Tundra of Colorado, U.S.A., Arctic and Alpine Research, 21:1, 71-82, DOI: 10.1080/00040851.1989.12002711

James, A.L., McDonnell, J.J., Tromp-van Meerveld, I. and Peters, N.E. (2010), Gypsies in the palace: experimentalist's view on the use of 3-D physics-based simulation of hillslope hydrological response. Hydrol. Process., 24: 3878-3893. https://doi.org/10.1002/hyp.7819

Jensen, M.E. and Haise, H.R. (1963) Estimating Evapotranspiration from Solar Radiation. Journal of the Irrigation and Drainage Division, 89, 15-41.

Jones, M. J. (1985). The weathered zone aquifers of the basement complex areas of Africa. Quarterly Journal of Engineering Geology and Hydrogeology, 18, 35-46.

Kahn, K.G., Ge, S., Caine, J.S. *et al.* (2008). Characterization of the shallow groundwater system in an alpine watershed: Handcart Gulch, Colorado, USA. *Hydrogeol J* **16,** 103–121. https://doi.org/10.1007/s10040-007-0225-6

Katsura, S., Kosugi, K., Mizutani, T., Okunaka, S., and Mizuyama, T. (2008), Effects of bedrock groundwater on spatial and temporal variations in soil mantle groundwater in a steep granitic headwater catchment, Water Resour. Res., 44, W09430, doi:10.1029/2007WR006610.

King, J. (2011). Characterization of the shallow hydrogeology with estimates of recharge at a high-altitude mountainous site, Niwot Ridge, Front Range, Colorado [master's thesis]. University of Colorado Boulder.

Knowles, J. F., Harpold, A. A., Cowie, R., Zeliff, M., Barnard, H. R., Burns, S. P., Blanken, P. D., Morse, J. F., and Williams, M. W. (2015). The relative contributions of alpine and subalpine ecosystems to the water balance of a mountainous, headwater catchment. *Hydrol. Process.*, 29: 4794– 4808. doi: 10.1002/hyp.10526.

Kormos, P. R., McNamara, J. P., Seyfried, M. S., Marshall, H. P., Marks, D., & Flores, A. N. (2015). Bedrock infiltration estimates from a catchment water storage-basedmodeling approach in the rain snow transition zone. Journal of Hydrology, 525, 231–248. https://doi.org/10.1016/j.jhydrol.2015.03.032

Kosugi, K., S. Katsura, M. Katsuyama, and T. Mizuyama (2006), Water flow processes in weathered granitic bedrock and their effects on runoff generation in a small headwater catchment, Water Resour. Res., 42, W02414, doi:10.1029/2005WR004275.

Kosugi, K., S. Katsura, T. Mizuyama, S. Okunaka, and T. Mizutani (2008), Anomalous behavior of soil mantle groundwater demonstrates the major effects of bedrock groundwater on surface hydrological processes, Water Resour. Res., 44, W01407, doi:10.1029/2006WR005859.

Langston, A. L., Tucker, G. E., Anderson, R. S., & Anderson, S. P. (2015). Evidence for climatic and hillslope-aspect controls on vadose zone hydrology and implications for saprolite weathering. *Earth Surface Processes and Landforms*, *40*(9), 1254–1269. https://doi.org/10.1002/esp.3718

Leopold, M., Völkel, J., Huber, J., and Dethier, D. (2013): Subsurface architecture of the Boulder Creek Critical Zone Observatory from electrical resistivity tomography. Earth Surface Processes and Landforms 38: 1417-1431, doi:10.1002/esp.3420.

Liu, F., Bales, R. C., Conklin, M. H., & Conrad, M. E. (2008). Streamflow generation from snowmelt in semi-arid, seasonally snow-covered, forested catchments, Valles caldera, New Mexico. Water Resources Research, 44(12), 1–13. https://doi.org/10.1029/2007WR006728

Liu, F., Williams, M. W., and Caine, N. (2004), Source waters and flow paths in an alpine catchment, Colorado Front Range, United States, *Water Resour. Res.*, 40, W09401, doi:10.1029/2004WR003076.

Losleben, M.V. 1990. Climatological data from Niwot Ridge, East Slope, Front Range, Colorado, 1989. University of Colorado Long-Term Ecological Research Data Report 90/1. 108 pp

Manning, A. H., and Caine, J. S. (2007). Groundwater noble gas, age, and temperature signatures in an alpine watershed: Valuable tools in conceptual model development. Water Resources Research, 43(4), 1–16. https://doi.org/10.1029/2006WR005349

Manning, A. H., and Solomon, D. K. (2003). Using noble gases to investigate mountain-front recharge. Journal of Hydrology, 275(3–4), 194–207. https://doi.org/10.1016/S0022-1694(03)00043-X

Manning, A. H., and Solomon, D. K. (2005). An integrated environmental tracer approach to characterizing groundwater circulation in a mountain block. Water Resources Research, 41(12), 1–18. https://doi.org/10.1029/2005WR004178

Maréchal, Jean-Christophe & Dewandel, Benoit & Ahmed, Shakeel & Galeazzi, Laurent & Zaidi, Faisal. (2006). Combined estimation of specific yield and natural recharge in a semi-arid groundwater basin with irrigated agriculture. Journal of Hydrology. 329.

Markovich, K., H, Manning, A. H., Condon, L. E., & McIntosh, J. C. (2019). Mountain-block recharge: A review of current understanding. Water Resources Research, 55, 8278– 8304. https://doi.org/10.1029/2019WR025676

Martin, C, Kampf, SK, Hammond, JC, Wilson, C, and Anderson, SP (2021): Controls on streamflow densities in semiarid Rocky Mountain catchments. Water 13(4), 521, doi: 10.3390/w13040521

Maurer, D.K., and D. L. Berger, Subsurface flow and water yield from watersheds tributary to Eagle Valley hydrographic area, west-central Nevada, U.S. Geological Survey Water-Resources Investigation Report 97-4191, 1997.

Maurya, A. S., Shah, M., Deshpande, R. D., Bhardwaj, R. M., Prasad, A., & Gupta, S. K. (2011). Hydrograph separation and precipitation source identification using stable water isotopes and conductivity: River ganga at Himalayan foothills. Hydrological Processes, 25(10), 1521–1530. https://doi.org/10.1002/hyp.7912

McFarlane, M.J. (1992). Groundwater movement and water chemistry associated with weathering profiles of the African surface in parts of Malawi. Geological Society, London, Special Publications, 66, 101-129, 1 https://doi.org/10.1144/GSL.SP.1992.066.01.06

McGlynn, B. L., J. J. McDonnell, J. B. Shanley, and C. Kendall. (1999). Riparian zone flowpath dynamics during snowmelt in a small headwater catchment, J. Hydrol., 222, 75– 92.

Miller, M. P., Tesoriero, A. J., Capel, P. D., Pellerin, B. A., Hyer, K. E., and Burns, D. A. (2016), Quantifying watershed-scale groundwater loading and in-stream fate of nitrate using high-frequency water quality data, Water Resour. Res., 52, 330– 347, doi:10.1002/2015WR017753.

Mills, TJ, Anderson, SP, Bern, C, Aguirre, A, and Derry, LA (2017): Colloid mobilization and seasonal variability in a semi-arid, headwater stream. J Environ. Qual. 46 (1): 88-95, doi:10.2134/jeq2016.07.0268.

Montgomery, DR, Dietrich, WE, Torres, R, Anderson, SP, Heffner, JT, and Loague, K (1997): Hydrologic response of a steep unchanneled valley to natural and applied rainfall. Water Resources Research 33(1): 91-109.

Morse, J. and M. Losleben. 2019. Air temperature, ET, and solar radiation data for B1 data logger (DP219), 1987 - 2006. ver 5. Environmental Data Initiative. https://doi.org/10.6073/pasta/24c259ffafc46ebf7b6c21d2e9362c68 (Accessed 2021-06-29).

Mulholland, P. J. (1993), Hydrometric and stream chemistry evidence of three storm flowpaths in Walker Branch Watershed, J. Hydrol. Amsterdam, 151, 291– 316, doi:10.1016/0022-1694(93)90240-A.

Nathan, RJ and McMahon, TA. (1990). Evaluation of automated techniques for base flow and recession analyses. Water Resources Research 26: 1465-1473.

National Atmospheric Deposition Program (NRSP-3). (2021). NADP Program Office, Wisconsin State Laboratory of Hygiene, 465 Henry Mall, Madison, WI 53706.

Niwot Ridge Long-Term Ecological Research Site (LTERS). (2021). http://culter.colorado.edu/NWT/site_info/climate/climate.html. Cited 9 July 2021

Noguchi, S., Y. Tsuboyama, R. C. Sidle, and I. Hosoda (1999), Morphological characteristics of macropores and the distribution of preferential flow pathways in a forested slope segment, Soil Sci. Soc. Am. J., 63, 1413– 1423.

Pandey, S. and Rajaram, H. (2016): Modeling the influence of preferential flow on the spatial variability and time-dependence of mineral weathering rates. Water Resources Research 52 (12): 9344-9366, doi: 10.1002/2016WR019026

Peet, RK (1981): Forest vegetation of the Colorado Front Range: Composition and dynamics. Vegetatio 45 (1): 3-75.

Pollock, D.W., 2012, User guide for MODPATH version 6—A particle-tracking model for MODFLOW: U.S. Geological Survey Techniques and Methods, book 6, chap. A41, 58 p.

Prudic, D.E., Konikow, L.F., and Banta, E.A. (2004). new streamflow-routing package (SFR1) to simulate stream-aquifer interaction with MODFLOW-2000: U.S. Geological Survey Open-File Report 04-1042, p. 95.

Reynolds, J.F. and Knight, D.H. (1973). Magnitude of snowmelt and rainfall interception by litter in lodgepole pine and spruce-fir forests in Wyoming. Northwest Sci. 1973, 47, 50–60

Rossi, M. W., Anderson, R. S., Anderson, S. P., & Tucker, G. E. (2020). Orographic controls on subdaily rainfall statistics and flood frequency in the Colorado Front Range, USA. Geophysical Research Letters, 47, e2019GL085086. https://doi.org/10.1029/2019GL085086

Rush, M, Rajaram, H, Anderson, RS, and Anderson, SP (in review): Modeling aspect-controlled evolution of ground thermal regimes on montane hillslopes. JGR- Earth Surface. Submitted 13 Feb 2021.

Rutledge, A. T. 1998. Computer Programs for Describing the Recession of Ground-Water Discharge and for Estimating Mean Ground-Water Recharge and Discharge from Streamflow Records - Update. In Water-Resources Investigations Report. Reston, Virginia: U.S. Geological Survey

Saberi, L., McLaughlin, R. T., Crystal Ng, G. H., La Frenierre, J., Wickert, A. D., Baraer, M., … Mark, B. G. (2019). Multi-scale temporal variability in meltwater contributions in a tropical glacierized watershed. Hydrology and Earth System Sciences, 23(1), 405–425. https://doi.org/10.5194/hess-23-405-2019

Sánchez-Murillo, Ricardo & Brooks, Erin & Elliot, William & Gazel, Esteban & Boll, Jan. (2014). Baseflow recession analysis in the inland Pacific Northwest of the United States. Hydrogeology Journal. 23. 287-303. 10.1007/s10040-014-1191-4.

Sanford,W., Plummer, L.,McAda,D., Bexfield, L.,&Anderholm, S. (2004).Use of environmental tracers to estimate parameters for a predevelopment ground-water-flowmodel of theMiddle Rio Grande Basin, NewMexico,U.S. *Geological SurveyWater-Resources Investigations Report*, *03-4286*, 110.

Scanlon, B. R., Healy, R. W., Cook, P. G. (2002). Choosing appropriate techniques for quantifying groundwater recharge. *Hydrogeology Journal*, *10*:18–39.

Shea, N. (2013). Spatial Patterns of Mobile Regolith Thickness and Meteoric 10Be in Gordon Gulch, Front Range, CO [master's thesis]. University of Connecticut.

Smull, E. (2015). Nitrate removal along a Colorado montane headwater stream: The role of bidirectional hydrologic exchange to catchment scales [master's thesis]. Colorado State University.

Somers, LD, McKenzie, JM. (2020). A review of groundwater in high mountain environments. *WIREs Water*. 7:e1475. https://doi.org/10.1002/wat2.1475

St. Clair, J., Moo, S., Holbrook, W. S., Perron, J. T., Riebe, C. S., Martel, S. J., et al. (2015). Geophysical imaging reveals topographic stress control of bedrock weathering. Science, 350(6260), 534–539. https://doi.org/10.1126/science.aab2210

Tokunaga, T. K., Wan, J., Williams, K. H., Brown, W., Henderson, A., Kim, Y., et al. (2019). Depth- and time-resolved distributions of snowmelt-driven hillslope subsurface flow and transport and their contributions to surface waters. Water Resources Research, 55, 9474– 9499. https://doi.org/10.1029/2019WR025093

Uchida, T., Y. Asano, N. Ohte, and T. Mizuyama (2003), Seepage area and rate of bedrock groundwater discharge at a granitic unchanneled hillslope, Water Resour. Res., 39(1), 1018, doi:10.1029/2002WR001298.

Van der Hoven, S. J., Solomon, D. K., and Moline, G. R. (2003), Modeling unsaturated flow and transport in the saprolite of fractured sedimentary rocks: Effects of periodic wetting and drying, Water Resour. Res., 39, 1186, doi:10.1029/2002WR001926, 7.

Voeckler, H. M., Allen, D. M., & Alila, Y. (2014). Modeling coupled surface water-groundwater processes in a small mountainous headwater catchment. Journal of Hydrology, 517, 1089–1106. https://doi.org/10.1016/j.jhydrol.2014.06.015

Weirman, D., Walker, J., and Udita, T. (2019). How much water is in the Guadalupe? A baseflow analysis. https://gato-docs.its.txstate.edu/jcr:c39ea6a9-6537-4d16-bd82-8f323b5f6c76

White, T, Brantley, S, Banwart, S, Chorover, J, Dietrich, W, Derry, L, Lohse, K, Anderson, S, Aufdenkampe, A, Bales, R, Kumar, P, Richter, D, and McDowell, B (2015): Chapter 2—The role of critical zone observatories in critical zone science. In: Developments in Earth Surface Processes 19:15-78, doi:10.1016/B978-0-444-63369-9.00002-1.

Wilson, J. L., and H. Guan (2004). Mountain-block hydrology and mountain-front recharge. In Hogan, J. F., Phillips, F. M., and Scanlon, B. R., (eds.), *Groundwater Recharge in a Desert Environment: The Southwestern United States Volume 9* (pp. 113−137). Washington, D.C.: American Geophysical Union.

Wilson, S. (2017). Groundwater-surface water exchange within montane and alpine regions of the Front Range and Rocky Mountains, Colorado, 102.

Wright, E.P. (1992). The hydrogeology of crystalline basement aquifers in Africa. *Geological Society, London, Special Publications, 66*, 1 - 27.

Xie, J., Liu, X., Wang, K., Yang, T., Liang, K., & Liu, C. (2020). Evaluation of typical methods for baseflow separation in the contiguous United States. Journal of hydrology, 583, . doi: 10.1016/j.jhydrol.2020.124628

Appendix A. Summary of Geologic Investigations in Gordon Gulch

The four primary hydrogeologic units of Gordon Gulch include soil, saprolite, weathered bedrock, and bedrock. A comprehensive literature review was performed to identify the range in thickness and values of hydraulic conductivity for each geologic unit. Findings from the literature review on the differences in the thickness of the hydrogeologic units are summarized in **Table A-1**.

Table A-2 summarizes the range of hydraulic conductivity values identified for the four hydrogeologic units from the literature review. Cited literature includes studies done in Gordon Gulch, along with values for similar rock types across different locations. The range in values of hydraulic conductivity was used during model calibration as upper and lower constraints of appropriate values to be modeled.

Table A-1. Summary of the thickness and depth to the four hydrogeologic units in Gordon Gulch based on studies performed in the catchment.

Unit	Hydrogeologic Unit Thickness (m)				Depth to Hydrogeologic Unit (m)			Reference
	Avg.	Range	Avg. North-*Facing* Slope	Avg. South-*Facing* Slope	Avg. Depth to Layer	Avg. – North-*Facing* Slope	Avg. South-*Facing* Slope	
Soil	0.9	0.3 – 2.0			N/A			Befus et al., 2011
		0.1 - 0.8						Leopold, 2013
	0.39	0.3 to 2.5	0.44	0.37				Shea, 2013
			2.3±0.76	2±0.80				Bandler, 2016[1]
	0.90	0.20-1.70	0.74	1.1				Eilers et al., 2012
			0.4 - 0.45	0.3 - 0.35				Hinckley et al., 2014a
Saprolite			8	10				Bandler, 2016
					3.2 ± 1.9			Befus et al., 2011
		0.4 - 5.1			3.0 – 4.1			Leopold, 2013
		5 to 10						Henning, 2016
			2.4					Anderson and Ragar, 2021a; Anderson and Ragar, 2021b
	8.8	8 – 14			3.3	8		Dethier and Lazarus, 2006[2]
						12.2		Anderson and Ragar, 2021a; Anderson and Ragar, 2021b
					4.3 ± 3.0			Leopold, 2013
	10	2 – 21*				< 10	5 - 7	Befus et al., 2011
	15							Henning, 2016
Bedrock	N/A				0 to 30	15	5 to 10	Dethier & Lazarus, 2006
					10 to 40			St. Clair, 2015
						8.5	14	Eldam et al., 2016
						14.6	7.6	Anderson and Ragar, 2021a; Anderson and Ragar, 2021b
						15	10	Leopold, 2013
						10.9± 3.6	8.7 ± 1.3	Bandler, 2016
					11.7 to 14.8	15	5 - 10, avg = 8	Befus et al., 2011

1. Reported from seismic survey results which includes soil and mobile regolith.
2. Depth and thickness of saprolite inferred from well log data interpolated throughout the foothills using a kriged surface in ArcGIS.

Table A-2. Summary of literature review of hydraulic conductivity values for soil, saprolite, weathered bedrock, and bedrock in Gordon Gulch or similar settings.

Unit	Average Hydraulic Conductivity (m/d)	Range in Hydraulic Conductivity (m/d)	Location	Source
Soil	5.0	0.2 - 20.7 m/d	Gordon Gulch	Hinckley et al., 2014a
	0 – 10cm: 2.8			
	10 -25cm: 7.1			
	2			Henning, 2016
	7.6			Langston et al., 2015
	6.9	0.1 - 45		Buraas, 2009
		0.9 – 0.09	Handcart Gulch, CO	Caine et al., 2006
	17.3			Kahn et al., 2008
Saprolite	1		Gordon Gulch	Henning, 2016
	0.02			Langston et al., 2015
		10^{-2} – 10	Saprolite aquifer in Zambia & Tanzania	Jones, 1985
	0.3	0.05 – 3.5	Victoria Province	Houston and Lewis, 1988
	0.09	0.006 – 0.9	Burkina Faso	Compaore et al., 1997
	0.35	0.012 – 0.9	Africa	Wright, 1992
	0.09		Africa	Jones, 1985
	0.04	0 – 0.4	Malawi	McFarlane, 1992
	0.008		Tennessee	Van der Hoven, 2003
	0.2		Andhra Pradesh, India	Dewandel et al., 2006
Weathered Bedrock	3.2×10^{-2}		Gordon Gulch	Henning, 2016
		0.001 – 0.01	Niwot Ridge, CO	King, 2011
	0.9		Andhra Pradesh, India	Dewandel et al., 2006
		0.09 – 17.3	Panola hillslope, GA	James et al., 2010
Bedrock	0.05 m/d (fractured granite)		Gordon Gulch	Anderson, Rajaram, Anderson, 2019
	3.2×10^{-3}			Henning, 2016
	2 (fractured bedrock)			Langston et al., 2015
		0.00009 – 0.09	Handcart Gulch, CO	Caine et al., 2006
	0.0004			Kahn et al., 2008
		0.0009 – 0.2	Panola hillslope, GA	James et al., 2010

1. Value not measured; hydraulic conductivity value for granitic bedrock sourced from Freeze and Cherry, 1979

Appendix B. Precipitation Data

Precipitation data was collected from three meteorological stations; two within Gordon Gulch (the North and South MET stations) and a third located approximately 2 km southwest of Gordon Gulch (CO94 station). Of these three precipitation stations, none had a complete precipitation record for water years 2012 through 2020. Additionally, winter precipitation data from the MET stations in Gordon Gulch cannot be used because precipitation gages are unheated, so precipitation cannot be separated by rain or snow. Therefore, a gap-fill ranked procedure was applied to create a complete precipitation record for water years (WY) 2012 – 2020. CO94 station was used as the base dataset. Inaccurate or missing measurements in the CO94 dataset, such as during September 2013 and after 2017 when the CO94 data record ends, were replaced with data from the South MET station. However, the South MET station was missing and/or produced inaccurate precipitation measurements from September 2013 and throughout water years 2016 – 2017. During these periods, data was instead replaced with measurements from the North MET station. Lastly, an average water year precipitation record was produced by calculating the mean daily amount across each individual day of water years 2012 – 2020. Due to extreme precipitation events in September 2013 and July 2015, data from these two months were excluded from the average dataset, so as not to skew mean precipitation towards these extreme events. The compiled dataset of mean daily precipitation measurements showing measured daily values from the gap-fill ranked procedure and the mean daily measurements are presented in **Table B-1** and **Figure B-1**. The compiled dataset of precipitation measurements was used for model calibration.

During the gap-fill ranked procedure, precipitation records from the North and South MET stations were compared to identify differences between them. The two MET stations are

located on opposing hillslopes. The South MET station is located in an exposed clearing while the North MET station is located under the tree canopy. Both stations are located approximately 1m above ground surface and neither precipitation gage is heated. Rainfall records from the North and South MET stations were compared to identify differences between them. On average, the South MET station records 20% more precipitation annually than the North MET station (0.55 m per year vs 0.40 m per year, respectively). The difference in precipitation is likely a result of canopy interception at the North MET station. This phenomenon is well known (Hamilton and Rowe, 1949), and is consistent with a Reynolds and Knight (1973) finding that rain events less than 10 mm in subalpine forests rarely penetrated soil layers because the rain was mostly intercepted by the canopy or absorbed by forest litter (Reynolds and Knight, 1973; Cowie, 2010).

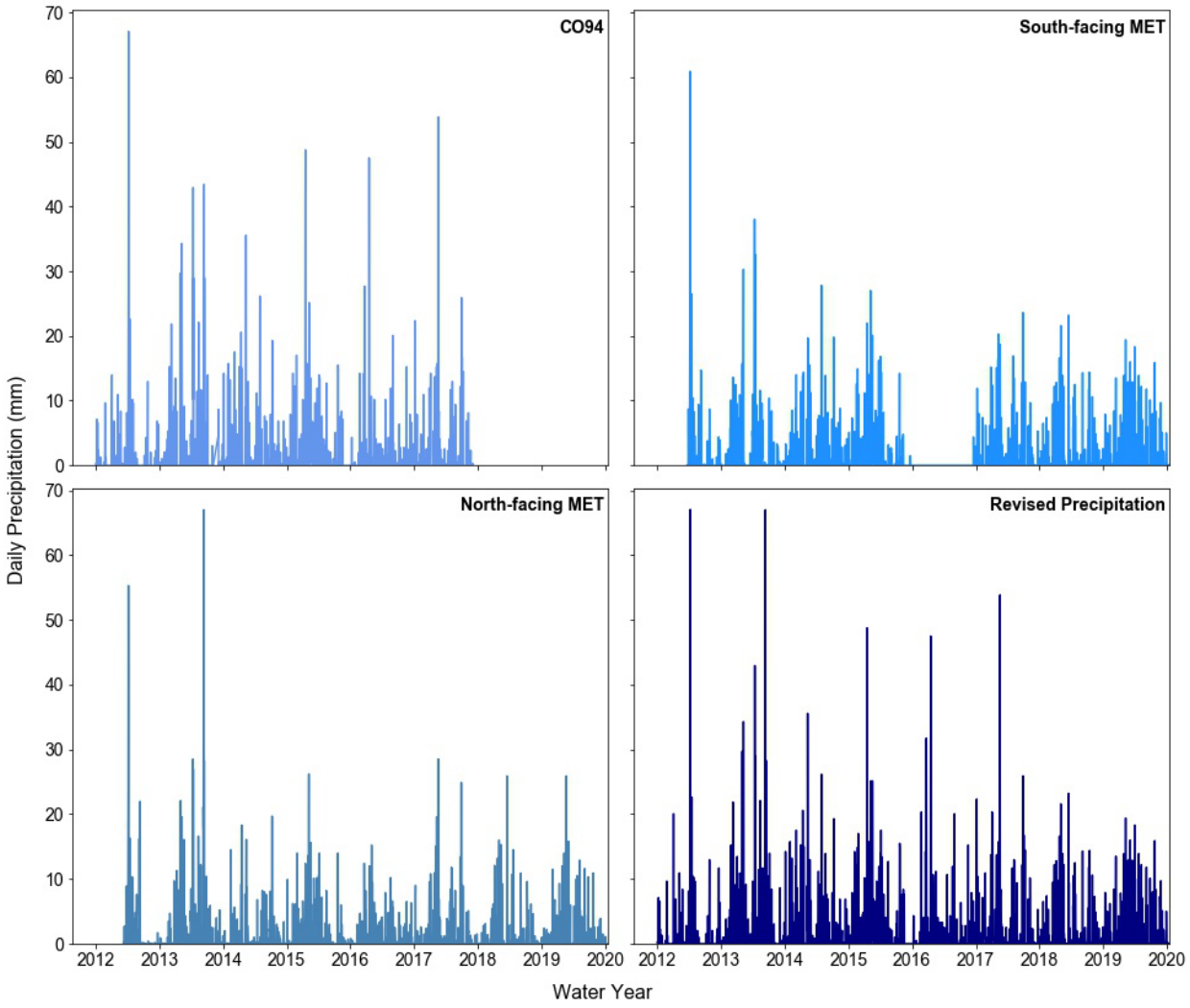

Figure B-1. Graph of total daily precipitation measurements recorded at the North-facing and South-facing MET stations, the CO94 station, and the rank-filled revised precipitation record for water years 2012 through 2019.

Table B-1. Summary of precipitation data, reported by month of the water year for years 2012 – 2020. The total annual precipitation, along with the mean monthly precipitation across the data record is also reported. Dashes indicate data is unavailable.

Month of Water Year	Total Monthly Precipitation, by Water Year (m)									Mean Monthly Total (m)
	2012	2013	2014	2015	2016	2017	2018	2019	2020	
October	0.16	0.030	0.035	0.026	0.050	0.012	0.059	0.053	0.049	0.039
November		0.002	0.000	0.024	0.030	0.024	0.022	0.024	0.029	0.019
December		0.034	0.021	0.017	0.000	0.040	0.015	0.006	0.023	0.019
January	0.021	0.007	0.055	0.016	0.006	0.077	0.013	0.037	0.002	0.026
February	0.014	0.061	0.052	0.099	0.024	0.027	0.023	0.010	0.056	0.041
March	0.000	0.060	0.055	0.021	0.090	0.038	0.035	0.052	0.044	0.044
April	0.036	0.079	0.070	0.135	0.098	0.082	0.049	0.055	0.037	0.071
May	0.041	0.108	0.110	0.140	0.054	0.136	0.081	0.094	0.030	0.088
June	0.014	0.016	0.006	0.039	0.015	0.006	0.041	0.083	0.039	0.029
July	0.214	0.125	0.081	0.086	0.029	0.033	0.051	0.064	0.034	0.080
August	0.025	0.081	0.057	0.030	0.042	0.052	0.007	0.036	0.012	0.038
September		0.233	0.034	0.005	0.032	0.054	0.020	0.036	-	0.052
Total Annual Precipitation (m)	0.53	0.84	0.58	0.64	0.47	0.58	0.42	0.55	0.36*	

*Total annual precipitation is not a complete record due to months without precipitation data.

Appendix C. Snow Data

Snow depth, snow cover duration, and density data were measured by the BcCZO using snow poles and snow pits in Gordon Gulch for water years 2012 through 2020. Snow depth was visually estimated by reviewing time-lapse imagery at 10-minute intervals from two cameras, each aimed at a snow pole with 10 cm intervals marked; one was stationed on the north-facing slope, and one on the south-facing slope (Anderson and Ragar, 2021c). Snow density was measured in snow pits on 16 dates between 2012 and 2018, using a snow cutter.

The average daily snow depth is 0.08 m in Gordon Gulch, but depth varies greatly over the winter and across the north- and south-facing slopes, as shown in **Table C-1** and **Figure C-1**.

Table C-1. Average daily snow depth measured on the north and south facing slopes for years 2012 through 2020.

Year	Average Daily Snow Depth (m)		
	North-facing slope (m)	South-facing slope (m)	Difference (m)
2012	0.29	0.06	0.31
2013	0.05	0.05	0.04
2014	0.03	0.07	0.04
2015	0.19	0.04	0.15
2016	0.12	0.03	0.07
2017	0.10	0.02	0.06
2018	0.07	0.01	0.06
2019	0.11	0.03	0.11
Mean	**0.12**	**0.04**	**0.12**
SD	0.08	0.02	0.09

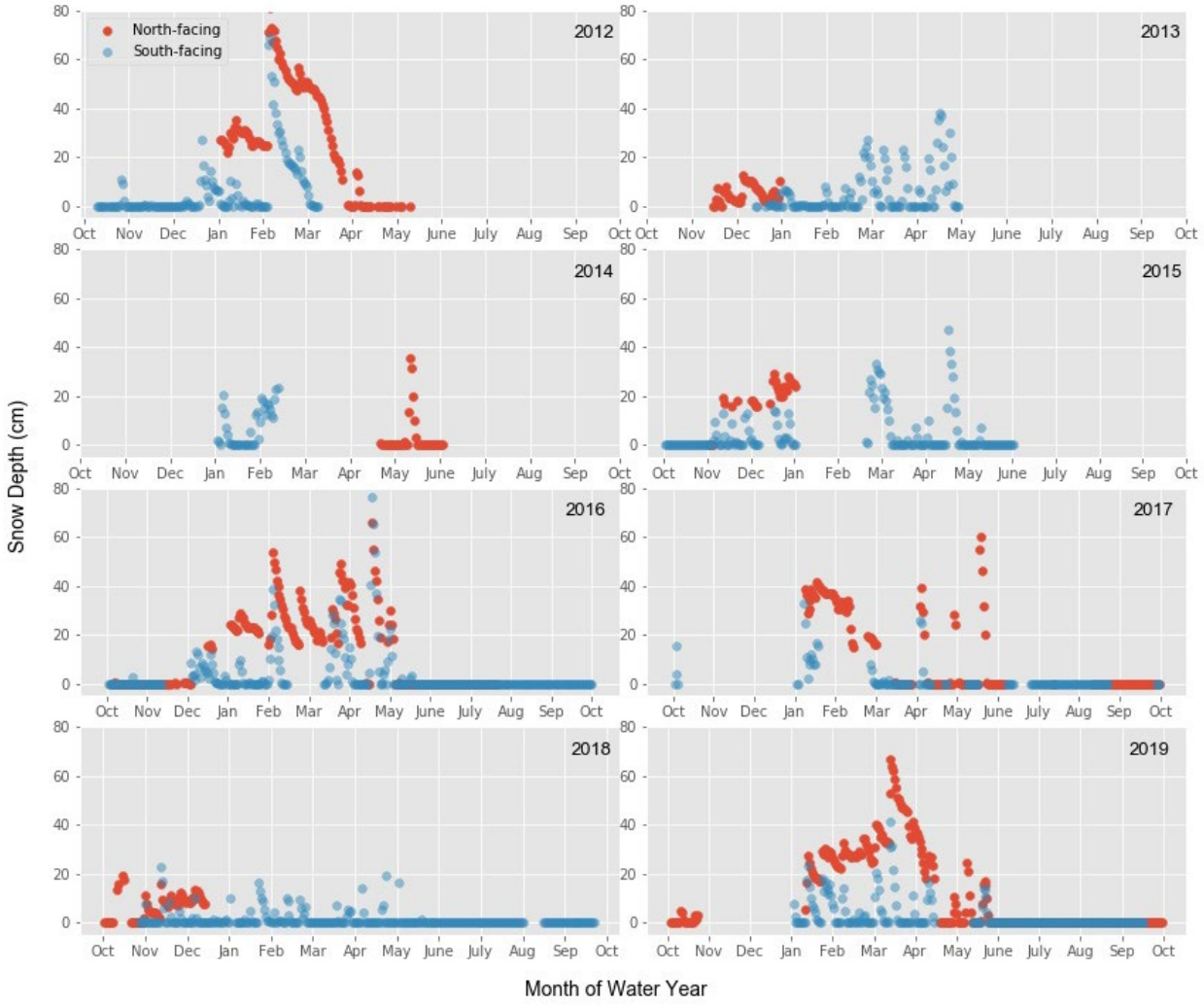

Figure C-1. Daily snow depths measured by snow poles on the north- and south-facing slopes throughout water years 2012 through 2019.

The daily change in snow depth was calculated to identify days with negative changes in depth, which were assumed to be due to melt (ignoring compaction). Next, average snow density was calculated using density cutter measurements taken from 16 snow pits in Gordon Gulch between 2008 to 2017 (Anderson, 2020). On average, snow density was 264 kg/m^3 but ranged from 214 to 323 kg/m^3, as shown in **Table C-2**. SWE was calculated by multiplying the negative change in daily snow depth by the average snow density. Since snow density data wasn't

available for water years 2018 and 2019, the nine-year snow density average (from 2008 – 2017) was applied instead.

Table C-2. Summary of average annual snow density, by water year

Year	Average Snow Density (kg/m^3)	Standard Deviation	Number of measurements
2008 – 2009	323.81	36	56
2010	319.26	81	128
2011	263.51	71	119
2012	225.39	79	131
2013	224.45	75	81
2014	284.92	70	104
2014	214.75	68	42
2016	233.62	50	26
2017	251.18	71	51
Mean	264	83	74
Std. deviation	39	14	38

To calculate snowmelt in Gordon Gulch, the snow water equivalent (SWE) was estimated from snow depth and density measurements. The average annual snow density was multiplied by the daily decline in snow depth to estimate the total snowmelt available as SWE. Since snow density data wasn't available for water years 2018 and 2019, the nine-year snow density average (from 2008 – 2017) was applied instead. **Figure C-2** plots daily estimated SWE on the north- and south-facing slopes for Gordon Gulch for water years 2012 through 2019.

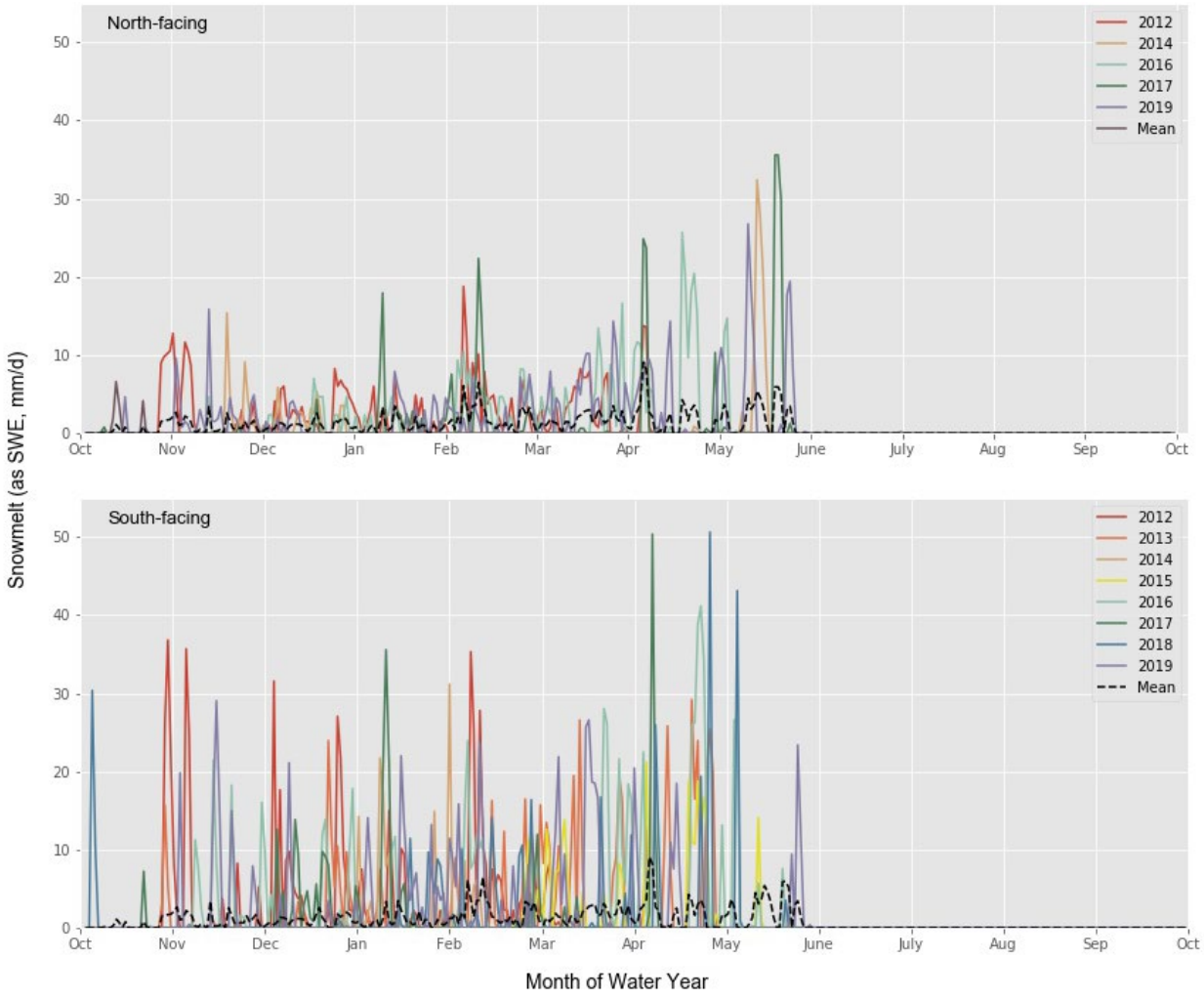

Figure C-2. Daily estimate of snowmelt as SWE on the north- and south-facing slopes in Gordon Gulch for water years 2012 through 2019.

Several other metrics were also derived including the number of melting events and the lag time between melting events. The persistence of snow was obtained by counting the number of days between the first day of snow and the last day of snow observed at the two snow poles. There were 19 discrete snow events on the north-facing slope for years 2012 through 2020. On the south-facing slope, there were 98 events over the same time period. On average, there were two major melt events on the north-facing slopes, while on the south-facing slopes there was an average of 11 melt events, as summarized in **Table C-3**.

Table C-3. Number of days with snow coverage on the north- and south-facing slopes by season. Data reported is an average value across years 2012 to 2020.

Year	Number of snow events	
	North-facing slope	South-facing slope
2012	1	8
2013	3	14
2014	2	14
2015	1	7
2016	1	9
2017	4	6
2018	1	12
2019	4	23
Mean	2	11
Standard Deviation	1.3	5.1

The lag time between snow melt events on the north and south facing slopes was also quantified by examining seven discrete spring melting events in 2012 and 2016-2019 as shown in **Table C-4**. The lag time is defined as the period between one slope having no snow present on the ground until the other slope also has no snow on the ground (recorded as 0 m depth of snow). This calculation is made by comparing the greatest differences in precipitation recorded at the MET stations (which mostly occur in the fall and the spring) and reviewing images of the ground surface to determine when snow is present. On average, snow melts entirely from the south facing slope 10 days prior to complete melt on the north facing slope. The start of melting occurs 1-2 days earlier on the south facing slope than on the north facing slope.

Table C-4. Days between snow melting events

Year	Days between Melt	Month
2012	27	March
2016	12	April
2016	2	May
2017	18	March
2017	2	April
2019	6	April
2019	2	May
Mean	10	
Standard deviation	9	

To characterize snow by aspect, the snowpack on the north-facing slope is persistent, deeper, and melts in one or two major events, whereas the snowpack on the south facing slope is intermittent and shallower. The snowpack on the north-facing behaves like a snowpack for a typical of alpine systems in the western United States. Conversely, the snowpack on the south-facing slope is episodic and experiences an average of 11 melt events per year. The difference in the number of melt events is attributed to a higher solar radiation due to less vegetation relative to the north-facing slopes (Langston et al., 2015). Snow is also observed on the ground longer on the north-facing slopes than the south-facing slopes, averages 154 days (5 months) vs. 4.5 days, respectively during the winter months (defined as December through March), see **Table C-3**. In 2011, snow remained on south-facing slopes for a maximum duration of 8 days and reached a maximum depth of 30 cm (Langston et al., 2015). During the same period on the north-facing slopes, snow remained on the surface from October through April, with a maximum depth of 35 cm (Langston et al., 2015). Hale (2018) determined that snow persistence on the south-facing slope was 33% and 58% on the north-facing slope (Hale, 2018). Langston et al. (2015) modeled six snowmelt events on the north facing slope and 20 snowmelt events on the south-facing slope over a 2-year period from 2010-2012 (Langston et al., 2015). As a result, there is more total SWE available from the south-facing slope than the north-facing slope (0.45 m vs. 0.40 m per

water year, respectively) due to the episodic melts. During the big melt in the spring, snow melts from the south-facing slopes one to two days prior to melt on the north-facing slopes.

Appendix D. Evapotranspiration Literature Review

A literature review was conducted to identify the range in ET values for Gordon Gulch estimated or used in other studies. A summary of the literature review is presented in **Table D-1**.

Previous works have stated that overall ET rates are higher on the south-facing slopes than the north-facing slopes due to higher temperatures, higher radiations, and less shade (Langston et al., 2015; Cowie, 2014). The periodic melting of snow on the south-facing slopes throughout the winter produce more supply of water to be used for ET. However, the concentrated snowmelt on the north-facing slope in the spring results in a greater availability and volume of water available for ET in the late spring and summer months, thus resulting in a shorter duration of high summer ET (this is also suspected to be the driver of a higher density of trees on the north facing slopes) (Cowie, 2010).

Table D-1. Summary of evapotranspiration measurements or values used in other studies for Gordon Gulch or similar environments.

ET (mm/yr)	Period of Record	Description	Location	Source
647	2010 - 2013	Estimated ET through the Budyko framework and a 10-year average end-of-century climate anomalies from the Weather Research Forecasting model (WRF)	Gordon Gulch	Hale, 2018[1]
955				
182.5 – 365	Not reported	ET rates used in a 2D numerical model of vadose zone dynamics under concentrated and episodic wetting conditions		Langston et al., 2015
710	2006 - 2009	Estimated from precipitation data, assuming 33% of precipitation consumed by ET	Saddle catchment, Niwot Ridge, CO	King, 2011
941	1987 – 2006	Daily ET measurements at B1 station, an upper montane ecological zone at an elevation of 2591 m	B1 Station, Niwot Ridge, CO	Niwot Ridge LTER[2]
930	1951 – 1980	Daily ET measurements at C1 station, a subalpine environment at an elevation of 3022 m	C1 Station, Niwot Ridge, CO	
54 - 178	2004 - 2005	Estimated ET using water budget and assumed ET ranged from 10% to 33% of precipitation	Handcart Gulch, CO	Kahn et al., 2008
474	2008 – 2012	ET estimated using the Hamon method	Como Creek, CO	Knowles et al., 2020
971		ET estimated using the Priestley-Taylor Method		
1297		ET estimated using the Penman Method		
257	1951 - 1985	Daily ET measurements at D1 station, an alpine tundra environment at an elevation of 3739 m	D1 Station, Niwot Ridge, CO	Greenland, 1989[3]
Not reported	1987	Direct measurements of ET using lysimeters and indirect measurements using the Penman method	Niwot Ridge, CO	Isard and Belding, 1989
2190	1980 – 2009	Daily forecast reference ET estimated by NOAA using temperature, cloud coverage, and solar radiation to be used as a reliable predictor for actual evapotranspiration	United States	NOAA Forecast Reference ET (FRET)
2555 - 4380		Network of agricultural weather stations in Colorado that calculate ET for various crops	Colorado	CoAgMET[4]

1. Used PET in the Distributed Hydrology Soil Vegetation Model (DHSVM) to investigate effects of climate change in Gordon Gulch. A rate of 647 mm/yr was applied as the base case, while 955 mm/yr was applied under a warming scenario. The basis for these values is based off the Budyko (1974) framework which is an empirical relationship that relates a catchment's evaporative fraction to an index of its aridity (PET/P).
2. LTER = long-term ecological research program
3. This study also determined that ET accounts for 41% to 66% of precipitation losses
4. Colorado Agricultural Meteorological Network (CoAgMet). No stations were located near Gordon Gulch or at similar elevations.
5. Greenland, 1989 quantified that 33% of precipitation was lost to ET at the D1 station and 50% of precipitation was lost to ET at the C1 station.

Appendix E. Groundwater Level Data

Three of the six wells, wells 1, 2, and 6, are equipped with Solinist Levelogger Junior pressure non-vented transducers set to automatically measure and record pressure at ten-minute intervals. The pressure transducer has a full-scale range of 10 m, and accuracy of ±1%; this results in accuracy of ±10 mm. The signal must be corrected for atmospheric pressure, which is measured with a Solinst Barologger suspended in a tree nearby in upper Gordon Gulch. There is also a Solinst Barologger suspended from a tree in lower Gordon Gulch that can be used to correct for errors in pressure readings, particularly during periods when temperatures drop below the datalogger specifications of -20°C. The pressure measurements are converted to depth to water measurements through a compensation process that corrects for sensor errors and uses the length of the cord attached to the pressure transducer (**Figure E-1**). Depth to water is then measured by subtracting the air-pressure corrected water pressure from the depth of the transducer (**Table E-1**). Manual depth to water measurements are also taken by the BcCZO field staff on a monthly basis for quality control purposes along with downloading the recorded data from the pressure transducers and collecting water samples. The resulting measurements in depth to water from period 11/21/2011 to 9/10/2019 from the compensation process are shown in **Figure E-2**.

Table E-1. Elevation of well tops and depth of pressure transducer in the well for the three monitored wells.

Well ID	Elevation of Well Top (m)	Depth to transducer[1] (m)
Well 1	2633.40	10.34
Well 2	2623.22	1.37
Well 6	2642.90	7.42

1. As measured by BcCZO field staff in July 30, 2020.

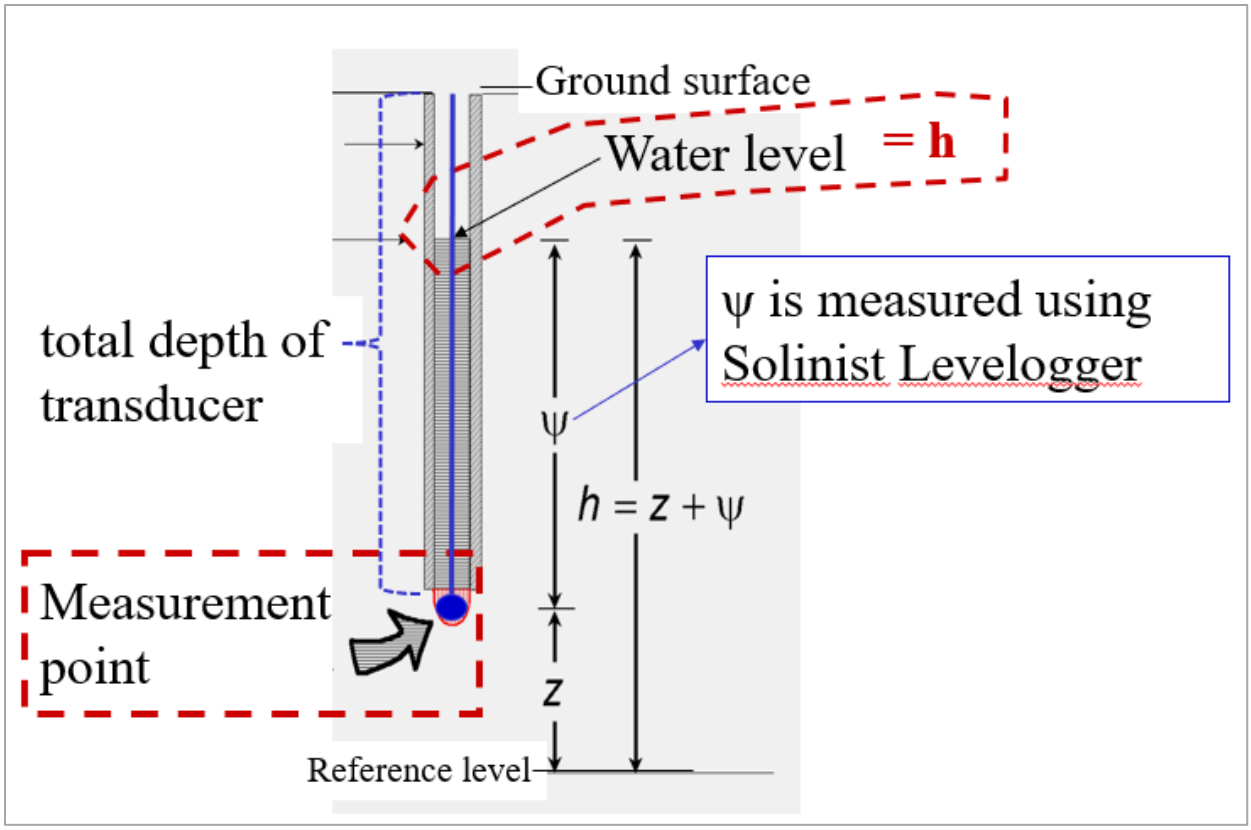

Figure E-1. Well schematic illustrating the method of measuring water levels in the three active monitoring wells in Gordon Gulch using a Solinist Levelogger and correcting for the depth to the transducer.

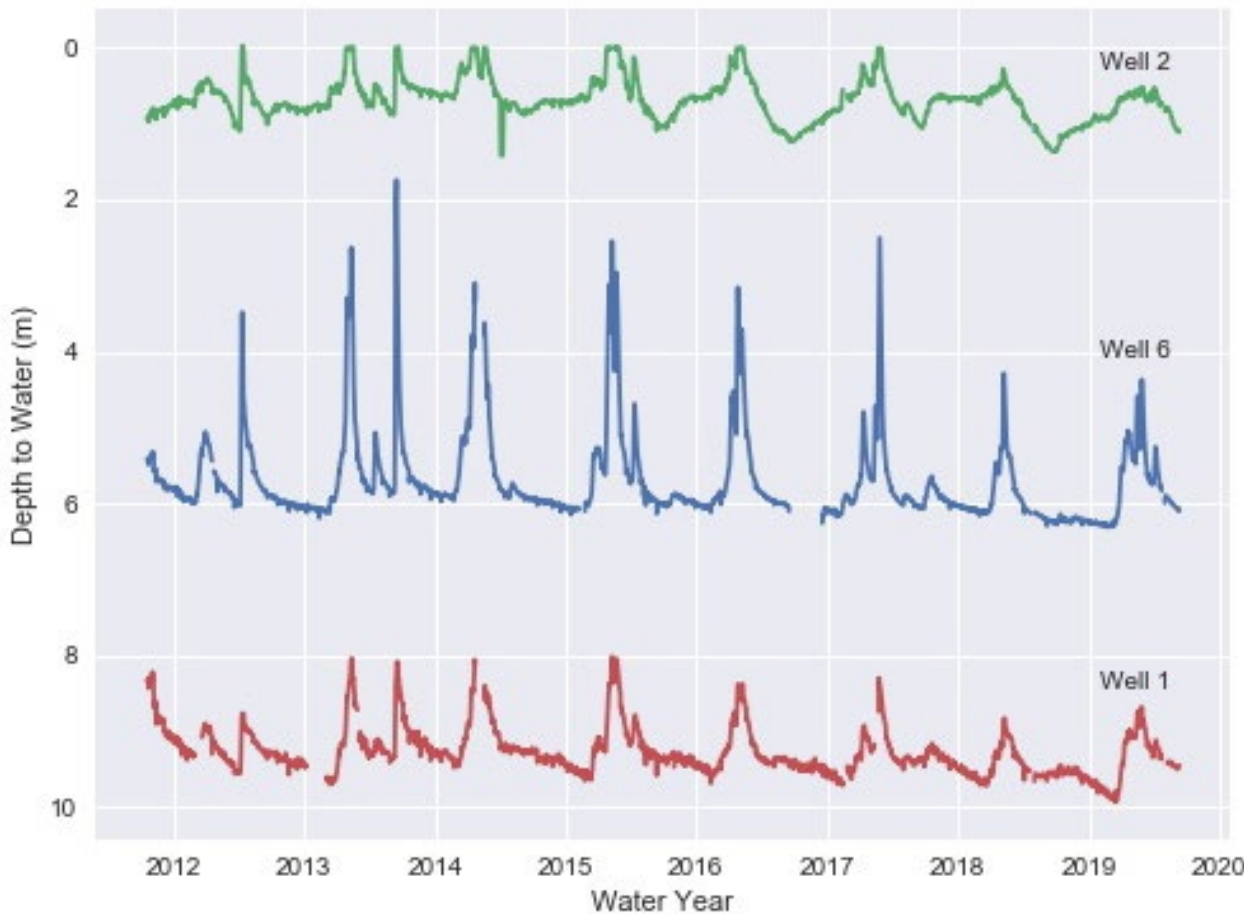

Figure E-2. Time series data of compensated depth to water measurements for wells 1, 2, and 6 for water years 2012 through 2020.

Appendix F. Baseflow

Description of Baseflow and Common Methods

Baseflow is an important component of streamflow; groundwater sustains stream discharge during dry periods when precipitation is low. Despite its importance, separating baseflow from streamflow is challenging, leading to some ambiguity about the term. For instance, some define baseflow by water source, usually identified as a source from deep groundwater (e.g., Hall, 1968; Weirman et al., 2019), while others define baseflow as the slowly varying component of hydrographs (Hewlett and Hibbert, 1967; Foks et al., 2019). Another approach is to use stream chemistry to identify baseflow (e.g., Hooper et al., 1990). While the details differ, baseflow is associated with the background flow in the channel, which most would attribute to discharge from long, deep flowpaths that travel in groundwater.

There are several methods of performing baseflow separation including isotopic or chemical tracers, which can be costly, time-intensive, and require field measurements, or non-tracer based methods which estimate baseflow using only streamflow discharge data through graphical and digital filter methods. Graphical methods estimate baseflow by identifying and connecting low-flow points of a streamflow hydrograph. Digital filter methods estimate baseflow by separating high and low-frequency signals from direct runoff and baseflow, respectively. For our purposes, a graphical method is the easiest approach to identifying baseflow. Xie et al. (2020) evaluated nine baseflow separation methods (four graphic methods and five digital filter methods) and found that the Eckhardt (2005) digital filter method had the best performance and the method's performance was independent of catchment characteristics (Xie et al., 2020).

The Eckhardt method is a recursive, two-parameter digital filter that parses streamflow hydrographs into two components: direct runoff and baseflow. Baseflow is associated with water

discharged from groundwater storage into the stream and is identified by low-frequency variations in streamflow (Eckhardt, 2005). Direct runoff is associated with surface runoff and interflow and identified by high-frequency variations in streamflow (Eckhardt, 2005). The Eckhardt two-parameter filter expands upon the common form of the digital filter method and establishes two assumptions: 1) total streamflow at each timestep is the sum of baseflow and direct runoff, and 2) during long periods of streamflow recession (in which streamflow is assumed to be maintained only by groundwater), groundwater discharge from the aquifer to the stream is linearly proportional to the aquifer's storage. The filter relies on two parameters, a recession constant (α) and the maximum baseflow index (BFI_{max}).

The recession constant, α, describes baseflow decay in terms of the rate of volumetric storage depletion between timesteps; it is essentially the rate at which streamflow declines in the absence of groundwater recharge (Foks et al., 2019; Eckhardt, 2005):

$$\alpha = e^{\frac{-\Delta t}{\tau}} \quad (1)$$

where Δt is the time step length (typically, equal to one day) and τ is the characteristic recession time constant (days per log cycle) (Eckhardt, 2008). Typical values of the recession constant range from 0.90 to 0.978 with values of 0.925 and 0.978 being common in cited literature (Nathan and McMahon, 1990; Chapman, 1991). The recession constant can be determined through recession analysis in which the recession curve, or the falling limb of a streamflow hydrograph, is related to groundwater storage depletion and flow to a stream (Rutledge, 1998). In the USGS Groundwater Toolbox, the RECESS program offers an automated approach to reviewing recession curves and estimating values of the recession time constant and recession constant from daily stream hydrographs.

The second parameter, BFI_{max}, is the long-term maximum value of the baseflow index (BFI) for a given recession constant. BFI is defined as the ratio of baseflow to streamflow and is influenced by catchment geology (Bloomfied et al., 2009). Short-term values of BFI may exceed BFI_{max}. This parameter is less established and currently there are no objective methods to estimate BFI_{max}. Generally, BFI_{max} should reflect the hydrologic and hydrogeologic conditions of the stream catchment (Barlow et al., 2017). Eckhardt (2008) suggested values of BFI_{max} based on hydrogeological conditions for three types of catchments: BFI_{max} = 0.8 for perennial streams with porous aquifers, 0.5 for ephemeral streams with porous aquifers, and 0.25 for perennial streams with hard rock aquifers. However, to estimate site-specific values of BFI_{max} without a field investigation of hydrogeological conditions, Collischonn and Fan (2013) developed a backwards filter method that uses stream discharge and estimated the recession constant to calculate BFI_{max}. Collischonn and Fan's method to estimate BFI_{max} uses the relationship between the recession constant and baseflow, which is expressed as (Nathan and McMahon, 1990):

$$b_k = \alpha b_{k-1} \tag{2}$$

where b_k is baseflow (L^3/t^{-1}) and b_{k-1} is baseflow from the prior timestep (k-1) (L^3/t^{-1}). Eq. (2) can be transformed into a backwards moving filter that by rearranging the terms. The backwards filter can then be applied to a stream hydrograph to estimate the maximum possible value of baseflow for a given value of α, where:

$$b'_{k-1} = \frac{b'_k}{\alpha} \tag{3}$$

where b' and b'_{k-1} are estimates of baseflow obtained by the backwards filter. The backwards filter of Eq. (3) can then be applied to a stream hydrograph which ends with a recession (ex: August 30), when observed streamflow is assumed to be entirely composed of baseflow (Collischonn and Fan, 2013). The backwards filter is applied to estimate baseflow for the day

prior to the end of the recession period (b'_{k-1}, ex: August 29) and the procedure is repeated backwards to the first day of observed recession period (ex: July 1). Results from the backwards filter estimate a hydrograph of b' which represents the maximum amount of possible baseflow for a given recession period, for a given value of α. The value of BFImax can then be estimated by dividing the sum of calculated daily baseflow values (b') by the sum of daily streamflow values:

$$BFI_{max} = \frac{\sum_{k=1}^{N} b\prime_k}{\sum_{k=1}^{N} y_k} \quad (4)$$

where BFI_{max} is the ratio of total baseflow to total streamflow, N is the length of the recession period (days), y_k is the total streamflow (L^3t^{-1}) at time step k, and b' is baseflow obtained from the backwards filter. Collischonn and Fan's backwards filter has been implemented in the USGS Groundwater Toolbox, which offers an automated approach to apply the backwards filter to stream hydrographs, obtain estimates of b', and ultimately, estimate BFI_{max} from daily stream hydrographs.

After obtaining estimates for α and BFImax, the Eckhardt two-parameter filter can be applied to the stream hydrograph to estimate baseflow:

$$b_k = \frac{[(1-BFI_{max})\alpha b_{k-1} + (1-\alpha)BFI_{max} y_k]}{(1-\alpha BFI_{max})} \quad (5)$$

subject to $b_k \leq y_k$. The Eckhardt two-parameter filter is passed over the streamflow hydrograph only once (as opposed to the single parameter filter method in which the filter can be passed over as many times as desired to increase the 'smoothing' effect of the filter). For values of $b_k < 0$ and the initial value of baseflow where k=1, b_k is set to:

$$b_k = 0.9(BFI_{max})(y_k) \quad (6)$$

The final result is a daily estimate of baseflow, derived from daily streamflow records.

Estimating Baseflow in Gordon Gulch

The USGS Groundwater Toolbox (Barlow et al., 2017) was employed to estimate the two digital filter parameters, α and BFI_{max}, and then apply the Eckhardt two-parameter filter to estimate baseflow in Gordon Gulch using. The process involved four-steps:

1. Select recession curves to analyze from the streamflow record and select the duration of recession period
2. Estimate α from the recession curves
3. Estimate BFI_{max} using the estimate of α and a backwards filter
4. Apply the Eckhardt two-parameter filter using estimates of α and BFI_{max} to compute baseflow

Baseflow was estimated from average daily streamflow measurements from the lower gauge for water years 2012 to 2019.

Step 1. Recession Analysis:

The recession analysis for Gordon Gulch streamflow was performed using the RECESS program of the USGS Groundwater Toolbox (Barlow et al., 2017; Rutledge, 1998). The recession curve, or the falling limb of a streamflow hydrograph, is related to groundwater storage depletion and groundwater discharge to the stream. The recession constant (α) can be determined by constructing a master discharge recession curve over a period of declining streamflow. The length of time to analyze recession following a discharge peak is a matter of some discussion; if the number of days in a recession period is too large, then too few recession periods will be detected. Previous studies cite a range of recession lengths from 10 days (Miller et al., 2016), 32 days (Sanchez-Murillo et al. 2015; Brutsaert and Lopez, 1998), up to 67 days (Sanchez-Murillo et al. 2015; Brutsaert and Lopez, 1989). Eckhardt (2005) states that the standard recession length

is 45 days while Rutledge (1998) recommends a recession period of 10 – 20 days with at least 20 recession periods to analyze.

We found a recession period of at least10 days to be appropriate for streamflow in Gordon Gulch. For years with complete records of streamflow, the recession period was applied and USGS Groundwater Toolbox identified a number of recession periods starting from one day after peak streamflow until the next increase in streamflow. These graphs of streamflow recession were reviewed and non-linear graphs were modified (periods shortened to remove any non-linearity) or removed entirely. An example of a good recession graph from May 2017 to June 2017 is provided in **Figure F-1**. The slope of the semilogarithmic recession graph is equal to the characteristic recession time constant (τ) which can be used to solve for the recession constant, per Eq. (1).

In total, 19 recession curves were analyzed using Gordon Gulch streamflow data, as shown in **Table F-1**. In Gordon Gulch, the majority of recession periods occurred in July. Estimated time constants ranged from 7 to 40 days with a median value of 21 days, indicating that recession periods in the Gordon Gulch stream lasted approximately three weeks long. There were seasonal differences in the recession periods, however, with September having the shortest average recession period (nine days) and July having the longest recession period (26 days). The majority of substantial recession periods (those exceeding 10 days) occurred between May and August, with only one in September. Estimated values of the recession constant ranged from 0.905 - 0.985, with a mean value of 0.956.

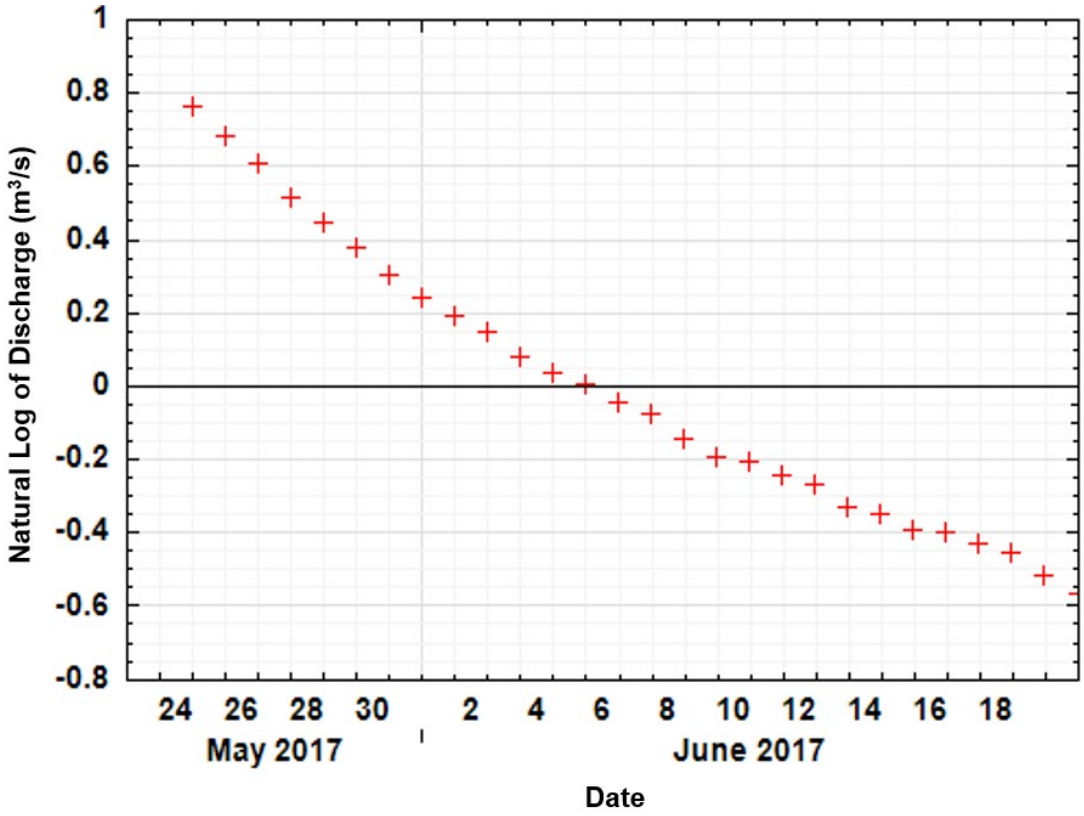

Figure F-1. Recession curve from May to June 2017 used for analysis of the recession constant for the stream in Gordon Gulch. The plot is a good example of a linear recession curve shape, which was used to estimate the slope of the recession curve and therefore the recession constant (α). The slope of the line is 1/τ, here about 0.073 d^{-1}, yielding a value of τ of about 13 days.

Table F-1. Summary of recession periods and estimated values of the recession time constant (τ) and the recession constant analyzed from the Gordon Gulch streamflow record between 2012 and 2019, reported by month of the water year.

Month of water year	# of recession periods	Average recession time constant (τ, days)	Recession constant (α)
May	6	21	0.953
June	4	24	0.959
July	5	26	0.962
August	3	19	0.948
September	1	9	0.894
Mean	4	22	0.956
Median	4	21	0.963

Step 2. Estimate BFI_{max}

A range of BFI_{max} estimates were then obtained using the estimated values of the recession constant obtained from RECESS and commonly cited values of α, 0.925 of 0.978 (Nathan and McMahon, 1990; Chapman, 1991). Estimating BFI_{max} is a more subjective process. The USGS Groundwater Toolbox employs Collischonn and Fan's (2013) backwards filter method to estimate BFI_{max} per Eq. (3) and (4). Daily streamflow measurements, the estimated recession constants (from step #1), and minimum number of recession days were input into the USGS Groundwater Toolbox. Visual inspections of the backwards filter were performed to remove any estimates that weren't a good visual fit for the data (i.e. non-linear trends or inconsistencies in recession). As summarized in **Table F-2**, BFI_{max} ranged from 0.28 to 0.56, with a mean BFI_{max} of 0.34.

Table F-2. Summary of BFI_{max} estimates using variable recession periods and recession constants estimated in the USGS Groundwater Toolbox for Gordon Gulch streamflow from 2012 to 2019. Values reported produced a good visual fit from the backwards filter in the USGS Groundwater Toolbox.

α	**Minimum recession length (N, days)**	**BFI_{max}**			
		Min	**Max**	**Mean**	**Median**
0.985	45	0.00	0.48	0.26	0.28
	32	0.00	0.78	0.31	0.33
	15	0.00	0.66	0.27	0.29
	10	0.00	0.78	0.35	0.38
	Mean	*0.00*	*0.67*	***0.30***	***0.32***
0.978	15	0.00	0.84	0.37	0.44
	10	0.00	0.84	0.42	0.49
	5	0.00	0.86	0.49	0.52
	Mean	*0.00*	*0.84*	***0.42***	***0.48***
0.971	45	0.00	0.71	0.43	0.56
	15	0.00	0.87	0.43	0.56
	10	0.00	0.87	0.48	0.56
	Mean	*0.00*	*0.82*	***0.45***	***0.56***
	Mean	0.00	0.58	**0.29**	**0.34**

Step 3. Estimate Baseflow

Once α and BFI_{max} were estimated, the Groundwater Toolbox was again employed to calculate baseflow from Eq. (5). For various combinations of the estimated values of the recession constant and BFI_{max}, the Eckhardt two-parameter filter was applied to hydrographs of daily streamflow records from Gordon Gulch in the USGS Groundwater Toolbox to estimate daily records of baseflow.

The best suited combination of parameters for streamflow in Gordon Gulch were a recession constant of 0.978 and a BFI_{max} value of 0.34. Overall, total annual baseflow accounts for 34% of total annual streamflow. Results from the hydrograph separation process are shown in **Figure F-2**, which identifies daily baseflow and total daily streamflow for water years 2012 through 2019 in Gordon Gulch.

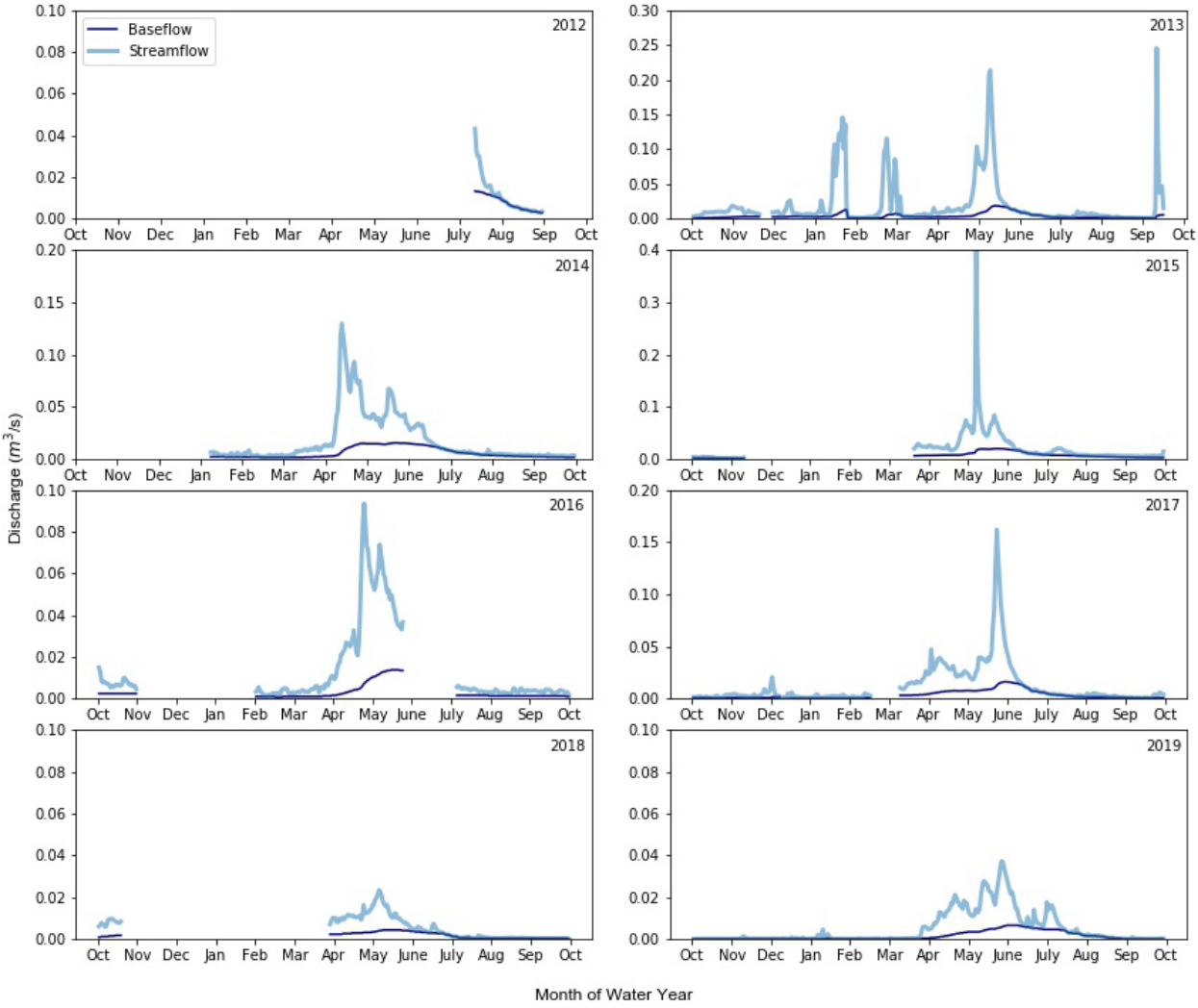

Figure F-2. Daily estimate of baseflow from the Eckhardt RDF method for water years 2012 through 2019. Daily streamflow is also plotted based on measurements from the lower gauge in Gordon Gulch.

Appendix G. Water Table Fluctuation Method

The water table fluctuation (WTF) method is based on the assumption that groundwater levels in an unconfined aquifer rise due to recharge (Healy and Cook, 2002). The WTF method is most often applied to aquifer systems that are responsive to discrete precipitation events, which are typically shallow, unconfined aquifers (Healy and Cook, 2002). If groundwater level measurements are available, recharge can be estimated as (Healy and Cook, 2002):

$$\Delta S_{gw} = R = S_y \frac{dh}{dt} = S_y \frac{\Delta h}{\Delta t} \quad (1)$$

where R is recharge, Sy is the specific yield (the ratio of water volume that drains from a saturated rock due to gravity to the total volume of the rock), dh or Δh is the rise in water table, and dt or Δt is the time interval over which the rise occurs.

There are three underlying assumptions that the WTF method relies on, which include:

1. A rise in groundwater level is caused only by recharge arriving to the water table
2. Specific yield is constant over the period of the water table fluctuations, and
3. The water level recession can be extrapolated to determine Δh/Δt (indicating long term records at appropriate temporal discretization are available).

To calculate recharge using the WTF method, groundwater level measurements and an estimate of the specific yield of the aquifer material are required. Groundwater level measurements are used to estimate Δh and Δt. First, peaks in the groundwater level hydrograph are identified. Where these peaks occur, an antecedent recession curve is extrapolated to continue the pattern of groundwater level decline that would occur in the absence of recharge. Δh is then estimated as the difference between the peak of the groundwater level rise and the low point of the extrapolated recession curve (**Figure G-1**). Δt is defined as the time between the start of the extrapolated recession curve until the peak in the groundwater hydrograph.

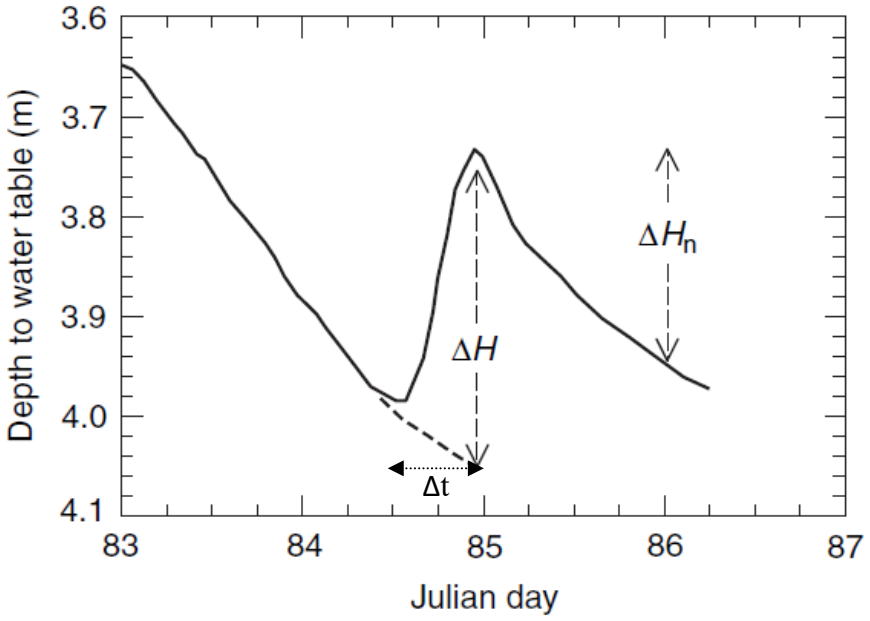

Figure G-1. Example calculation of ΔH and ΔH_n (net change in groundwater level). Solid black lines are the measured groundwater levels, dashed black lines are extrapolated antecedent curves, the vertical dashed lines identify ΔH and ΔH_n, and the dotted black line identifies Δt. Groundwater recharge is then calculated as Sy times ΔH. Adapted from Healy and Cook, 2002.

The WTF method deemed appropriate for use in this study because conditions in Gordon Gulch overcome several of the limitations of the method which include:

1. Variable recharge rates within a watershed because of differences in elevation, geology, slope, vegetation, etc. To overcome this, it is recommended that multiple wells be used throughout a watershed to ensure estimates of recharge represent the entire watershed and not just one specific site. Three wells sited in Gordon Gulch were used to estimate recharge, representing conditions on the north-facing slope (well 1), south-facing slope (well 6), and in the riparian area of the valley (well 2). Additionally, precipitation is weakly dependent on elevation in this catchment (Rossi et al., 2020).
2. Limited measurements of groundwater levels; fewer measurements result in an underestimated rate of recharge (Delin et al., 2007). Delin et al. (2007) recommended that at least weekly measurements of groundwater levels be used for this method. Water level

measurements were available at 10-minute intervals from wells 1, 2, and 6 for water years 2012 – 2019, although the measurements used ultimately were daily mean values.

3. Heterogeneity of specific yield. Natural heterogeneity of geologic materials can result in variations of specific yield over short distances. Usually, specific yield can be determined through laboratory methods, field, methods, water budget methods, or numerical modelling. However, if this data isn't available, specific yield is difficult to measure and there is no widespread method of deriving it from other data. Therefore, estimating the specific yield of the aquifer at the depth of the zone of the water table fluctuation can be a huge challenge and represents uncertainty in the estimate of recharge using the WTF method. No available estimates of specific yield were available for Gordon Gulch, so this represents the greatest uncertainty in estimating recharge via the WTF method.

Daily mean groundwater levels from wells 1, 2, and 6 for water years 2012-2019 were used to estimate recharge in Gordon Gulch. These wells are unaffected by human activities, pumping, cycles of the ocean, etc. so there is a fair assumption that rises in the water table are due to precipitation. Since values of specific yield are unknown for the aquifer in Gordon Gulch, a graphical procedure was applied to first obtain an estimate of specific yield of the aquifer. Using estimates of specific yield, recharge was then calculated by applying the WTF method to groundwater levels measured at the three wells in Gordon Gulch, as described below.

Estimating specific yield:

No estimates of specific yield were available for the hydrogeologic units in Gordon Gulch. Therefore, we applied the water budget method to estimate specific yield (Delin et al., 2007; Healy, 2010; King, 2011):

$$R = P - \frac{Q}{A} \quad (2)$$

where R is recharge, P is precipitation, Q is streamflow, and A is the area of Gordon Gulch (2.6 km^2). The recharge term in Eq. (1) was substituted into Eq. (2) and then be rearranged to solve for S_y:

$$S_y = \frac{P - {}^{Q}/_{A}}{{}^{\Delta h}/_{\Delta t}} \quad (3)$$

Eq. (3) was applied to observed rises in groundwater levels that occurred in mid to late summer in the hydrographs for the three wells in Gordon Gulch. During this period (approximately June through September) streamflow and groundwater levels are generally in recession and all precipitation arrives as rain. Antecedent recession curves were manually extrapolated on the hydrographs of wells 1, 2, and 6 to estimate values of $\Delta h/\Delta t$ (an example of this is presented in **Figure G-2**). The estimate of Δt was used to constrain the period to calculate total precipitation and total stream discharge. Daily values of precipitation and stream discharge measurements were available for this time period, as described in Appendix B and Appendix F.

The results from estimating specific yield for wells 1, 2, and 6 are presented in **Table G-1**, **Table G-2**, and **Table G-3**, respectively. The average specific yield across all three wells for water years 2012-2019 was 0.14, but ranged from 0.02 to 0.32 depending on the precipitation event and well. The average estimate of specific yield varied by well with an average value of 0.14 at well 1, 0.17 at well 2, and 0.10 at well 6. The range in the estimates of specific yield reflect the range in the aquifer material at the level of the water table fluctuation. Wells 1 and 6 are screened in saprolite, weathered bedrock, and bedrock (at varying thicknesses) whereas well 2 is screened exclusively in saprolite. A literature review was also performed (**Table G-4**) to compare estimated values of specific yield with those for similar hydrogeologic units. Compared

to cited values of specific yield for saprolite, the estimates from the water budget method tended to fall in the upper range of cited values.

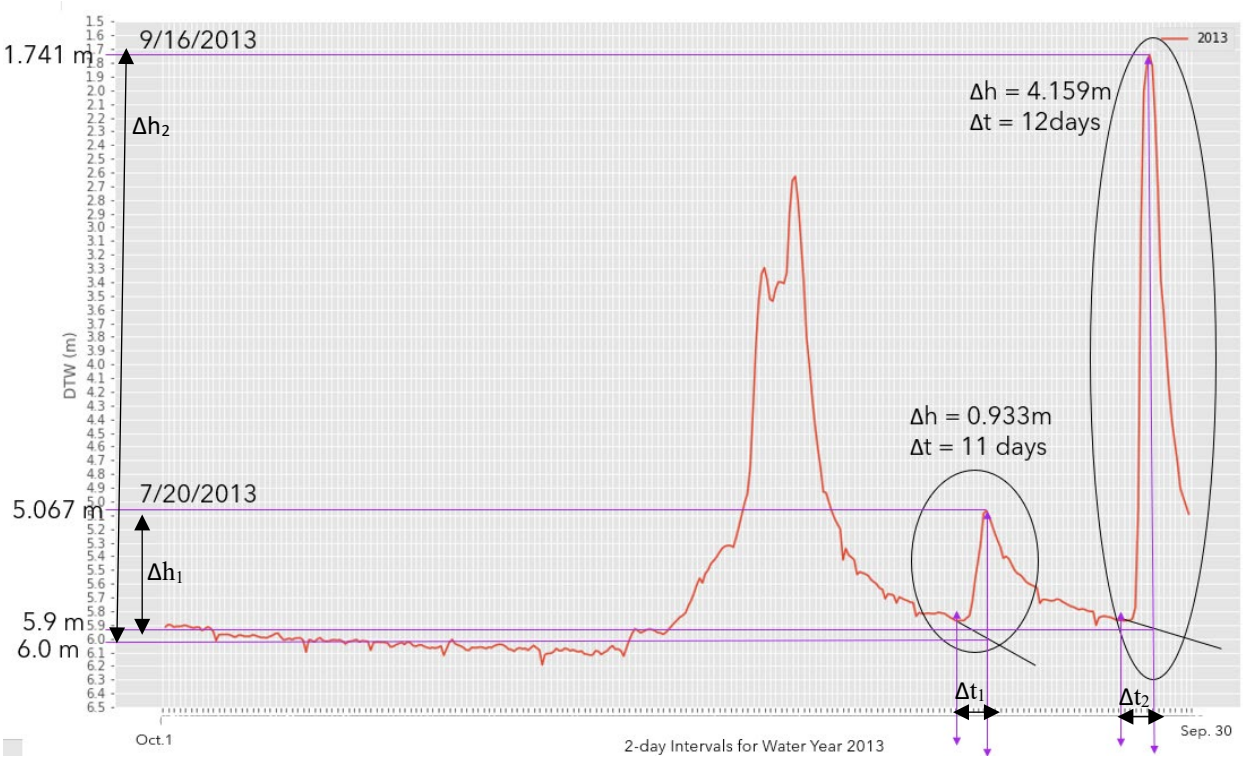

Figure G-2. Example calculation of Δh and Δt to use to estimate Sy for two peaks in the 2013 hydrograph from well 6. Δh_1 and Δt_1 occurred in July 2013; Δh_2 and Δt_2 occurred in September 2013. Red lines are depth to water measurements, black circles identify the summer peaks, black lines are the extrapolated antecedent curves off the two hydrograph peaks, and purple lines identify the values of h and t to be used to calculate Δh and Δt.

Table G-1. Estimates of specific yield for well 1 using the water budget method for water years 2012 – 2019. P is the rate of precipitation, Q is the total stream discharge over time (Δt), A is the area of Gordon Gulch, Δh is the change in head over a period of time, and Sy is the estimated value of specific yield from Eq. (3).

Water Year	P (m/d)	Q/A (m/d)	Δh (m)	Δt (days)	Month of Water Year	Sy
2012	0.014	0.00035	0.83	10	July	0.16
2013	0.001	0.00027	0.29	7	July	0.02
2013	0.027	0.00237	1.29	7	September	0.13
2014	0.004	0.00019	0.16	7	August	0.17
2015	0.006	0.00047	0.58	14	July	0.14
2016	0.001	0.00015	0.10	4	August	0.05
2017	0.004	0.00013	0.16	14	August	0.30
2019	0.004	0.00042	0.22	10	July	0.14
Mean	**0.01**	**0.00055**	**0.46**	**9**	**August**	**0.14**
SD	**0.01**	**0.00070**	**0.39**	**3**	**--**	**0.08**

Table G-2. Estimates of specific yield for well 2 using the water budget method for water years 2012 – 2019. P is the rate of precipitation, Q is the total stream discharge over time (Δt), A is the area of Gordon Gulch, Δh is the change in head over a period of time, and Sy is the estimated value of specific yield from Eq. (3).

Water Year	P (m/d)	Q/A (m/d)	Δh (m)	Δt (days)	Month of Water Year	Sy
2012	0.005	0.00043	1.17	6	July	0.02
2013	0.010	0.00018	0.34	9	July	0.26
2013	0.022	0.00112	0.92	8	September	0.19
2014	0.004	0.00014	0.18	12	August	0.27
2015	0.007	0.00032	0.63	10	July	0.10
2017	0.003	0.00011	0.2	12	August	0.18
2018	0.001	0.00002	0.1	8	August	0.09
2019	0.001	0.00006	0.2	8	August	0.05
2019	0.003	0.00024	0.09	9	July	0.32
Mean	**0.01**	**0.00029**	**0.43**	**9**	**August**	**0.17**
Std.	**0.01**	**0.00032**	**0.37**	**2**	**--**	**0.10**

Table G-3. Estimates of specific yield for well 6 using the water budget method for water years 2012 – 2019. P is the rate of precipitation, Q is the total stream discharge over time (Δt), A is the area of Gordon Gulch, Δh is the change in head over a period of time, and Sy is the estimated value of specific yield from Eq. (3).

Water Year	P (m/d)	Q/A (m/d)	Δh (m)	Δt (days)	Month of Water Year	Sy
2013	0.008	0.00016	0.93	11	July	0.09
2013	0.018	0.00008	4.16	12	September	0.05
2014	0.004	0.00014	0.24	10	August	0.18
2015	0.006	0.00039	1.14	11	July	0.06
2016	0.002	0.00010	0.03	1	August	0.08
2017	0.004	0.00001	0.13	5	September	0.16
2019	0.004	0.00033	0.56	8	August	0.05
Mean	**0.01**	**0.00017**	**1.03**	**8**	**August**	**0.10**
Std.	**0.00**	**0.00013**	**1.33**	**4**	**--**	**0.05**

Table G-4. Literature review of specific yield values for similar hydrogeologic units to Gordon Gulch (saprolite and weathered bedrock).

Reference	Geology and Specific Yield	Location
King, 2011	0.033 (fractured rock)	Niwot Ridge, Colorado
Durand et al., 2017	0.07 to 0.15 (saprolite) 0.01 to 0.03 (fractured rock)	Brittany, France
Maréchal et al., 2006	0.014 (fractured granite)	Andhra Pradesh State, India
Creutzfeldt, 2010	0.024 (saprolite)	Wetzell, Germany
Hisz and Murdoch, 2006	0.0001 to 0.5 (saprolite)	Piedmont Physiographic Province, eastern U. S

Estimating recharge using the WTF method:

Using the range of estimates of specific yield obtained in the previous step, recharge was estimated by applying the WTF method (Eq. 1) to wells 1, 2, and 6. The cumulative individual rises of groundwater level for each year were obtained for each well by adding up individual recharge events over each water year. Estimates of recharge were then calculated for each well by multiplying the range of specific yield estimates from the previous step to the net cumulative groundwater rise for each water year.

Table G-5, **G-6**, and **G-7** summarize the results of estimating recharge as a percentage of total annual precipitation for wells 1, 2, and 6, respectively, for water years 2012-2019. Despite estimating specific yield using a graphical method, specific yield represents a considerable uncertainty. The mean estimate of specific yield (0.14) produced unreasonable results of recharge (i.e. recharge exceeded total precipitation), as did any estimate of specific yield greater than 0.086. Ultimately, we applied the lowest estimate of specific yield of 0.02 to the WTF method to estimate recharge. Specific yield of 0.02 may be the minimum estimate across the three wells in Gordon Gulch, but it is comparable to other estimates of specific yield for saprolite and fractured rock found in cited literature (**Table G-4**). Mean annual recharge ranged from 19% (well 2) to 38% (well 6) of total precipitation. The greatest annual recharge occurred in 2013 across the three wells, attributed to the extreme precipitation event in September of 2013. The minimum annual recharge occurred in 2018 where total annual precipitation was the lowest of the data record from 2012 to 2019. Mean annual recharge was consistently largest at well 6 and consistently lowest at well 2. Variation in the recharge rates across the three wells reflects the differences in the distribution of precipitation, snowmelt, hillslope position, and hydrogeologic unit(s) that the water table fluctuations occur. Well 6 is located on a long, planar south-facing

hillslope, is recharged by upslope infiltration and lateral flow, and recharge is stored within weathered bedrock. Well 2 is located in the riparian zone, is recharged from shallow flow and lateral, upslope flow, and recharge is stored in saprolite.

Figure G-3, **G-4**, and **G-5** plot the annual recharge (Sy = 0.02) versus the corresponding total annual precipitation for wells 1, 2, and 6, respectively. Total annual precipitation had the strongest effect on recharge at well 6 ($R^2 = 0.74$) and weakest effect on recharge at well 2 ($R^2 = 0.42$).

Table G-5. Estimated recharge as a percentage of total precipitation (P) at well 1 for a range of specific yield values using the WTF method. P is precipitation, Δh is the total annual rise in head, and specific yield values were estimated for each well using the graphical water budget method as described in Appendix G. Selected values of recharge using a specific yield of 0.02 are in **bold**.

Year	P (m)	Δh (m)	Δt (m)	Recharge (% of P)			
				S_y = 0.02	S_y = 0.033	S_y = 0.086	S_y = 0.14
2012	0.53	4.95	176	**39%**	62%	166%	271%
2013	0.84	4.32	149	**25%**	41%	109%	177%
2014	0.58	4.77	179	**34%**	54%	145%	236%
2015	0.64	5.53	196	**32%**	52%	139%	226%
2016	0.47	4.29	199	**34%**	54%	144%	235%
2017	0.58	4.60	186	**31%**	50%	134%	219%
2018	0.42	3.88	189	**36%**	57%	153%	250%
2019	0.55	3.79	169	**30%**	48%	128%	208%
Mean	0.57	4.51	180.4	**33%**	52%	140%	228%
std.	0.12	0.54	15.1	**32%**	6%	16%	26%

Table G-6. Estimated recharge as a percentage of total precipitation (P) at well 2 for a range of specific yield values using the WTF method. P is precipitation, Δh is the total annual rise in head, and specific yield values were estimated for each well using the graphical water budget method as described in Appendix G. Selected values of recharge using a specific yield of 0.02 are in **bold**.

Year	P (m)	Δh (m)	Δt (m)	R (% P)			
				S_y = 0.02	S_y = 0.033	S_y = 0.086	S_y = 0.14
2012	0.53	3.54	193	**25%**	42%	109%	177%
2013	0.84	3.43	188	**16%**	26%	68%	111%
2014	0.58	3.88	219	**22%**	37%	96%	157%
2015	0.64	3.26	209	**18%**	29%	77%	125%
2016	0.47	2.63	207	**20%**	33%	85%	139%
2017	0.58	2.48	188	**17%**	27%	72%	117%
2018	0.42	2.18	212	**18%**	29%	77%	125%
2019	0.55	1.95	161	**16%**	27%	69%	113%
Mean	0.57	2.84	197.1	**19%**	31%	82%	133%
std.	0.12	0.66	17.4	**3%**	5%	13%	22%

Table G-7. Estimated recharge as a percentage of total precipitation (P) at well 6 for a range of specific yield values using the WTF method. P is precipitation, Δh is the total annual rise in head, and specific yield values were estimated for each well using the graphical water budget method as described in Appendix G. Selected values of recharge using a specific yield of 0.02 are in **bold**.

Year	P (m)	Δh (m)	Δt (m)	Recharge (% of P)			
				S_y = 0.02	S_y = 0.033	S_y = 0.086	S_y = 0.14
2012	0.53	5.4	198	**38%**	62%	163%	265%
2013	0.84	9.3	206	**40%**	65%	170%	277%
2014	0.58	5.3	203	**33%**	55%	143%	233%
2015	0.64	8.6	201	**49%**	81%	210%	342%
2016	0.47	5.5	195	**44%**	72%	187%	305%
2017	0.58	5.8	164	**45%**	74%	192%	313%
2018	0.42	3.6	200	**31%**	52%	135%	220%
2019	0.55	4.5	195	**31%**	51%	133%	216%
Mean	0.57	5.8	194.83	**38%**	63%	165%	268%
Std.	0.12	1.8	12.33	**6%**	10%	27%	44%

Figure G-3. Total annual precipitation vs. total annual recharge (Sy = 0.02) estimated at well 1 for water years 2012 – 2019.

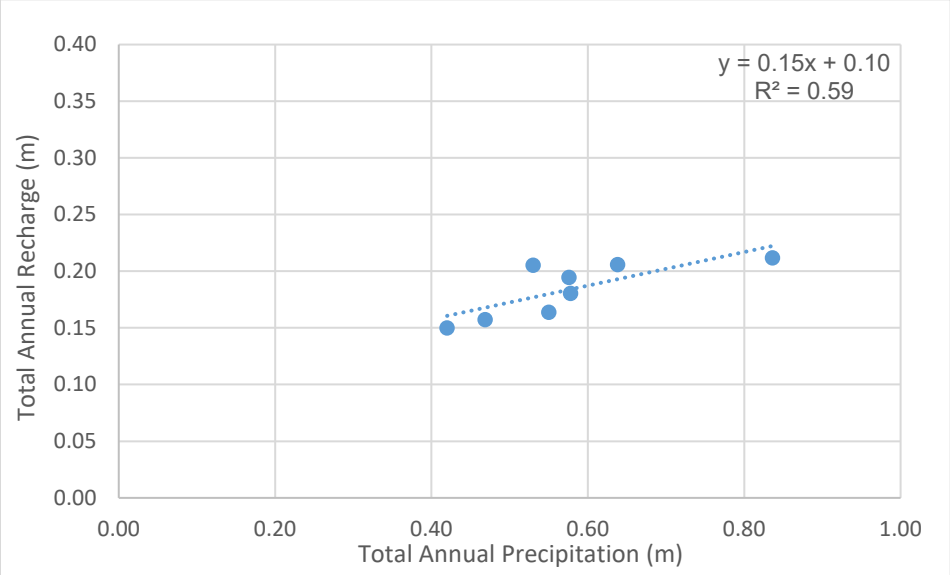

Figure G-4. Total annual precipitation vs. total annual recharge (Sy = 0.02) estimated at well 2 for water years 2012 – 2019.

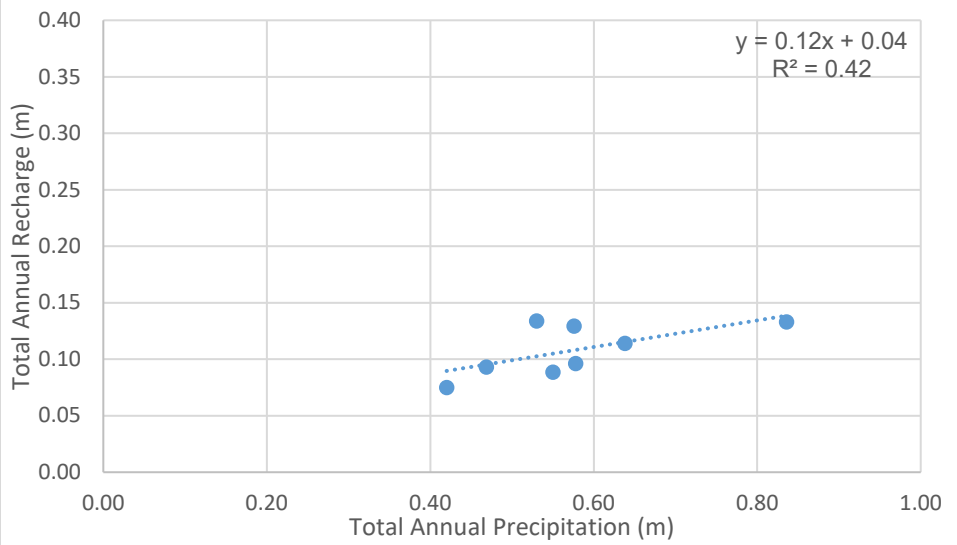

Figure G-5. Total annual precipitation vs. total annual recharge (Sy = 0.02) estimated at well 6 for water years 2012 – 2019.